ENERGY MIGRATION IN RARE EARTH COMPLEXES

By

John Jerome Freeman

Facsimile Price $ 14.50

Microfilm Price $ 6.77

Available from the
Office of Technical Services
Department of Commerce
Washington 25, D. C.

A Dissertation

Submitted in Partial Fulfillment of the

Requirements for the Degree of

Doctor of Philosophy in Chemistry

The University of New Mexico

1963

DISCLAIMER

"And further, by these, my son, be admonished: of many books there is no end; and much study is a weariness of the flesh . . . ."

Ecclesiastes 12: 12

ACKNOWLEDGMENTS

I wish to express my appreciation to Dr. Glenn A. Crosby for his valuable suggestions and advice.

The research presented in this dissertation was sponsored by Sandia Corporation under P. O. No. 51-5134.

ABSTRACT

Complexes of trivalent samarium, europium, terbium, and dysprosium were prepared for investigations of the luminescence properties of complexed rare earth ions. Rare earth chelates derived from benzoylacetone, dibenzoylmethane, and acetylacetone; rare earth chlorides solvated with water and deuterium oxide; and rare earth oxides dissolved in sodium metaphosphate glasses were synthesized for these studies.

Initial investigations were conducted on the β-diketone chelates dissolved in organic glasses at 77°K. The luminescence spectra of the samples, arising from excitation by ultraviolet light, are reported, and groups of spectral lines are given J-J assignments. The luminescence decays of the rare earth ion emissions, arising from radiative transitions originating at the lowest resonance level of the ions, were measured. The decay curves were analyzed statistically, and a lower limit of 5×10^5 sec.$^{-1}$ is reported for the rate constant associated with intramolecular energy transfer. From a consideration of the rate of energy transfer and the magnitude of the molecular phosphorescence decay times of of the chelates, it is concluded that intramolecular energy transfer cannot originate at the same level from which phosphorescence occurs. Intramolecular energy transfer rate

constants for transfer of energy to the ions from higher levels of the triplet energy systems in these compounds are discussed.

The visible absorption spectra of solutions of rare earth chelates and rare earth chlorides are presented and analyzed. Rare earth ion radiative transition probabilities, calculated from the weak ion absorption bands, are reported. It is shown that the increased luminescence decay times of the chelated rare earth ions as compared to the solvated rare earth ions must be due to a decrease in quenching of the ion states, not to a decrease in the radiative transition probabilities.

The luminescence investigations were also carried out on microcrystalline chelates, crystalline solvated chlorides, and metaphosphate glasses. The emission spectra are presented and J-J assignments are made. Measurements of spectral lines arising from vibronic coupling of chelated rare earth ions are given. The luminescence decay curves of the complexes are reported, and decay times calculated from the curves are tabulated. For a few of the samples, the temperature dependencies of the luminescences are also reported.

Quite significant differences were found in the luminescence intensities and decay times of rare earth ions in different environments. Possible mechanisms for quenching of rare earth ion states are presented, and it is concluded that the variations of the luminescence properties of the ions are due to variations in vibronic quenching efficiency.

The nature of the vibronic quenching in each of the different rare earth complex systems is discussed.

Secondary environmental effects on the rare earth ion luminescences are considered, and it is shown that factors such as the nature of the solvent and the method of sample preparation must be considered in any quantitative discussion of the luminescence properties. The origins of the discrepancies among the luminescence decay times reported by other authors are also considered.

TABLE OF CONTENTS

Page

LIST OF TABLES

LIST OF FIGURES

1. Introduction

It has been known for some time that the near ultraviolet, visible, and near infrared spectra of the trivalent rare earth ions, lanthanum through lutetium, arise from "forbidden" electronic transitions between states derived from 4f electrons. The absorption spectra of the complexed ions are characterized by sharp lines possessing very small extinction coefficients (1,2), while the emission spectra are characterized by very sharp lines similar to those in the spectra of the free ions. Due to shielding of the 4f electrons by the outer 5s and 5p electrons of the ions, the wave lengths of the lines in the absorption or emission spectra are not very dependent upon the environments of the ions. The central problems in the spectroscopy of the trivalent rare earth ions have been to characterize the electronic states giving rise to the visible and near visible spectra and to delineate the paths of energy migration within the rare earth complexes.

The characterization of the 4f electronic states of the rare earth ions has been conducted through a study of the absorption and emission spectra of, for the most part, crystalline inorganic salts of the metals (3). As the spectra of the complexed ions are very similar to the atomic spectra of the free ions, the electronic states of the complexed rare

earth ions have been classified according to the spin quantum number, S, the orbital angular momentum quantum number, L, and the total angular momentum quantum number, J, of the parent atomic states. Weak interactions between the 4f electrons and the surrounding ligands may partially or wholly remove the electronic degeneracies of the parent atomic states giving rise to crystal field multiplets. Whereas a transition between atomic J states of the free ion would give rise to a single spectral line, transitions between the crystal field multiplets lead to a group of spectral lines. The problems involved in the characterization of the crystal field multiplets, and the accomplishments that have been made in this field have been reviewed by McClure (3). Recent extensive analyses of the crystal field structure of the spectra of the rare earth ions have been reported by Dieke and coworkers (4,5,6,7,8,9).

Quantitative measurements of energy migration in inorganic salts were first reported by Rinck (10). Detailed studies of the relative intensities of emission and the luminescence decay times were conducted using crystals of europic sulfate, $Eu_2(SO_4)_3 \cdot 8H_2O$. It was found that although the 4f electrons of the europium ion were being excited directly by the absorption of near ultraviolet light, the depopulation of the excited electronic states of the europium ion occurred mainly through quenching processes. The data indicated that over 95% of the electronic energy was being converted to vibrational motion of the surrounding lattice, and that less than 5% of the energy was reappearing as radiation. Similar

results were obtained by Geisler and Hellwege (11) in a study of the emission of terbium bromate, $Tb(BrO_3)_3 \cdot 9H_2O$.

The energy migration mechanisms become even more complex in the β-diketone chelates of the rare earth ions. It has been shown (12,13,14,15) that for these complexes, the 4f electrons are not excited directly by the absorption of the ultraviolet light, but rather that the surrounding organic ligands absorb the exciting radiation, and the energy is then transferred to the 4f electrons of the rare earth ion. Detailed studies of the spectra of the β-diketone chelates by Crosby and coworkers (16,17,18,19,20,21) have established that intramolecular energy transfer to the 4f electrons of the rare earth ion occurs *via* the lowest triplet state of the organic complex or *via* a nearby excited triplet.

Although the spectral measurements of the rare earth chelates revealed the important role played by the triplet state in the intramolecular energy transfer process, it was not known with certainty which of the levels of the lowest triplet system were involved in the energy transfer process. Furthermore, the spectral measurements gave no measure of the rate of intramolecular energy transfer, and it was not known if the energy transfer process controlled the rate of decay of the rare earth ion luminescences.

In an effort to obtain more detailed information about energy migration processes in rare earth complexes, an investigation of the luminescence decay times and the luminescence spectra of complexed rare earth ions was undertaken. Complexes

selected for study were those compounds of trivalent samarium, europium, terbium, and dysprosium which commonly give rise to bright line emission characteristic of the rare earth ion. Beta-diketone chelates, solvated chlorides, and oxides dissolved in sodium metaphosphate glasses were used in the investigations.

The purposes of the investigations presented here are as follows:

(a) to establish limits on the rate of intramolecular energy transfer in rare earth chelates and to determine whether the transfer process controls the rate of decay of ion luminescence,

(b) to obtain information about the nature of the excited energy levels of the rare earth chelate from which intramolecular energy transfer occurs,

(c) to determine whether the quenching processes, which play such an important role in the depopulation of excited electronic states of the solvated rare earth salts, are also operative in other types of rare earth complexes; and to obtain information about the nature of the quenching processes.

2. Experimental Details

2.1. Preparation of Compounds

2.1.1. Chelates Derived from Benzoylacetone and Dibenzoylmethane

Rare earth trisbenzoylacetonate dihydrates ($MB_3 \cdot 2H_2O$) and rare earth trisdibenzoylmethides (MD_3) were prepared in the same manner as described by Whan and Crosby (20). The rare earth oxides (99.9+% purity) were obtained from Research Chemicals, Inc. The dibenzoylmethane and benzoylacetone (both Eastman White Label grade) were not purified before use. In the case of the europium trisdibenzoylmethide, a portion of the preparation was not subjected to the usual prolonged vacuum drying at elevated temperatures described in reference 20. Analysis of this compound revealed that the chelate contained one extra mole of chelating agent (dibenzoylmethane) per mole of chelate.

2.1.2. Chelates Derived from Acetylacetone

One gram of rare earth oxide was converted to the chloride by treatment with a concentrated hydrochloric acid solution. The excess hydrogen chloride was removed by gently boiling away the excess liquid. The moist crystals of the rare earth chloride were dissolved in 200 ml. of water, and

4 ml. of redistilled acetylacetone were added to the solution. Concentrated ammonium hydroxide was added to the mixture, drop by drop with vigorous stirring, until precipitation of the white microcrystalline chelate was complete.

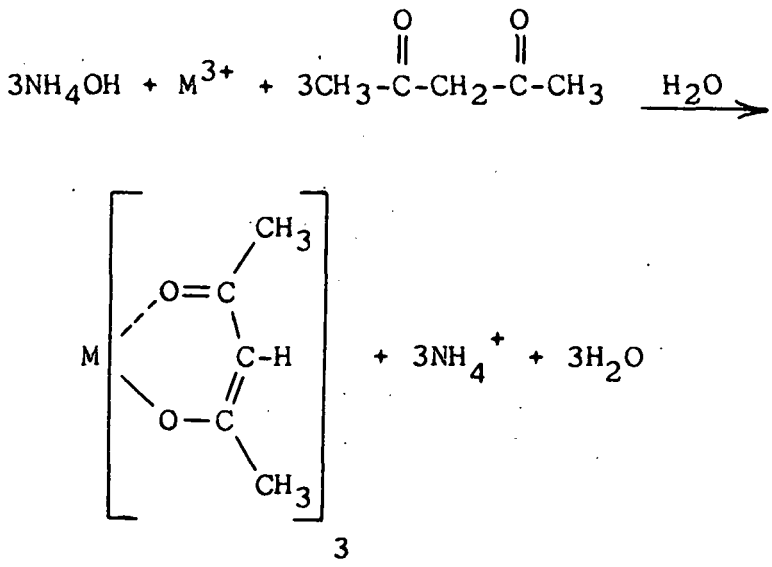

Addition of excess concentrated ammonium hydroxide was avoided.

The precipitated chelate was collected by vacuum filtration on a medium, sintered-glass, filter funnel, washed three times with distilled water, and air dried. Acetone was added to dissolve the dried material while it was still on the filter funnel, and the solution was drawn off under vacuum. The chelate was then crystallized from the boiling acetone solution and vacuum dried at room temperature for twelve to sixteen hours. Quantitative analyses of the compounds revealed that the final product existed as the monohydrate. Attempts to remove the extra mole of water from the product by vacuum drying at elevated temperatures were not successful. The melting points of the rare earth trisacetylacetonate monohydrates

are reported in Table 2.1.2.1.

2.1.3. Solvated Rare Earth Chlorides

Hydrated rare earth chlorides were prepared by treating the rare earth oxide with a concentrated hydrochloric acid solution. The excess hydrogen chloride was removed by gently boiling away the excess solvent until only moist crystals remained. The material was dissolved in distilled water and the solution was again evaporated down to moist crystals. The crystalline chloride was then collected on a sintered-glass filter funnel and air dried.

Rare earth chlorides solvated with deuterium oxide were obtained through the courtesy of Dr. Kathryn E. Lawson of Sandia Corporation, Albuquerque, New Mexico. These compounds were prepared in precisely the same manner as were the rare earth chlorides solvated with water except that deuterium chloride in deuterium oxide was used to convert the rare earth oxide to the solvated chloride. During the preparation of these compounds, the solutions were evaporated to dryness in a vacuum desiccator to prevent contamination of the materials with water. The final products were also stored in a vacuum desiccator.

No chemical analyses were performed on the crystalline solvated rare earth chlorides, however, Dr. Lawson obtained X-ray powder patterns of the chlorides prepared in the manner just described. The powder patterns of the rare earth chlorides of trivalent samarium, europium, terbium, and dysprosium solvated with either water or deuterium oxide indicate

TABLE 2.1.2.1.

MELTING POINTS OF RARE EARTH TRISACETYLACETONATE MONOHYDRATES

Compound	m. p., °C
$SmA_3 \cdot H_2O$[a]	136-139[b]
$EuA_3 \cdot H_2O$	136-139
$GdA_3 \cdot H_2O$	142-145
$TbA_3 \cdot H_2O$	130-132
$DyA_3 \cdot H_2O$	137-139

[a]Abbreviations used for organic groups here and throughout the text are:

A = acetylacetonate ion,

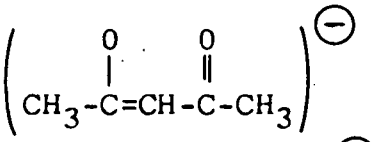

B = benzoylacetonate ion,

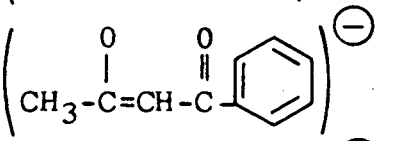

D = dibenzoylmethide ion,

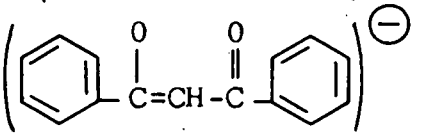

DH = dibenzoylmethane molecule,

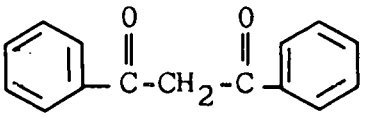

[b]None of the compounds exhibited sharp melting points. Decomposition occurred during melting.

that the samples were all isostructural with crystalline gadolinium trichloride hexahydrate ($GdCl_3 \cdot 6H_2O$).

2.1.4. Rare Earth Oxide-Sodium Metaphosphate Glasses

Rare earth oxide and sodium dihydrogenphosphate, $NaH_2PO_4 \cdot H_2O$ (Baker's Analyzed reagent, C. P. grade), were weighed out directly into a porcelain crucible. The mixture was heated gently with a Meeker burner until the evolution of water had ceased. The opaque glassy residue was then fused by vigorous heating with the burner. Heating was continued, with occasional swirling of the melt, until all of the rare earth oxide had been dissolved by the molten sodium metaphosphate. The melt was poured onto a piece of polished stainless steel sheet and allowed to cool. Rare earth oxide-sodium metaphosphate glasses containing 0.1, 1.0, 2.0, and 10.0% by weight europium or terbium oxide, and glasses containing 2.0% by weight dysprosium or samarium oxide were prepared in this manner. The total weight of an individual sample was about 8 gm., and the resultant glass bead was two to three centimeters in diameter and about a half centimeter thick at the center.

The dissolution of the rare earth oxide in the molten sodium metaphosphate probably occurs according to the reaction

$$M_2O_3 + 3NaH_2PO_4 \cdot H_2O \xrightarrow{\Delta} 2MPO_4 + Na_3PO_4 + 6H_2O.$$

The dissolution process is definitely not just a dispersion of

the rare earth oxide in a sodium metaphosphate matrix since the glass samples were perfectly transparent, and if they did possess color, it was the color characteristic of the inorganic salt of the particular rare earth ion, not the color of the oxide of the rare earth ion.

For glasses containing 2% by weight or less of rare earth oxide, the samples possessed all the characteristics of a true glass. The samples were perfectly transparent, fractured conchoidally, and revealed curved strain patterns when viewed through crossed polaroids. The glasses were slightly hygroscopic, and they fractured when immersed in boiling liquid nitrogen.

Samples containing 10% by weight rare earth oxide were no longer transparent, but contained a dispersion of white opaque solid. The glass beads fractured when cooled to room temperature. This was not surprising, since stoichiometric considerations indicate that they may contain as much as 80% by weight rare earth phosphates, and such large amounts of phosphate would not be completely dissolved in the remaining sodium metaphosphate.

No chemical analyses were performed on the metaphosphate glass samples. Per cent compositions were estimated from the weights the rare earth oxide and sodium dihydrogenphosphate used in preparing the samples.

2.2. Quantitative Analyses of Rare Earth Chelates

A volumetric procedure for determining the rare earth

metal content of β-diketone chelates of the trivalent rare earths has been reported by Whan (20,22). An alternative method of analysis by a combustion technique is described below. Although this method is neither more accurate nor faster than the volumetric procedure, it can be accomplished with fewer laboratory manipulations of the sample.

About 100 mg. of rare earth chelate was weighed out in a carefully dried and tared porcelain combustion crucible. Ignition of the sample was performed without a crucible cover. The samples were first heated with a very low, Meeker-burner flame. At no time was the temperature of the sample allowed to rise so high that vigorous boiling or splattering of the liquid residue occurred. When the liquid residue had been reduced to a black carbonaceous solid, the sample was treated for one half to one hour longer with a very hot flame. All analyses were run in triplicate.

Ignition of chelates of samarium, dysprosium, and europium yielded the white sesquioxide (23), while the terbium chelates yielded a black residue consisting of mixed oxides of trivalent and tetravalent terbium. According to Cotton and Wilkinson (24), terbium oxides formed by ignition of terbium compounds in air have variable compositions ranging from $TbO_{1.71}$ to $TbO_{1.81}$ with $TbO_{1.75}$ being most common. Results of ignition analyses of rare earth β-diketone chelates are listed in Table 2.2.1. Melting points were obtained on all other rare earth chelates which were prepared, although the latter were not analyzed for rare earth metal content. The melting points of these chelates agreed with those given by

TABLE 2.2.1.

RESULTS OF IGNITION ANALYSES OF RARE EARTH CHELATES

Compound	% Metal (found)	% Metal (theoretical)
EuD_3 [a]	18.6	18.5
$EuD_3 \cdot DH$	14.0	14.5
$SmA_3 \cdot H_2O$	33.2	32.3
$EuA_3 \cdot H_2O$	32.4	32.5
$GdA_3 \cdot H_2O$	33.4	33.2
$TbA_3 \cdot H_2O$	34.7 [b]	33.6
$DyA_3 \cdot H_2O$	33.7	34.0

[a] See Table 2.1.2.1. for abbreviations.

[b] Calculated on the assumption that the empirical formula for the terbium oxide was $TbO_{1.75}$.

Whan (22).

2.3. Measurements of Absorption Spectra

Absorption spectra of solutions of rare earth compounds were measured with a Cary Model 14 spectrophotometer. Cylindrical quartz cells varying from 1 cm. to 10 cm. in length were used to contain the solutions. Reagent grade solvents were used to prepare all solutions. In all instances, the solutions were prepared immediately before the measurements were made.

Absorption strengths are reported in either units of absorbance, A, or in terms of the molar extinction coefficient, ϵ. The molar extinction coefficient used here is related to the absorbance by the following form of the integrated Beer's law:

$$A = \log_{10}\left(\frac{I_o}{I}\right) = \epsilon c l \qquad 2.3.1.$$

where I_o = intensity of incident radiation,

I = intensity of transmitted radiation,

c = concentration in moles per liter of solution,

l = length of cell in centimeters.

The spectrum of the strong ligand absorption bands of the acetylacetonate complex was measured using an alcoholic solution of $GdA_3 \cdot H_2O$ at a concentration of 444 mg. per 50 ml. of solvent. A 1 cm. cell was used to contain the solution. In order to measure the very weak absorbances of the chelated rare earth ions, the compounds were dissolved in benzene,

acetone, or alcohol at concentrations around 0.01 M. Optical cells varying from 2.5 cm. to 10 cm. in length were used for measuring the absorption spectra of these solutions.

For the measurements of the weak rare earth ion transitions of the chlorides, about two grams of the rare earth oxide were carefully weighed out in a 250 ml. beaker and converted to moist crystals of the rare earth chloride as described in Section 2.1.3. The chloride crystals were then dissolved in water, and the solution transferred quantitatively to a 50 ml. volumetric flask and diluted to the mark. The absorption spectra of the resultant solutions ($\sim$0.2 M concentrations) were investigated using quartz cells varying in length from 2.5 cm. to 10 cm.

Only the visible region of the absorption spectrum was investigated for these studies because the strong organic ligand absorption band completely masked out other weak rare earth ion transitions which are reported by Halleck and Hartinger (25) to lie in the near ultraviolet region of the spectrum. A typical absorption spectrum of a chelated rare earth ion is shown in Fig. 2.3.1. The spectrum consists of small sharp absorption peaks of the rare earth ion superimposed on the long wave length tail of the ligand absorption band. As only the rare earth ion absorption strengths were desired, the absorption curve of the ligand was interpolated beneath the ion absorption peaks, and the absorbance due to the ligand was subtracted from the total absorbance.

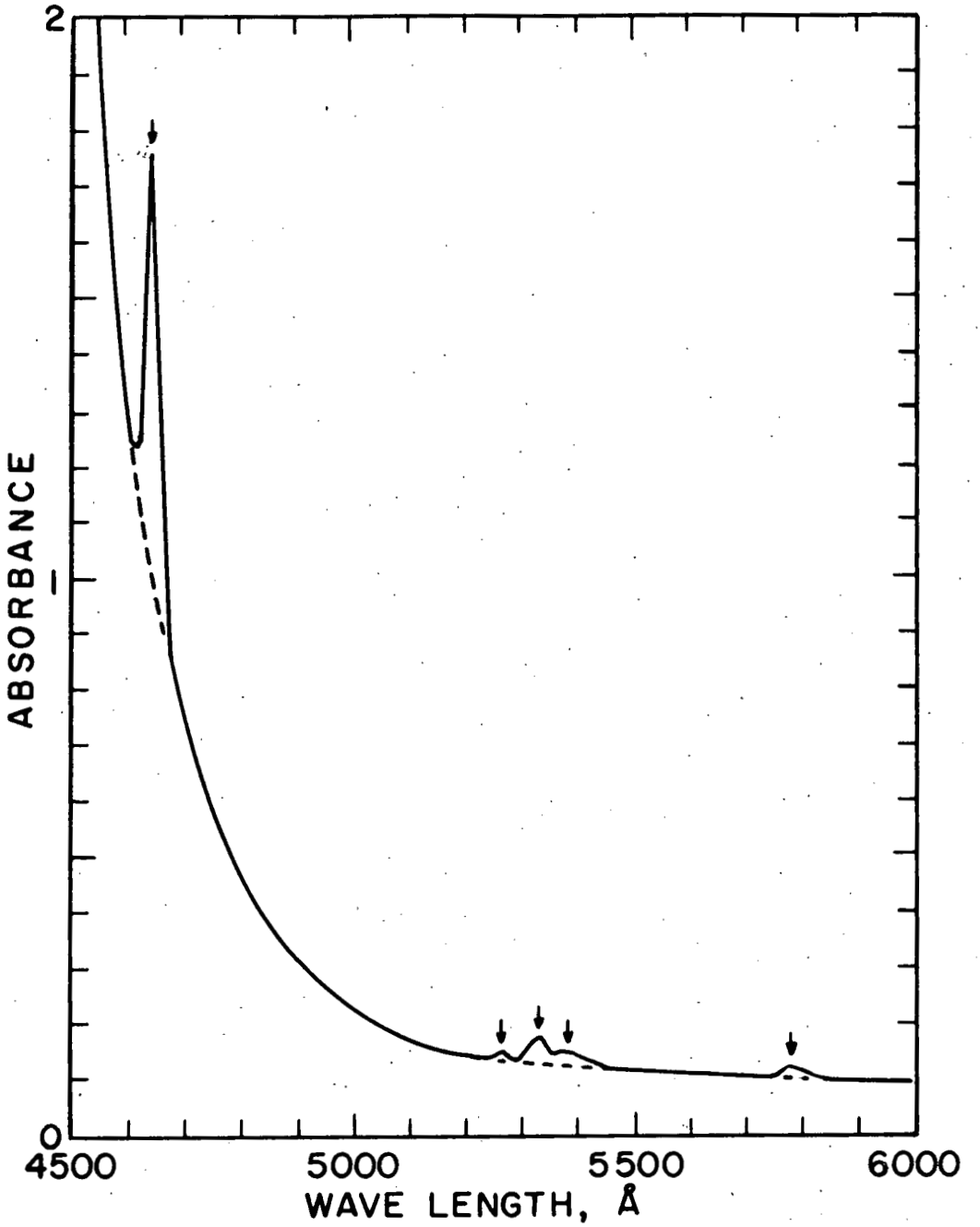

Fig. 2.3.1.--Absorption spectrum of 0.0122 M EuD_3 in benzene in a 10 cm. quartz cell.

↓ absorption peaks attributable to the europium ion

——— total absorption of the sample

------- interpolated absorption of the ligand

It is generally assumed (1) that the absorption strengths of the rare earth ions follow Beer's law. It was not possible to check whether the absorbances of the chelated rare earth ions also follow Beer's law since nearly saturated solutions had to be used to detect the weak absorption peaks of the ions. Due to the low intensities of the transitions observed and the method used in elimination of the absorbance of the ligand, calculated molar extinction coefficients of the rare earth ion absorption bands may be in error by as much as 10%. In some instances, the absorption intensities were so weak (less than 0.01 absorbance units) or the interpolated base line so curved that the calculated extinction coefficients may be in error by as much as 25%.

2.4. Measurements of Luminescence Spectra

2.4.1. Sample Preparation

For studying the luminescence properties of microcrystalline solids, the samples were mounted between two vicor glass plates. The following method was used in preparing the mounted samples. A thin gasket formed from double sided tape (Technical Tape Corp., Morris Heights, N.Y., 53, N.Y.) was placed around the perimeter of a 2 X 25 X 50 mm. vicor plate. (See Fig. 2.4.1.1.) The rare earth chelate powder or finely ground rare earth chloride was spread evenly on the face of the plate within the gasket. A second vicor plate was then pressed firmly down on the first plate. If sufficient pressure was applied, an airtight seal was formed between the tape

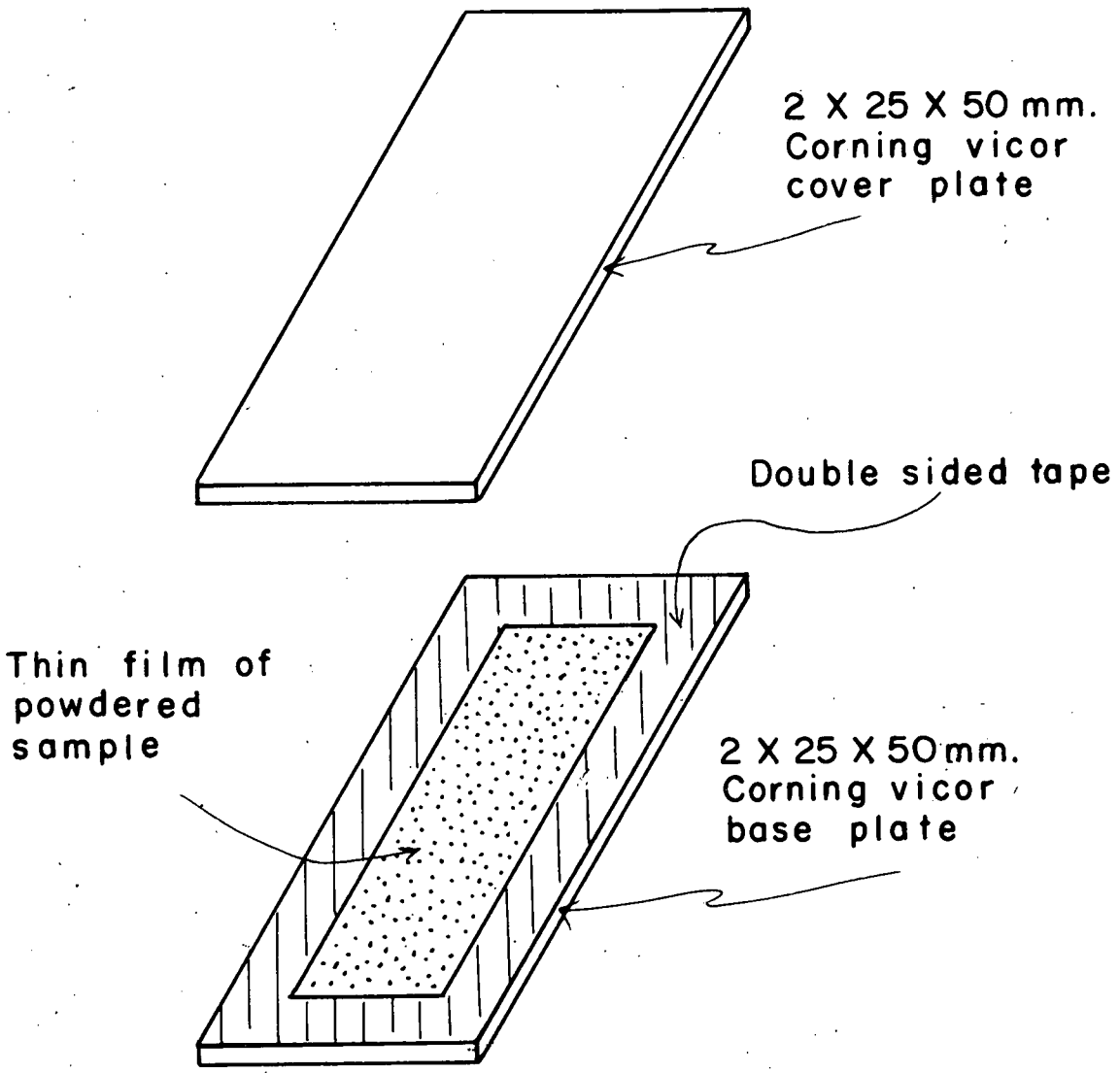

Fig. 2.4.1.1.--Preparation of microcrystalline powder samples for luminescence studies.

and the glass plates. The rare earth complex between the plates was pressed into a thin semitransparent layer when the glass plates were sealed together. Because the doublesided tape luminesces when exposed to ultraviolet light, the perimeter of the mounted sample was sprayed with flat black lacquer so that none of the tape was exposed either to the exciting light or to the instruments used to detect the sample luminescence. The mounted samples could be immersed directly into liquid nitrogen for low temperature studies.

For the investigations of the luminescence properties of the sodium metaphosphate glasses at room temperature, the glass beads were suspended in the path of the exciting light. For low temperature studies, the glass beads were immersed directly into the liquid nitrogen. Even though the glasses cracked upon immersion, the luminescence of the samples could still be readily recorded.

Rare earth chelates dissolved in rigid organic glasses at low temperatures were prepared as follows. Approximately one milligram of the chelate was accurately weighed and transferred to a 50 ml. volumetric flask. The sample was completely washed into the flask and dissolved in the desired combinations of organic solvents. After complete solution of the chelate was obtained, the solution was diluted with the appropriate organic solvents to the 50 ml. mark and thoroughly mixed. The solution was then transferred to a quartz sample tube which had a 2 cm. o. d. X 15 cm. body topped with a 1 cm. o. d. X 20 cm. neck. The top of the filled sample tube was sealed off with a rubber serum cap. Luminescence measurements

were made within two hours of the time at which solutions were prepared.

The following organic solvent combinations, all of which formed clear rigid glasses at low temperatures, were selected for this work:

(a) EMPA consisting of, by volume, two parts diethyl-ether, two parts 3-methylpentane, and one part absolute ethanol,

(b) EMP consisting of, by volume, one part diethyl-ether and one part 3-methylpentane,

(c) MP--pure 3-methylpentane.

The ethanol (U. S. Industrial Co., absolute, reagent quality) was distilled from magnesium ethoxide according to the method given by Fieser (26) before use. The diethylether (Mallinckrodt, anhydrous, analytical reagent grade) and the 3-methylpentane (Phillips Pure Grade, 99 mol % min.) were both distilled from sodium metal ribbon within the same day that the solvents were used for sample preparation.

2.4.2. Total Luminescence Measurements

Total luminescence spectra were recorded by observing the sample emission at right angles to the path of the exciting light. A diagram of the experimental arrangement for measuring the luminescence of samples at liquid nitrogen temperatures is shown in Fig. 2.4.2.1. A General Electric, 1000 W, pyrex jacketed, water cooled, high pressure, AH-6 mercury arc lamp was used as an ultraviolet light source for studying the

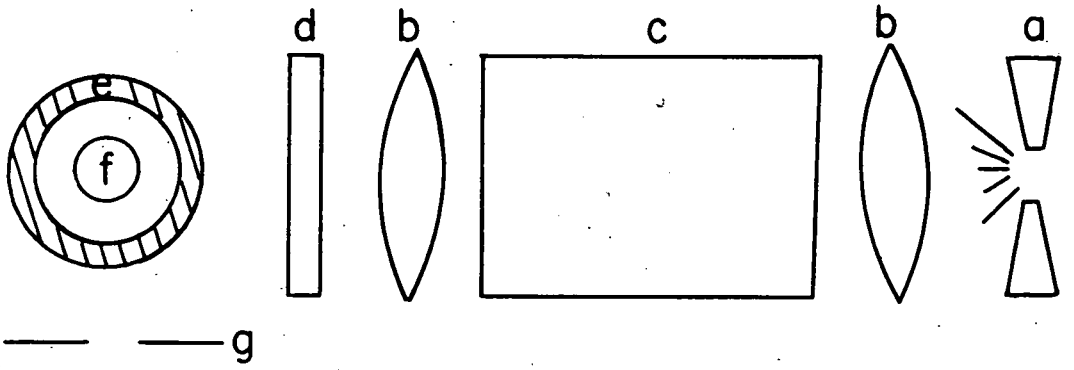

Fig. 2.4.2.1.--Arrangement of the equipment used for measuring total luminescence spectra of samples at 77°K.

a. GE AH-6 or Osram 500W mercury arc lamp

b. quartz condensing lenses

c. solution filter cell with quartz windows

d. Corning glass absorption filters

e. quartz dewar

f. sample

g. spectrograph slit

luminescence properties of all samples except the rare earth trisacetylacetonates. Because the first strong absorption band of the chelates derived from acetylacetone lies much further down in the ultraviolet region of the spectrum (2900 Å), an Osram, 500 W, quartz jacketed, air cooled, mercury arc lamp was used for an excitation source.

Glass absorption filters and solution filters were selected to absorb all light from the excitation source except light lying in selected narrow regions of the ultraviolet spectrum. (See Section 2.4.4. for details.) Quartz condensing lenses were used to focus the filtered ultraviolet light on the sample. For low temperature studies, the samples were placed in a quartz dewar filled with liquid nitrogen. The quartz dewar was only partially silvered. An unsilvered band, 5 cm. wide, was used for irradiation and observation of the sample. For room temperature studies the dewar was removed, and the sample was merely suspended in the path of the exciting light. The dewar, light filters, and condensing lenses were encased in a black lucite plastic box to prevent excess exciting light from entering the spectrograph.

2.4.3. Time Resolved Luminescence Measurements

For certain of the samples studied, it was desired to record only the spectra of the long-lived luminescence. A modified Becquerel phosphoroscope was used for this purpose. A diagram showing the arrangement of equipment used for measuring time resolved emission spectra of samples at low temperatures is given in Fig. 2.4.3.1. A complete description of the

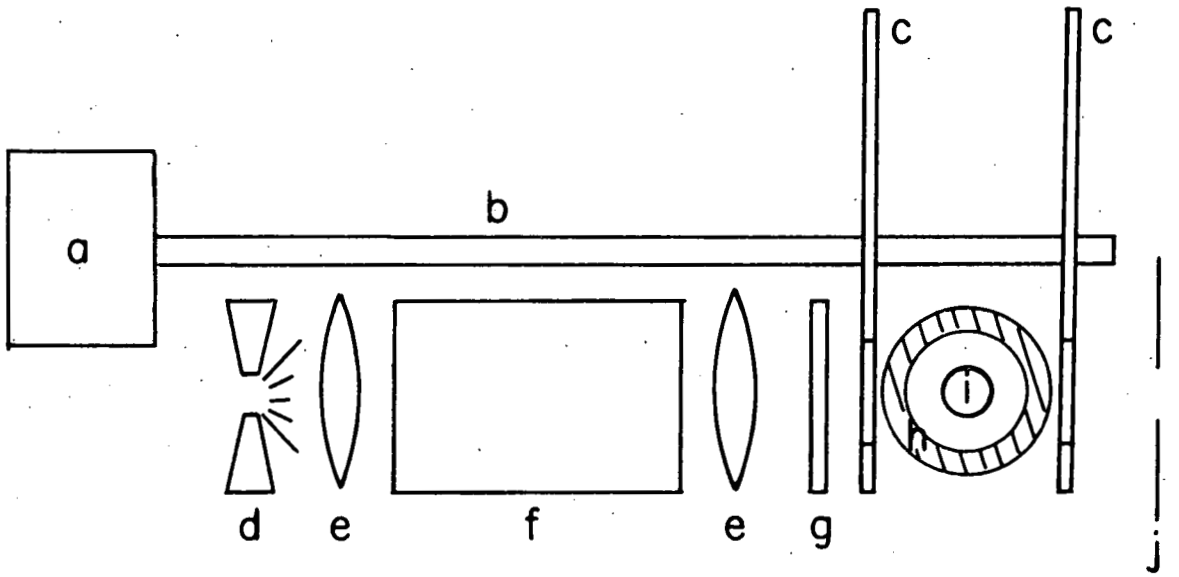

Fig. 2.4.3.1.--Arrangement of the equipment used for measuring long-lived luminescence spectra of samples at 77°K.

a. phosphoroscope motor

b. motor shaft

c. phosphoroscope blades

d. high pressure mercury lamp

e. quartz condensing lenses

f. solution filter cell with quartz windows

g. Corning glass absorption filters

h. quartz dewar

i. sample

j. spectrograph slit

construction and operation of the phosphoroscope is given by Whan (22). The instrument was operated with a resolution time of $\sim 10^{-4}$ sec.; that is, a time lapse of $\sim 10^{-4}$ sec. occurred between the moment one blade cut off the exciting light from the sample and the other blade opened to allow sample luminescence to reach the spectrograph. The light sources, light filters, and dewars used for these measurements were the same as those used for total luminescence measurements.

The construction of the phosphoroscope was such that the sample emission which reached the spectrograph came from the side of the sample opposite to the surface being irradiated with the ultraviolet light. This presented no problems with the organic and metaphosphate glasses since these samples were perfectly transparent. Powder samples proved to be a problem because the layer of powder in the mounted sample was nearly opaque. The long-lived emission spectra of these samples were obtained by making the powder layer between the vicor plates thin enough for the sample emission to pass through the semitransparent layer and be recorded through the spectrograph.

2.4.4. Light Filter Combinations

The light from the mercury arc source was filtered so that light from only narrow regions of the ultraviolet spectrum reached the sample. The light filter systems consisted of combinations of Corning, two inch square, polished, ultraviolet transmitting filters and aqueous solutions which were contained

in a brass cell 5 cm. in diameter by 5 cm. long fitted with quartz plates at the ends. For studying emissions of rare earth chelates, filter combinations were chosen such that only ultraviolet light corresponding to the first strong absorption band of the chelate reached the sample. For inorganic salts or metaphosphate glasses, the filter combinations allowed ultraviolet light, corresponding to the near ultraviolet absorption bands of the ion, to reach the sample.

As the Corning ultraviolet transmitting filters also transmit radiation in the red end of the spectrum beyond 7000 Å, it was necessary to use aqueous solutions of inorganic salts to filter out the red light from the mercury arc. Filter combinations were selected with the aid of the transmission data on Corning glass filters presented by Corning Glass Works (27), and transmission data on solution filters published by Kasha (28). The light filter combinations selected for use in this work are listed in Table 2.4.4.1, and their transmission characteristics are given in Fig. 2.4.4.1.

2.4.5. Recording the Luminescence Spectra

All luminescence spectra were photographed using a Steinheil Universal GH prism spectrograph. With the exception of one compound ($GdA_3 \cdot H_2O$) all the spectra were recorded with the instrument set at f/8 optics with a dispersion of 17 Å/mm. at 5000 Å. The instrument was adjusted so that the spectrum between 4500 and 7500 Å was recorded on the photographic plate. For investigating the luminescence properties of the gadolinium trisacetylacetonate complex, the spectrograph was set at f/3.5

TABLE 2.4.4.1.

ULTRAVIOLET TRANSMITTING LIGHT FILTER COMBINATIONS

Class of Compounds Studied	Wave Length of Light Desired, Å	Filter Combinations Used
$MA_3 \cdot H_2O$	2900	Corning #7-54[a] + $NiSO_4$[b]
$MB_3 \cdot 2H_2O$	3200	Corning #7-54 + $CuSO_4$[c]
MCl_3, MPO_4 MD_3	3600	Corning #7-60 + $CuSO_4$

(a)Corning catalog number for two inch square, polished glass filters.

(b)Aqueous solution of nickel sulfate (5 cm. path, 100 gm. of $NiSO_4 \cdot 6H_2O$ per liter of solution).

(c)Aqueous solution of cupric sulfate (5 cm. path, 100 gm. of $CuSO_4 \cdot 5H_2O$ per liter of solution).

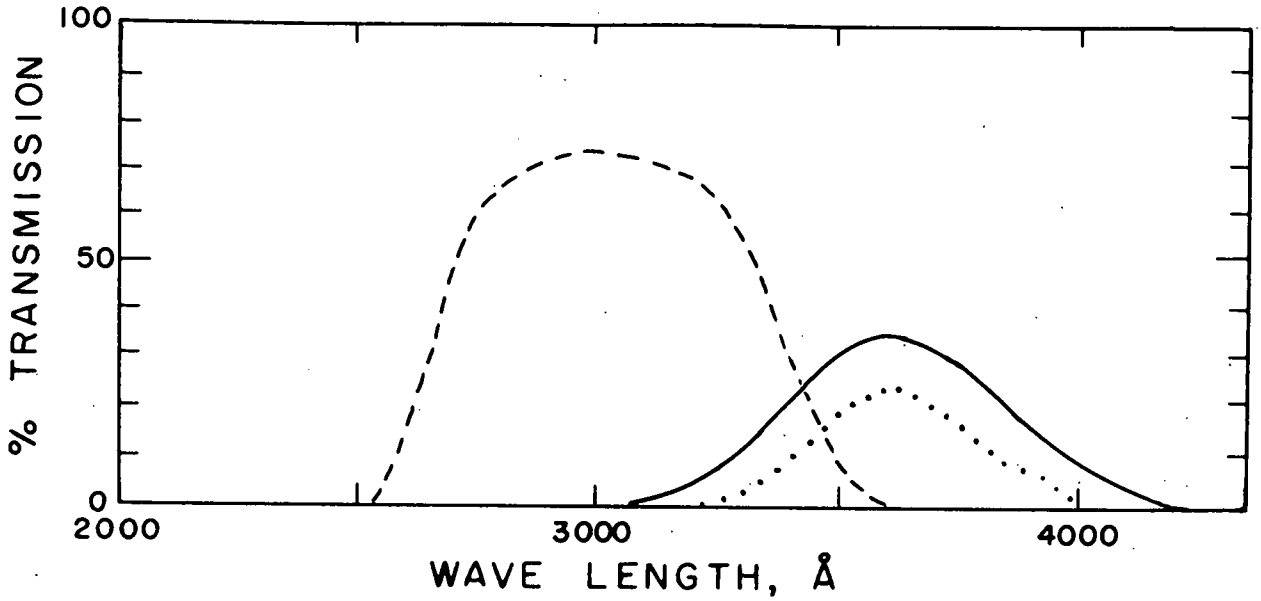

Fig. 2.4.4.1.--Transmission characteristics of ultraviolet transmitting light filter combinations.

– – – – – $NiSO_4$ solution plus Corning #7-54 filter

——— $CuSO_4$ solution plus Corning #7-54 filter

····· $CuSO_4$ solution plus Corning #7-60 filter

optics with a dispersion of approximately 40 Å/mm. at 5000 Å. In this case the instrument was adjusted so that the spectrum between 3800 and 5600 Å was recorded. All spectra were recorded on Kodak 103a-F spectrographic plates. Densitometer traces of the spectra were obtained from the photographic plates with a Jarrell-Ash automatic recording microphotometer.

For a study of the linelike emission spectrum characteristic of a complexed rare earth ion, it was of interest to know the detailed structure of both the strong lines and the weak lines of the spectrum. Because such information cannot be obtained from one exposure of the photographic plate, three to five separate exposures were made of the sample emission with the exposure times varying by a factor of four from one exposure to the next. Superimposed on each exposure was the calibration spectrum obtained from an argon gas discharge tube. Details of the determination of the wave lengths of the sample emission lines are given in Appendix 5.1. A typical photographic plate is shown in Fig. 2.4.5.1. As can be seen in the figure, the structure of the strongest lines is clearly discernible in the $\frac{1}{4}$ min. exposure, while the structure of the weak lines around 5300 Å is discernible in the 60 min. exposure. In Table 2.4.5.1. are listed some of the spectrograph slit widths and exposure times used for recording the emission spectra of the complexed rare earth ions.

2.4.6. Stability of Rare Earth Chelates to Prolonged Exposures to Ultraviolet Light

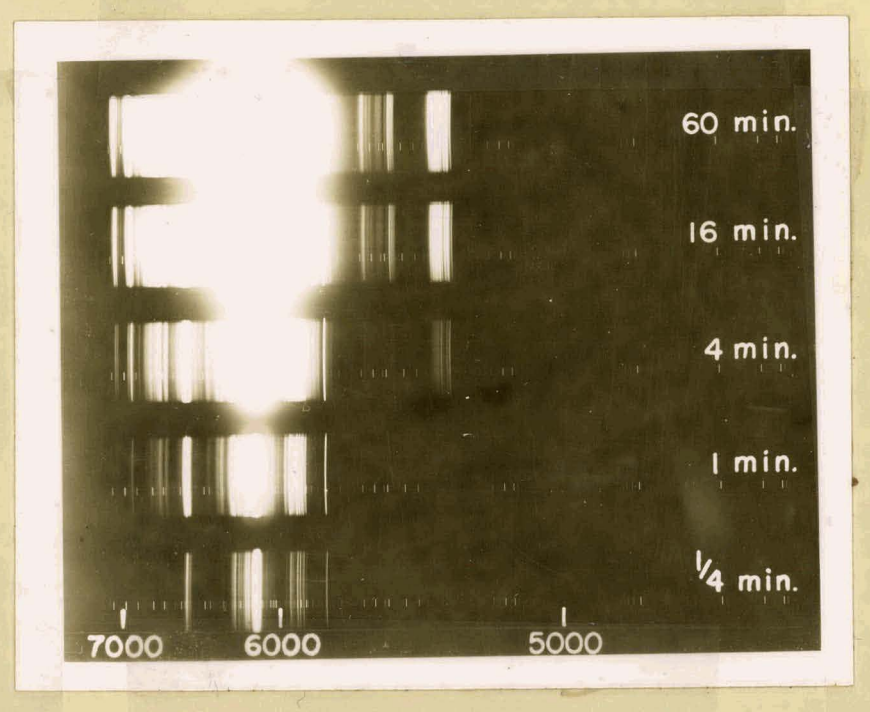

Fig. 2.4.5.1. Positive reproduction of a photographic plate displaying the emission spectrum of $EuD_3 \cdot DH$ solid at 77°K. (The spectra were obtained with a Steinheil Universal GH spectrograph set at f/8 optics yielding a dispersion of 17 Å/ mm at 5000 Å. A 50 micron slit width was used for recording the spectra on a Kodak 103a-F spectrographic plate. Exposure times are indicated to the right of each spectrum.)

TABLE 2.4.5.1.

TYPICAL SPECTROGRAPH SLIT WIDTHS AND EXPOSURE TIMES USED TO RECORD THE LUMINESCENCE SPECTRA OF COMPLEXED RARE EARTH IONS

Compound	Medium	Slit Width, Microns	Exposure Time, Minutes
$SmB_3 \cdot 2H_2O$	EMPA Glass at 77°K	20	4, 16, 60
$EuB_3 \cdot 2H_2O$	"	20	$\frac{1}{4}$, 1, 4, 16, 60
$TbB_3 \cdot 2H_2O$	"	20	1, 4, 16, 60
$DyB_3 \cdot 2H_2O$	"	20	1, 4, 16, 60
$SmB_3 \cdot 2H_2O$	Powder at 77°K	80	4, 16, 60
$EuB_3 \cdot 2H_2O$	"	40	$\frac{1}{4}$, 1, 4, 16, 60
$TbB_3 \cdot 2H_2O$	"	40	$\frac{1}{4}$, 1, 4, 16, 60
$DyB_3 \cdot 2H_2O$	"	40	4, 16, 60
$SmCl_3 \cdot 6H_2O$	Powder at 298°K	100	1, 4, 16, 60
$EuCl_3 \cdot 6H_2O$	"	50	$\frac{1}{4}$, 1, 4, 16, 60
$TbCl_3 \cdot 6H_2O$	"	50	$\frac{1}{4}$, 1, 4, 16, 60
$DyCl_3 \cdot 6H_2O$	"	100	1, 4, 16, 60
$SmPO_4$	$NaPO_3$ glass at 298°K	40	1, 4, 16, 60
$EuPO_4$	"	40	1, 4, 16, 60
$TbPO_4$	"	40	1, 4, 16, 60
$DyPO_4$	"	40	1, 4, 16, 60

An experiment, designed to test the stability of rare earth chelates in EMPA glasses at 77°X, was conducted in the following manner. Two samples of EuD_3 in EMPA ($\sim$1 mg./50 ml.) were prepared and placed in quartz sample tubes. One of the samples, immersed in liquid nitrogen, was continuously irradiated with filtered ultraviolet light for eight hours. The light filters used were the same as those in Table 2.4.4.1. selected for irradiation of MD_3 complexes. The luminescence spectrum of this sample was recorded at one hour intervals using a 2 min. exposure with a 40 micron slit width. The other sample was stored in liquid nitrogen and irradiated with ultraviolet light only for the short intervals necessary to record the emission spectrum. The emission spectrum of this sample was recorded once every two hours. The luminescence spectra of both these samples were recorded on the same photographic plate.

A visual inspection of the spectra obtained from the two EuD_3 samples indicated that there were no changes in the line positions or relative intensities regardless of the length of exposure to the ultraviolet radiation. No other tests were made on the stability of the chelates dissolved in organic glasses. It was noticed, however, that in the case of TbD_3 dissolved in an EMP glass a progressive and striking change occurred in the color of the emitted light. Within the first few minutes of exposure to ultraviolet radiation, the emission from the EMP glass turned from a weak, pale yellow-green to a slightly stronger, deep green. The phenomenon was confined to the small region of the rigid organic

glass under irradiation. This change in emission characteristics was attributed not to any large amounts of photodissociation, but rather to a minor amount of photodissociation of the sample which caused small shifts in the energies of nearly coincidental electronic states of this chelate. This phenomenon will be discussed in more detail in Section 3.3.2.6.

2.4.7. Effects of Concentration on the Emission Spectra of the Rare Earth Oxide-Sodium Metaphosphate Glasses

Sodium metaphosphate glasses containing 0.1, 1.0, and 10% by weight europium oxide or terbium oxide were prepared, and the emission spectra of the glasses were taken with the samples at room temperature. The emission spectra of the 0.1 % and 1.0 % oxide samples were identical, as far as structure and relative line intensities, with the emission spectra of the glasses containing 2% oxide. The spectra of the glasses containing 10% by weight rare earth oxide were almost the same as the glasses of lower compositions except that very sharp but weak lines characteristic of rare earth ions in inorganic crystals were superimposed upon the more diffuse line emission characteristic of the rare earth ions in the metaphosphate glasses at low concentrations. The sharp line emission probably arises from emission by the white, opaque, undissolved rare earth phosphate embedded in the clear glass.

2.5. Measurement of the Decay of Rare Earth Ion Luminescence

2.5.1. The Apparatus

The luminescence decays of the complexed rare earth ions were measured by flashing the sample with a short-lived, ultraviolet flash lamp, and by monitoring the luminescence intensity with a photomultiplier. A block diagram of the apparatus constructed for this purpose is shown in Fig. 2.5.1.1. Complete details describing the construction and operation of the apparatus are given in Appendix 5.2. An Edgerton, Germeshausen, and Grier FX-12 xenon lamp operating at one joule per discharge (0.08μF at 5000 V) was used for the flash source. Spontaneous discharge of the lamp was prevented by the use of a triggered spark gap which consisted of essentially two steel poles separated to such a distance that spontaneous discharge across the poles occurred at voltages slightly higher than the operating voltage of the lamp. Discharge of the storage capacitors across the spark gap and through the flash lamp was accomplished by momentarily ionizing the air between the steel poles with a spark from the thyratron spark source. With this apparatus, a flash with a mean lifetime of two microseconds could be obtained.

The sample emission was monitored with a RCA-2020 photomultiplier tube. (For studying the red emission of chelated Sm^{3+} a RCA-7102 photomultiplier was employed.) The phototubes, operated at a total potential of 1080 volts with an $\sim$10 KΩ anode to ground load resistance, had a response time of less than one microsecond. The photomultiplier signal was displayed on a Tektronix Model 535 oscilloscope on which the horizontal sweep trigger was adjusted so that a single sweep was initiated when the lamp was flashed. Time mark

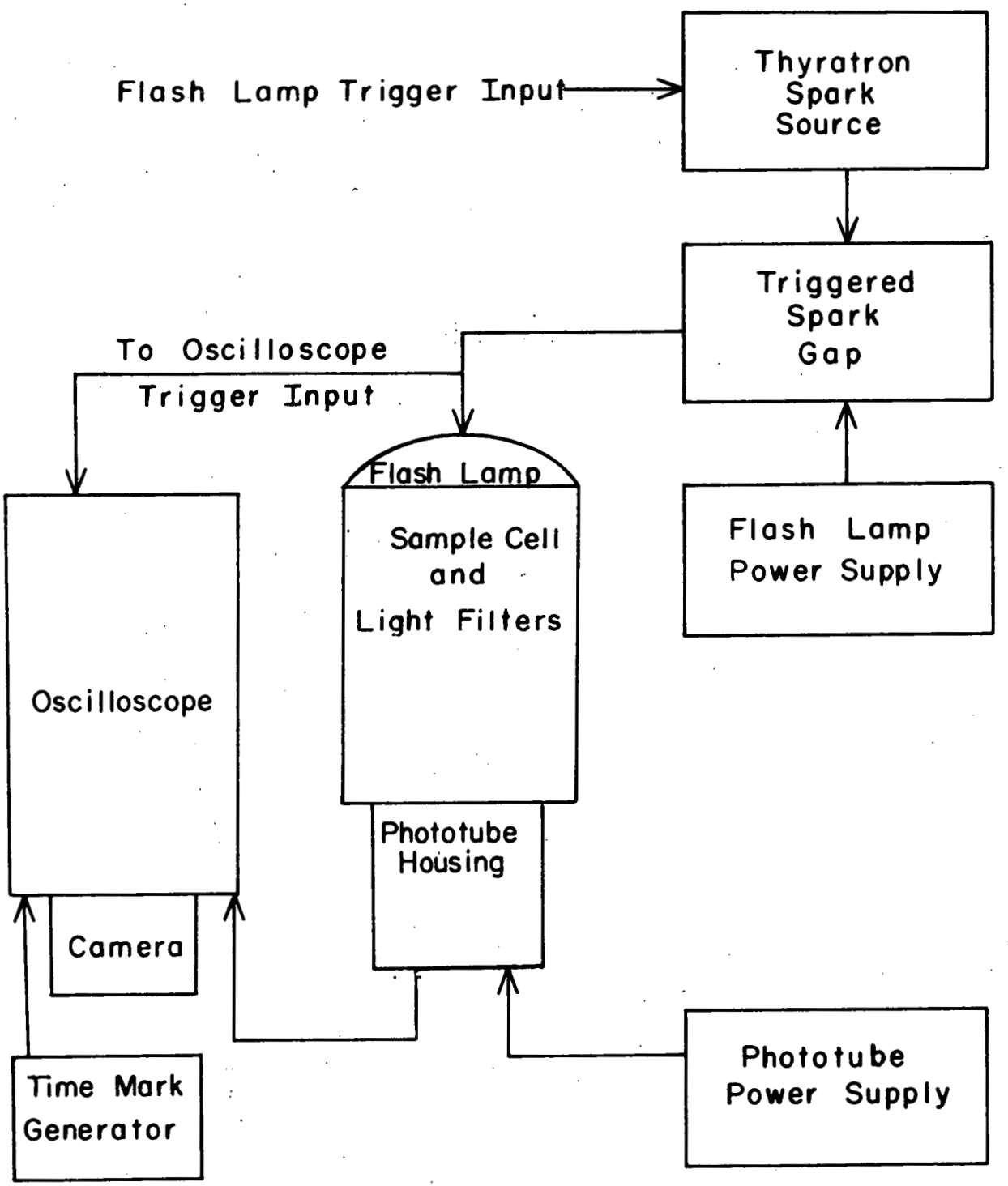

Fig. 2.5.1.1.--Block diagram of the apparatus used to measure luminescence decay times.

signals from a Tektronix Model 180 time mark generator were used as a standard for measuring the horizontal time scale of the oscilloscope. A Polaroid Land camera equipped with Polaroid 3000 speed film was employed to photograph the oscilloscope traces.

2.5.2. Preparation of Samples

The same microcrystalline powder samples and metaphosphate glass samples used for studies of the emission spectra were also employed when measuring the luminescence decays. The rigid organic glass samples were prepared in the same manner as those used for the emission spectra studies. For low temperature investigations, the samples were immersed in liquid nitrogen in the same quartz dewar that was used when photographing the luminescence spectra.

2.5.3. Light Filter Combinations

The light from the flash lamp was filtered through the same light filter combinations used in the luminescence spectra studies (See Table 2.4.4.1.). Two different methods were used to filter the sample emission so that light from only a selected narrow region of the spectrum reached the photomultiplier. One method was to interpose Corning glass cut-off filters, a solution filter, and an interference filter between the sample and the photomultiplier. The solution filter ($\sim 10^{-3}$ M dibenzoylmethane in absolute alcohol) and the cut-off filters absorbed all the ultraviolet light from the flash lamp, while various Balzar narrow band interference filters

($\sim$100 Å half width) were used to pass light from narrow regions of the visible spectrum. An iris diaphragm was employed to adjust the intensity of light falling on the photomultiplier.

The other method of filtering the sample emission was to place a Bausch & Lomb Monochromator (250 mm. focal length, 66 Å/mm. dispersion) between the sample and the detector. The monochromator was adjusted so that only sample emission from the desired region of the visible spectrum reached the photomultiplier. The intensity of light falling on the photomultiplier was adjusted by opening or closing the slits of the monochromator.

The regions of the visible spectrum selected, when monitoring the luminescence decay of the samples, are indicated on the illustrations of the emission spectra of each of the samples. These spectra are presented in the Discussion section (Section 3.).

2.5.4. Method of Recording and Measuring the Luminescence Decays

The proper combinations of light filters were mounted in the apparatus and the sample was centered in the sample compartment so that maximum illumination by the flash was obtained. The intensity of sample emission reaching the phototube, the vertical sensitivity of the oscilloscope, and the horizontal sweep speed of the oscilloscope were all adjusted so that the initial rise, the peak intensity, and the first two or three half-lives of the luminescence decay were displayed

on the oscilloscope screen. This oscillographic trace plus the base line trace and the time mark signals were all recorded by the camera on the same photograph. A typical photograph is given in Fig. 2.5.4.1.

For certain samples the first six to nine half-lives of the luminescence decay were recorded by utilizing both time bases of the Tektronix Model 535 oscilloscope. After ascertaining the approximate half life of the luminescence decay, the time base "B" of the oscilloscope was adjusted so that approximately ten half-lives were displayed on a single sweep. Using time base "A" in the Main Sweep Delayed mode and making proper adjustments of the vertical sensitivity of the preamplifier, the first three half-lives could be recorded on one photograph, the second three on another photograph, and so on, until the desired number of half-lives had been recorded or until the intensity of the sample emission became too weak to detect on time base "A.

The relative intensity of sample luminescence was taken as the vertical distance on the photograph between the luminescence decay curve and the base line. A pair of dividers and a millimeter scale were used to make the measurements. The data (using at least eight points from each photograph) were plotted on semilogarithmic paper for interpretive purposes. The statistical methods used in determining the mean life times from the decay curves are given in Appendix 5.3.

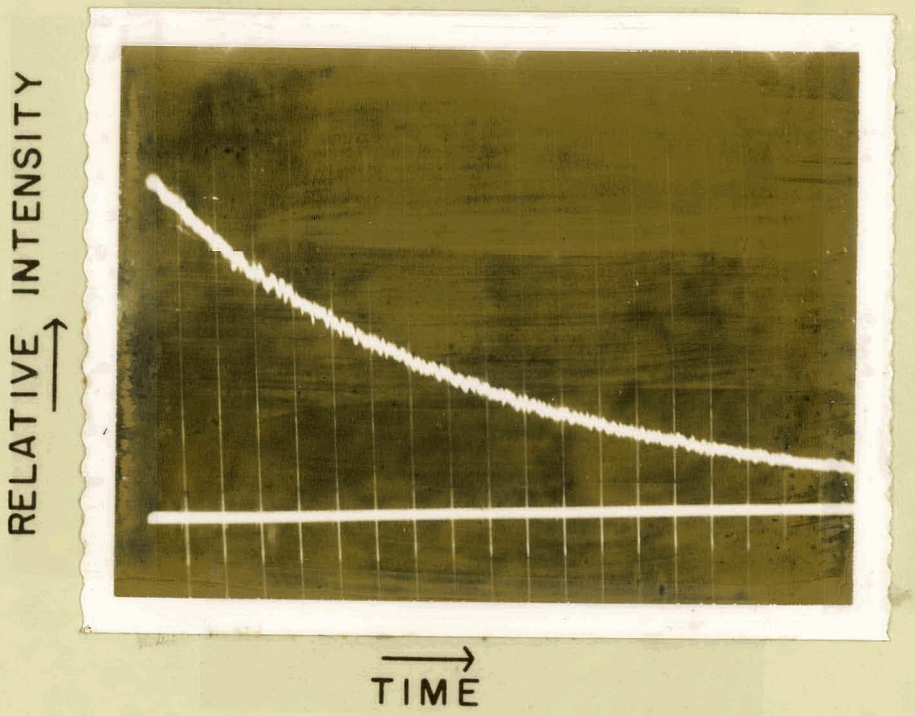

Fig. 2.5.4.1.--Luminescence decay of the 5400 Å lines of $TbA_3 \cdot H_2O$ in EMPA at 77°K.

| | | 100 microsecond time mark signals

luminescence intensity

——— base line

(The sample was excited with an Edgerton, Germesheusen, and Grier FX-12 flash lamp operating at one joule per discharge. The sample emission, filtered through a B & L monochromator (250 mm. focal length) set at 5400 Å with 2 mm. slit widths, was detected with a RCA-2020 photomultiplier operating at a 1080 V anode to cathode potential with a 10 KΩ load resistance. The photomultiplier signal was displayed on a Tektronix Model 535 oscilloscope employing a 50 millivolt per centimeter vertical sensitivity.)

2.5.5. Effects of Concentration on the Luminescence Decays of Rare Earth Oxide-Sodium Metaphosphate Glasses

Rare earth oxide-sodium metaphosphate glasses containing 0.1, 1.0, and 10% by weight europium oxide or terbium oxide used for the emission spectra studies reported in Section 2.4.7. were also used to determine the concentration effect on the luminescence decay times. The luminescence decay curves of all of the samples are shown in Fig. 5.5.1.3. and Fig. 5.5.1.4. The luminescence decay times measured from these curves were compared with the luminescence decay times of the glasses containing 2 % by weight rare earth oxide. In the case of the terbium oxide glasses, the luminescence decay times of the 0.1, 1.0, and 10% glasses were within 2 % of the luminescence decay time of the terbium glass containing 2 % by weight terbium oxide. In the case of the europium glasses, the luminescence decay times of the 0.1 % and 1.0 % glasses were within 2 % of the luminescence decay time of the sample containing 2 % by weight europium oxide. The luminescence decay time of the 10 % glass was significantly shorter than those of the glasses of lower composition.

Because the glasses containing 10 % by weight rare earth oxide were opaque, shattered easily, and appeared to contain two different rare earth species, they were discarded. Although the luminescence properties of the glasses containing 0.1, 1.0, and 2.0 % by weight rare earth oxide appeared to be identical, the glasses containing 2 % by weight rare earth oxide were chosen for detailed luminescence studies because of

the higher intensities of light emitted from these samples.

3. Discussion

3.1. Rate of Intramolecular Energy Transfer in Rare Earth Chelates

3.1.1. Luminescence Properties of Rare Earth Chelates

The probable structure of the chelates used in these studies is shown in Fig. 3.1.1.1. The octahedral or near octahedral arrangement of oxygen atoms around the central metal ion is exhibited by β-diketone chelates derived from acetylacetone and substituted acetylacetones. Luminescence is observed from these complexes when the compounds, dissolved to low concentrations in organic glasses at low temperature, are irradiated with near ultraviolet light corresponding to the first strong absorption band of the complexes.

The spectra consist of varying amounts of broad band molecular emission characteristic of the organic portion of the complex and sharp line emission characteristic of the chelated rare earth ion. By means of careful measurements of the molecular emissions plus observations upon the appearance or nonappearance of the rare earth ion emission, Crosby, Whan, and Alire (18) were able to determine the path of intramolecular energy transfer in rare earth chelates.

The energy transfer and luminescence mechanisms are indicated schematically in the energy level diagram shown in

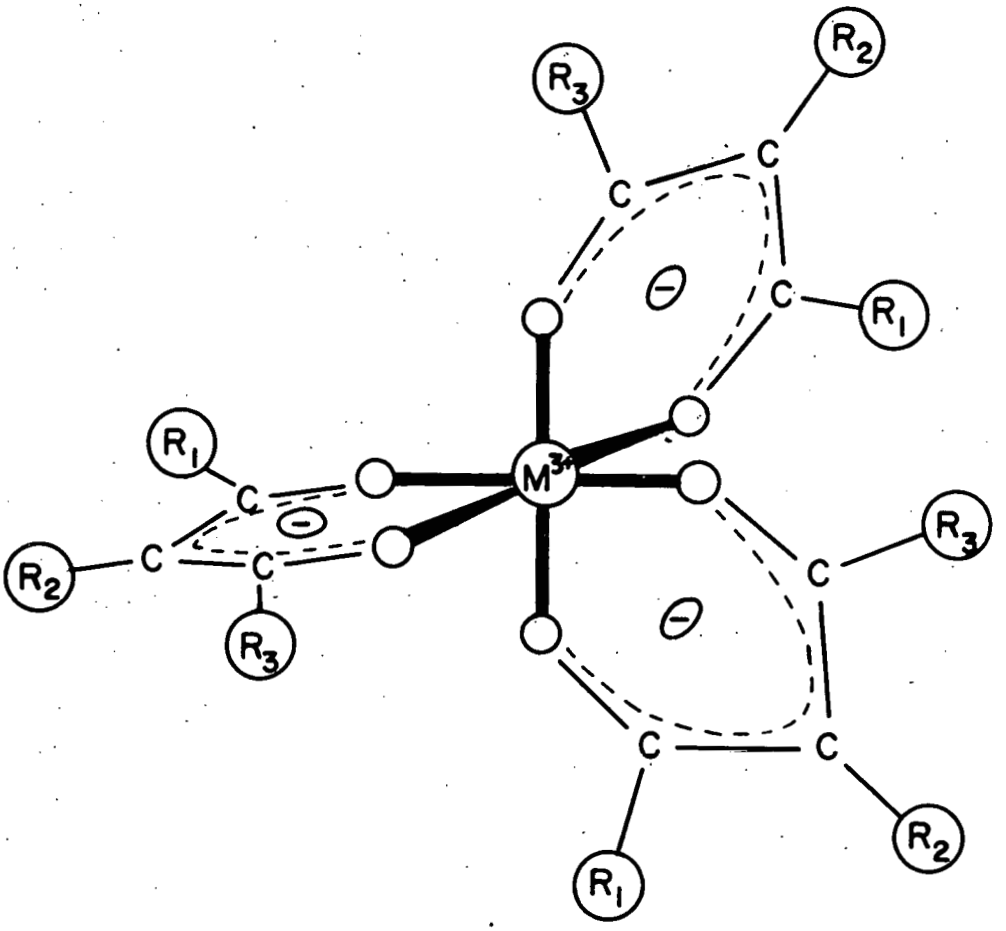

Fig. 3.1.1.1.--Probable structure of β-diketone chelates of trivalent rare earth ions.

For trisacetylacetonate chelates, $R_1 = R_3 = CH_3-$, and $R_2 = H$.

For trisbenzoylacetonate chelates, $R_1 = CH_3-$, $R_2 = H$, and $R_3 =$ 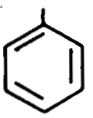 .

For trisdibenzoylmethide chelates, $R_2 = H$, $R_1 = R_3 =$ 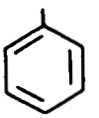 .

For tristribenzoylacetonate chelates, $R_1 = R_2 = R_3 =$

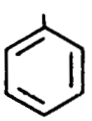 .

Fig. 3.1.1.2. Absorption by the complex of the near ultraviolet light excites the molecule to the first excited singlet state, S_1. The molecule may either lose its electronic energy *via* radiative combinations with the ground state ($S_1 \rightarrow S_0$), giving rise to molecular fluorescence, or it may undergo intersystem crossing ($S_1 \rightarrow T_1$) to the less energetic triplet state. Spin-forbidden radiative combinations of the triplet state with the ground state ($T_1 \rightarrow S_0$) result in long-lived molecular phosphorescence. The excited molecule may, on the other hand, undergo a nonradiative transition from the triplet state T_1 to the low-lying electronic levels of the chelated rare earth ion. These latter electronic levels arise from interactions among the 4f electrons of the trivalent rare earth ion.

Linelike emission characteristic of the complexed rare earth ion arises only when a resonance (emitting) level of the ion (such as R_1 in the diagram) lies at an energy which is equivalent to or less than the energy of the lowest triplet level, T_1. This emission arises from intramolecular energy transfer from the triplet state (T_1) to the resonance level (R_1) followed by radiative combinations of the resonance level with the lower lying ion levels. The transfer of energy from the first excited singlet state (S_1) to some lower lying resonance levels of the ion such as R_1 or R_2, although energetically possible, was not found to be operative in the populating of the electronic states of the chelated rare earth ion.

During the investigations of the phosphorescence spectra of the rare earth chelates, Whan (22) noticed that the rare

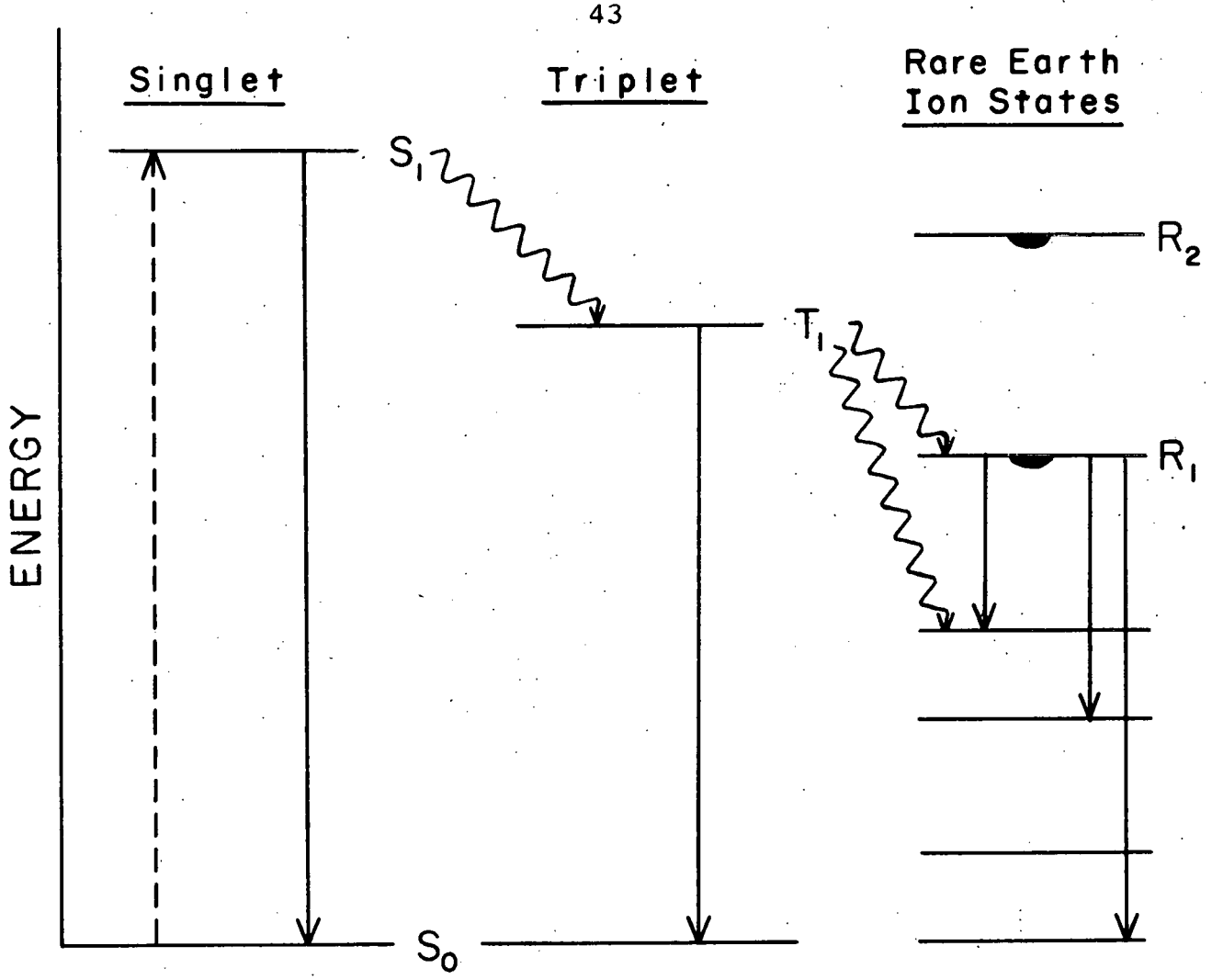

Fig. 3.1.1.2.--Energy level diagram for rare earth chelates.

- – – → transitions via absorption of radiation
- ——→ transitions via emission of radiation
- ∿∿∿→ radiationless transitions
- ——● denotes resonance level of the rare earth ion

earth ion emissions of the europium and terbium chelates could be readily recorded with the phosphorescence spectrum of the complexes through a phosphoroscope, while the linelike emissions characteristic of the samarium and dysprosium ions were never recorded in the phosphorescence spectra. As the resolution time of the phosphoroscope was 100 microseconds, it was concluded that the decay times of the samarium and dysprosium ion emissions were much less than 100 microseconds, while the decay times of the europium and terbium ion emissions were greater than 100 microseconds. Because the spectroscopic investigations gave no quantitative measure of the rate of intramolecular energy transfer, it was not known whether these variations in ion luminescence decay times were due to a slow, variable, rate determining intramolecular energy transfer step followed by very fast radiative decay of the ion, or a very fast intramolecular energy transfer step followed by slow, variable radiative decay of the ion.

In order to measure the rate of intramolecular energy transfer in rare earth chelates, this study of the luminescence exhibited by the chelated rare earth ions was undertaken. The experimental program consisted of detailed investigations of both the luminescence spectra and the luminescence decay times of the complexed rare earth ions.

3.1.2. Emission Spectra of Chelated Rare Earth Ions in Organic Glasses

Compounds selected for this study were chelates of trivalent terbium, europium, samarium, and dysprosium derived

from dibenzoylmethane, benzoylacetone, or acetylacetone. These chelates, with the exception of DyD_3, yield linelike emission characteristic of the complexed rare earth ion. Crosby, Whan, and Alire (18) showed that except for the DyD_3 chelate, the triplet levels of the benzoylacetonate and dibenzoylmethide complexes are of sufficient energy to populate the resonance levels of the rare earth ions via intramolecular energy transfer.

In order to be assured that the resonance levels of the rare earth ions in the acetylacetonate chelates would also be populated primarily through an intramolecular energy transfer process, a measure of the singlet state and triplet state energies of these complexes was needed. These data were obtained from the absorption and emission spectra of the $GdA_3 \cdot H_2O$ complex. The spectra of this compound are shown in Fig. 3.1.2.1. The complex exhibits a strong absorption maximum at approximately 35,000 $cm.^{-1}$ and negligible absorption below 30,000 $cm.^{-1}$. The first excited singlet state of the complex is therefore placed somewhere between 30,000 $cm.^{-1}$ and 35,000 $cm.^{-1}$. No detectable differences could be found between the total emission spectrum and the phosphorescence spectrum of this compound. This indicates that the molecular emission consists almost entirely of long-lived phosphorescence. The position of the first excited triplet state is taken as the energy of the first detectable emission peak on the high energy side of the phosphorescence band. This peak lies at approximately 25,100 $cm.^{-1}$. The first excited triplet level of the acetylacetonate

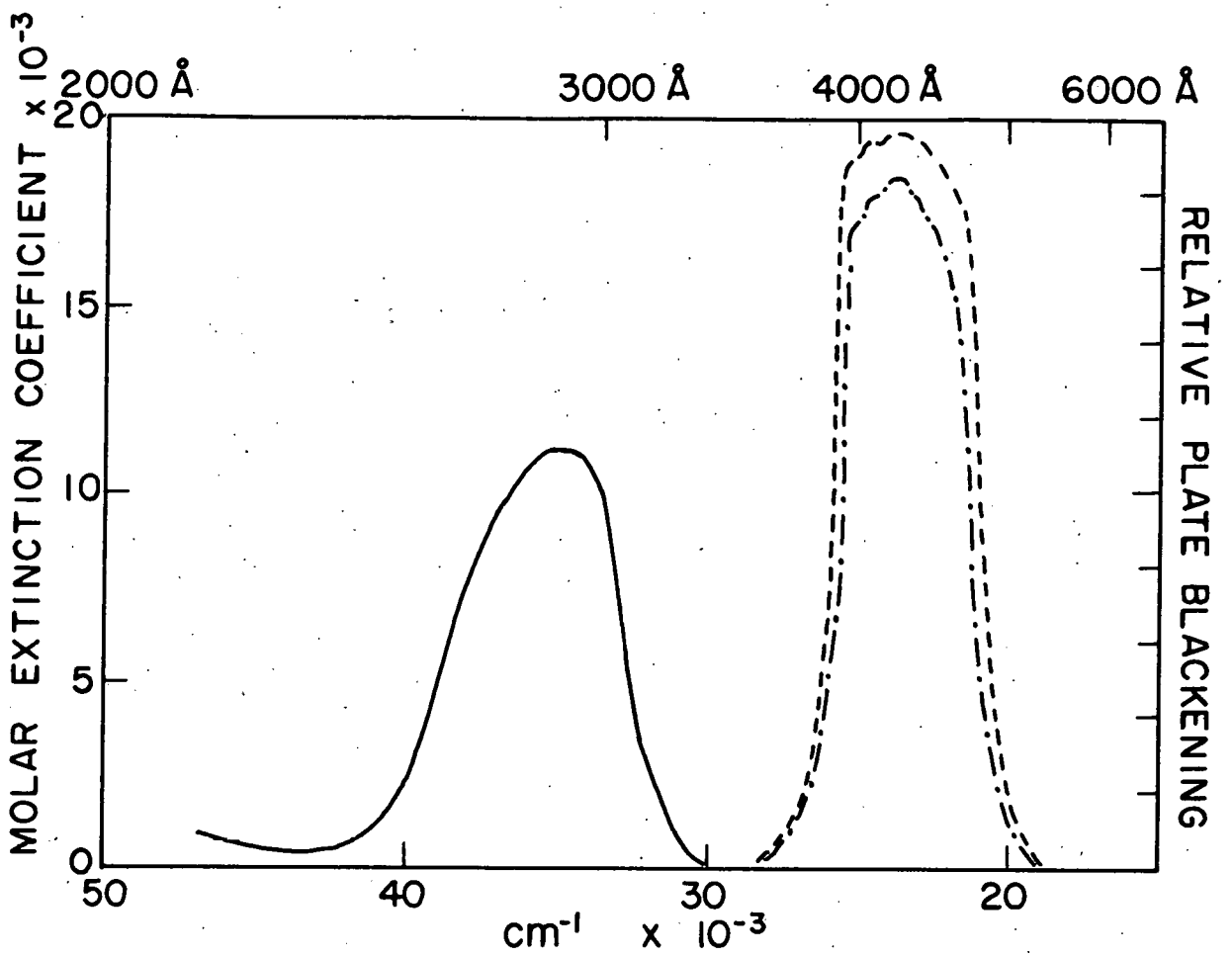

Fig. 3.1.2.1.--Emission and absorption spectra of $GdA_3 \cdot H_2O$.

——— absorption spectrum of $GdA_3 \cdot H_2O$ in absolute alcohol at room temperature in terms of molar extinction coefficient per mole of ligand

– – – – – total emission spectrum of $GdA_3 \cdot H_2O$ in an EMPA glass at 77°K in units of relative plate blackening

–·–·–·– phosphorescence emission spectrum of $GdA_3 \cdot H_2O$ in an EMPA glass at 77°K in units of relative plate blackening

complexes is therefore placed at or slightly higher than an energy of 25,100 $cm.^{-1}$--sufficiently energetic to populate, via intramolecular energy transfer, the resonance levels of all four of the above mentioned rare earth ions.*

An energy level diagram of all the β-diketone chelate systems studied is presented in Fig. 3.1.2.2. The positions of the triplet levels of the complexes plus the energies of the low-lying electronic states of the rare earth ions are presented. The triplet levels of the benzoylacetonate and dibenzoylmethide chelates are taken from the paper by Crosby, Whan, and Alire (18), while the energies of the rare earth ion states are those reported by Dieke (4) for the ions in the crystalline anhydrous chlorides. The rare earth ion levels are labeled according to the quantum number designations of the parent atomic states.

Densitometer traces of the emission spectra observed from the chelates in EMPA glasses at $77^{o}K$ are presented in Fig. 3.1.2.3. and Fig. 3.1.2.4. From the linelike structure of the emission, it is evident that the spectra arise from radiative transitions between electronic states derived from 4f electrons. Line emission characteristic of the rare earth ion was also observed in the emission spectra of the $SmA_3 \cdot H_2O$ and $DyA_3 \cdot H_2O$

---

*Crosby, Whan, and Alire (18) showed that the lowest triplet levels of different rare earth ions complexed with the same ligand lie in approximately the same energy. The energy of the triplet level of the gadolinium trisacetylacetonate complex is thus taken as the energy of the lowest triplet level of all the rare earth trisacetylacetonates.

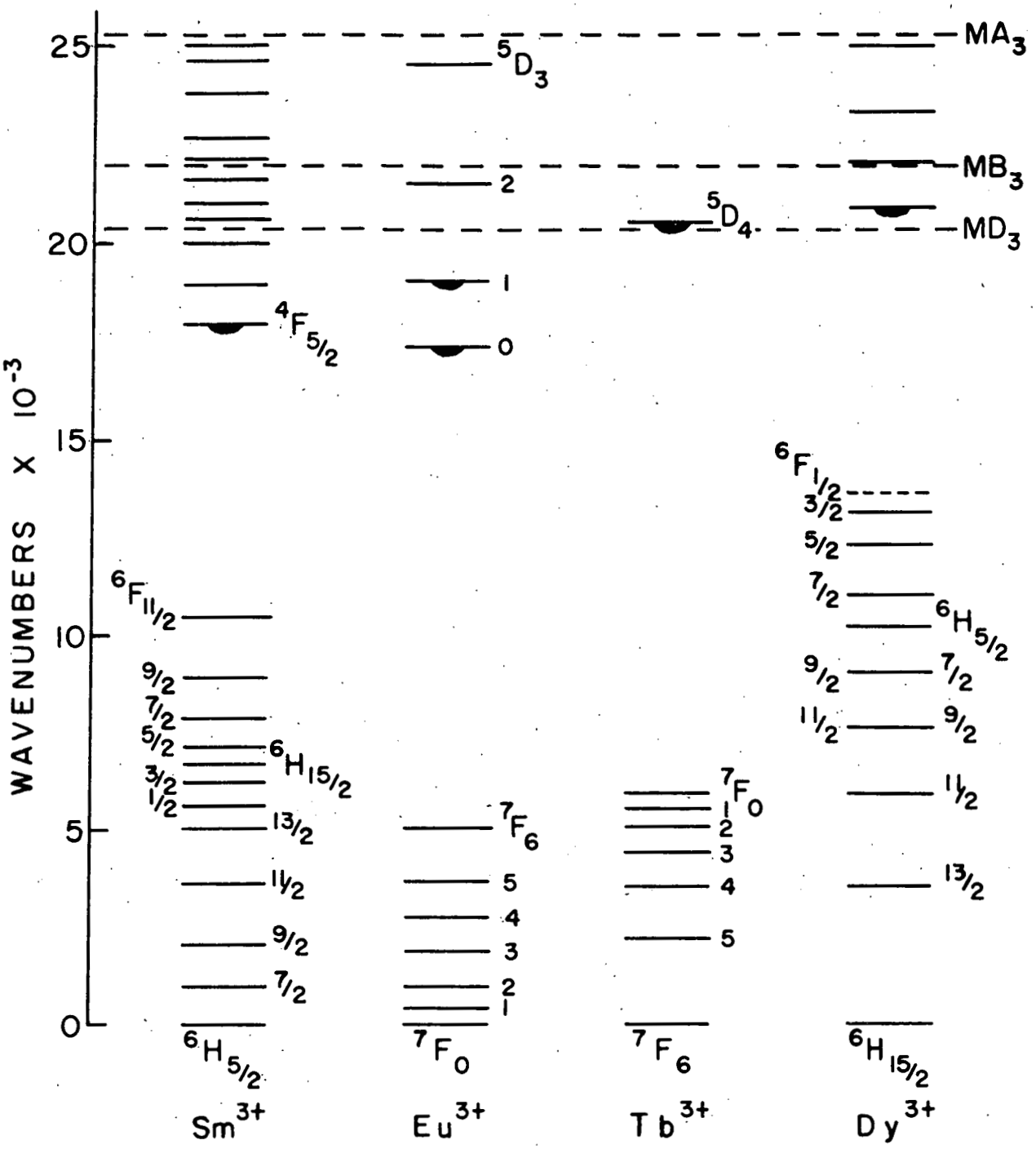

Fig. 3.1.2.2.--Energy level diagram for β-diketone chelates of trivalent terbium, europium, samarium, and dysprosium.

----- triplet energy level of the β-diketone complex

——— rare earth ion level

——●—— resonance level of the chelated rare earth ion

Fig. 3.1.2.3.--Emission spectra of β-diketone complexes of trivalent dysprosium, samarium, and terbium in EMPA glasses at 77°K.


transmission region of the filter system used for decay measurements

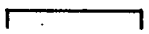
line group arising from indicated J-J transition

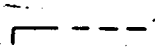
possible J-J assignment

(X, followed by a given number, is the factor by which the exposure time had to be multiplied in order to record the peaks shown in that spectral region. The time required to photograph the most intense group of lines for a given compound has been chosen as unity. Excitation source, intensity, geometry, etc. were all held constant for a series of exposures (displaced vertically) recorded on the same photographic plate for a particular compound with the exposures requiring progressively longer times. The final trace for a complex is a composite made up of the densitometer traces obtained from the series of exposures taken in the described way. This allows one to obtain an estimate of the relative line intensities for a given compound, although only a semi-quantitative one. No intensity comparisons can be made between different chelates from these traces.)

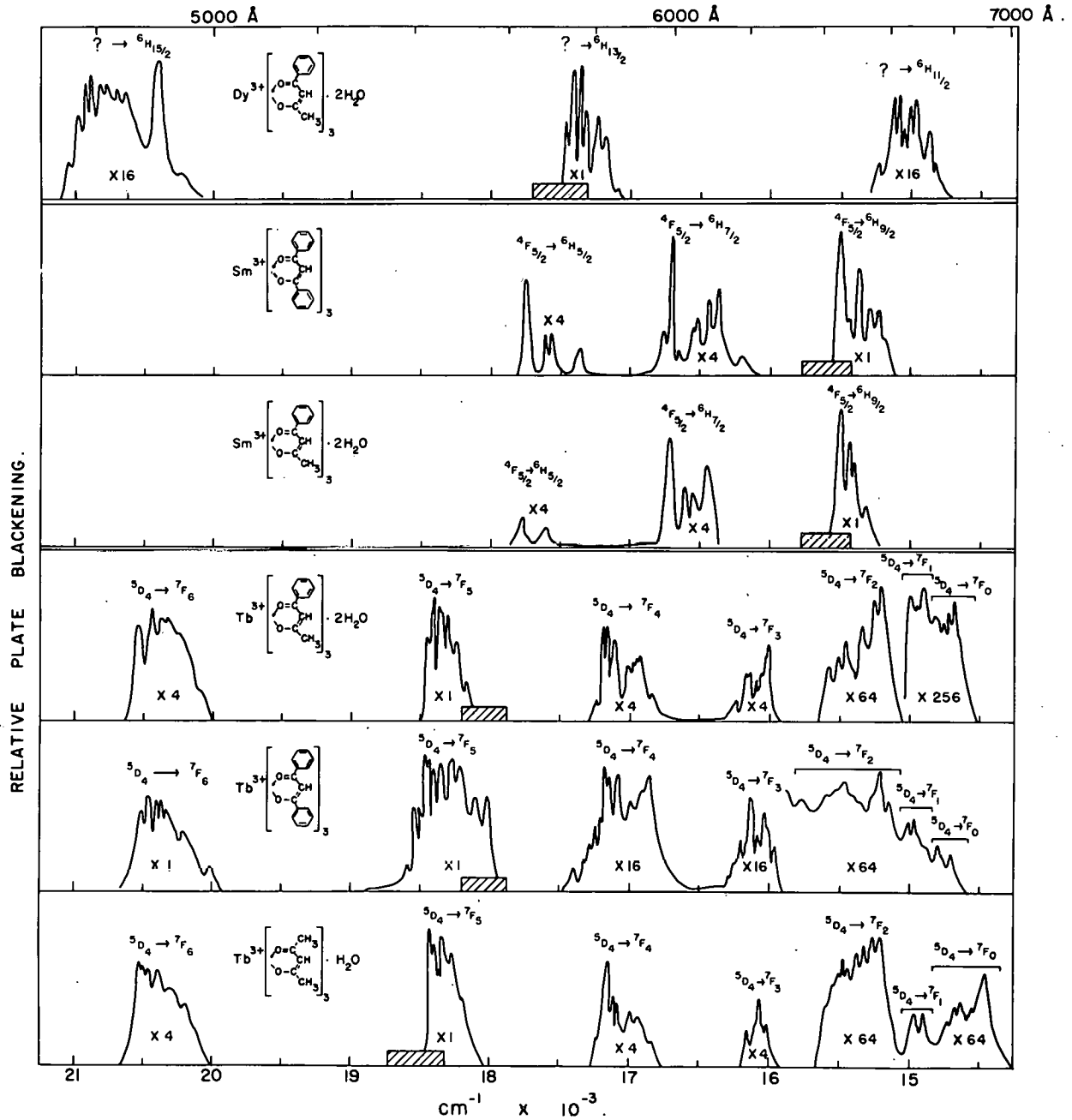
5000 Å
6000 Å
7000 Å
RELATIVE PLATE BLACKENING.
? → $^6H_{15/2}$
? → $^6H_{13/2}$
? → $^6H_{11/2}$
Dy^{3+} · $2H_2O$
Sm^{3+}
Sm^{3+} · $2H_2O$
Tb^{3+} · $2H_2O$
Tb^{3+}
Tb^{3+} · H_2O
$^4F_{5/2} \rightarrow {}^6H_{5/2}$
$^4F_{5/2} \rightarrow {}^6H_{7/2}$
$^4F_{5/2} \rightarrow {}^6H_{9/2}$
$^5D_4 \rightarrow {}^7F_6$
$^5D_4 \rightarrow {}^7F_5$
$^5D_4 \rightarrow {}^7F_4$
$^5D_4 \rightarrow {}^7F_3$
$^5D_4 \rightarrow {}^7F_2$
$^5D_4 \rightarrow {}^7F_1$
$^5D_4 \rightarrow {}^7F_0$
X 1
X 4
X 16
X 64
X 256
21
20
19
18
17
16
15
cm^{-1} x 10^{-3}

Fig. 3.1.2.4.--Emission spectra of β-diketone chelates of trivalent europium in EMPA glasses at 77°K. (For definitions of symbols see Fig. 3.1.2.3.).

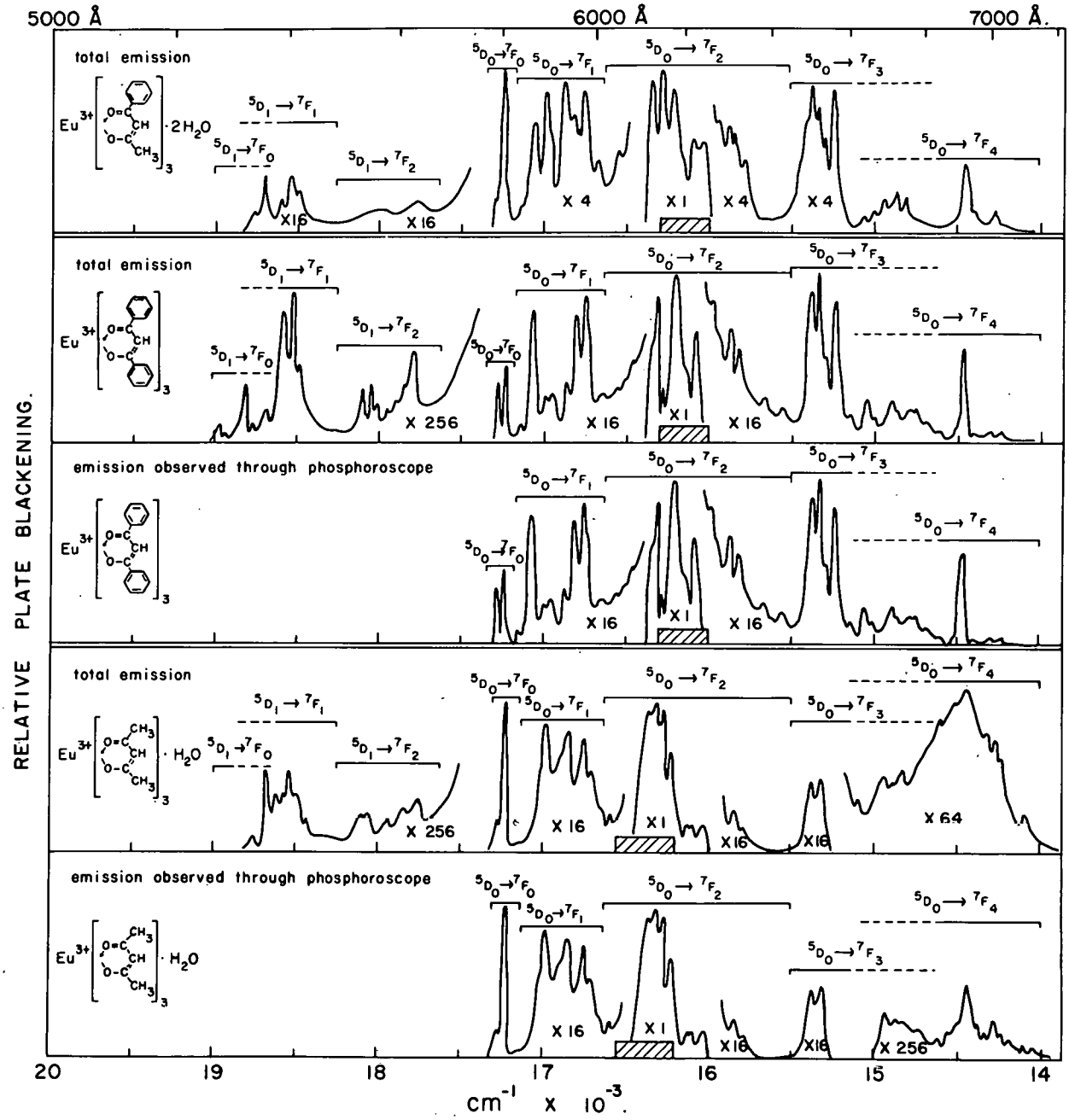
5000 Å
6000 Å
7000 Å.
total emission
$Eu^{3+}[\cdot]_3 \cdot 2H_2O$
$^5D_1 \rightarrow {}^7F_1$
$^5D_1 \rightarrow {}^7F_0$
$^5D_1 \rightarrow {}^7F_2$
$^5D_0 \rightarrow {}^7F_0$
$^5D_0 \rightarrow {}^7F_1$
$^5D_0 \rightarrow {}^7F_2$
$^5D_0 \rightarrow {}^7F_3$
$^5D_0 \rightarrow {}^7F_4$
X16
X 16
X 4
X 1
X 4
X 4
total emission
$Eu^{3+}[\cdot]_3$
X 256
X 16
X 1
X 16
emission observed through phosphoroscope
$Eu^{3+}[\cdot]_3$
X 16
X 1
X 16
total emission
$Eu^{3+}[\cdot]_3 \cdot H_2O$
X 256
X 16
X 1
X16
X16
X 64
emission observed through phosphoroscope
$Eu^{3+}[\cdot]_3 \cdot H_2O$
X 16
X 1
X16
X16
X 256
RELATIVE PLATE BLACKENING.
20
19
18
17
16
15
14
$cm^{-1} \times 10^{-3}$.

compounds, but because the emissions were quite weak, these two chelates were not investigated further.

Although transitions between electronic states of the free ion would give rise to isolated spectral lines, the spectra of the complexed rare earth ions are characterized by groups of lines. The interactions between the 4f electrons and the surrounding ligands partially or wholly remove the electronic degeneracies of the electronic states of the free ion and create a crystal field multiplet of states. It is the radiative transitions between these various crystal field multiplets of the two combining states of the ion which give rise to a group of lines in the emission spectra of the rare earth ions.

The emission spectra of the Tb^{3+}, Sm^{3+}, and Dy^{3+} ions arise from radiative transitions originating at only one resonance level yielding a single progression of line groups. Because of this relative simplicity of the spectra these groups of lines can be assigned to particular electronic transitions on the basis of energy differences only. Such J-J transitions are indicated above the spectral lines in Fig. 3.1.2.3.

The emission spectra of the chelated europium ion are complicated by the fact that the emission arises from two well characterized resonance levels ($^5D_0$, $^5D_1$), both of which are populated <u>via</u> intramolecular energy transfer in the chelates. Nevertheless, assignment of the groups of lines to transitions arising from unique resonance levels is possible by means of the technique of recording the emission spectra through a

Becquerel phosphoroscope. The transitions originating at the $^5D_1$ state are so short-lived that the phosphoroscope effectively eliminates these emissions from the luminescence spectra. Therefore, lines which appear in both the total emission spectra and the time resolved emission spectra can be assigned definitely to $^5D_0 \rightarrow {}^7F$ transitions. As can be seen in Fig. 3.1.2.4., three groups of weak lines corresponding to transitions originating at the $^5D_1$ level appear in the Eu^{3+} emission spectra between 17,250 $cm.^{-1}$ and 19,000 $cm.^{-1}$. From the energy level diagram of this ion, one would expect to find four additional groups of lines originating at the $^5D_1$ state at lower frequencies in the emission spectrum. The intensity changes in the region of 6700 Å to 7000 Å of the $EuA_3 \cdot H_2O$ emission spectra give only a hint of the existence of $^5D_1$ transitions. Other predicted transitions in the region of the spectrum between 5800 Å and 7000 Å are evidently so weak that they cannot be detected by the difference between the total emission spectrum and the time resolved emission spectrum.

3.1.3. Luminescence Decay Times of Chelated Rare Earth Ions in Organic Glasses

The strong intensities plus the long lifetimes of the rare earth ion emissions from the β-diketone chelates allowed the luminescence decays of the ions to be readily recorded with the apparatus described in Section 2.5. The emission from the rare earth chelate was passed through light filter combinations which allowed only ion emission corresponding to

transitions originating at the lowest resonance level of the ion to reach the photomultiplier tube. Because Tb^{3+}, Sm^{3+}, and Dy^{3+} emissions all originate at unique resonance levels, all the lines in the spectra of each of these ions had the same luminescence decay times. The strongest lines were selected for observation. The lines in the Eu^{3+} emission spectra originating at the $^5D_1$ resonance level were so weak and short-lived that a direct measure of their decay could not be obtained with the apparatus used in these studies. Measurements were restricted to the strong 6100 Å lines originating at the $^5D_0$ resonance level. The regions of the rare earth ion emission spectra passed by the light filter combinations are indicated by the crosshatched bars in Fig. 3.1.2.3. and Fig. 3.1.2.4.

The luminescence decay curves of the chelated rare earth ions are shown in Appendix 5.5. The salient features of the luminescence decays exhibited by the majority of samples are exemplified by the decay curve shown in Fig. 3.1.3.1. The luminescence intensities rose very rapidly, reached a maximum at time t_m, and decayed slowly, the semilogarithmic plot becoming linear at longer times.

For a few of the samples studied, the semilogarithmic plots of relative luminescence intensity versus time did not become linear at longer times, but curved away from the horizontal time axis. Such decay curves arise when the measured intensities originate from two different emitting species, each decaying with a slightly different lifetime. The two species could correspond to two different isomers of the rare

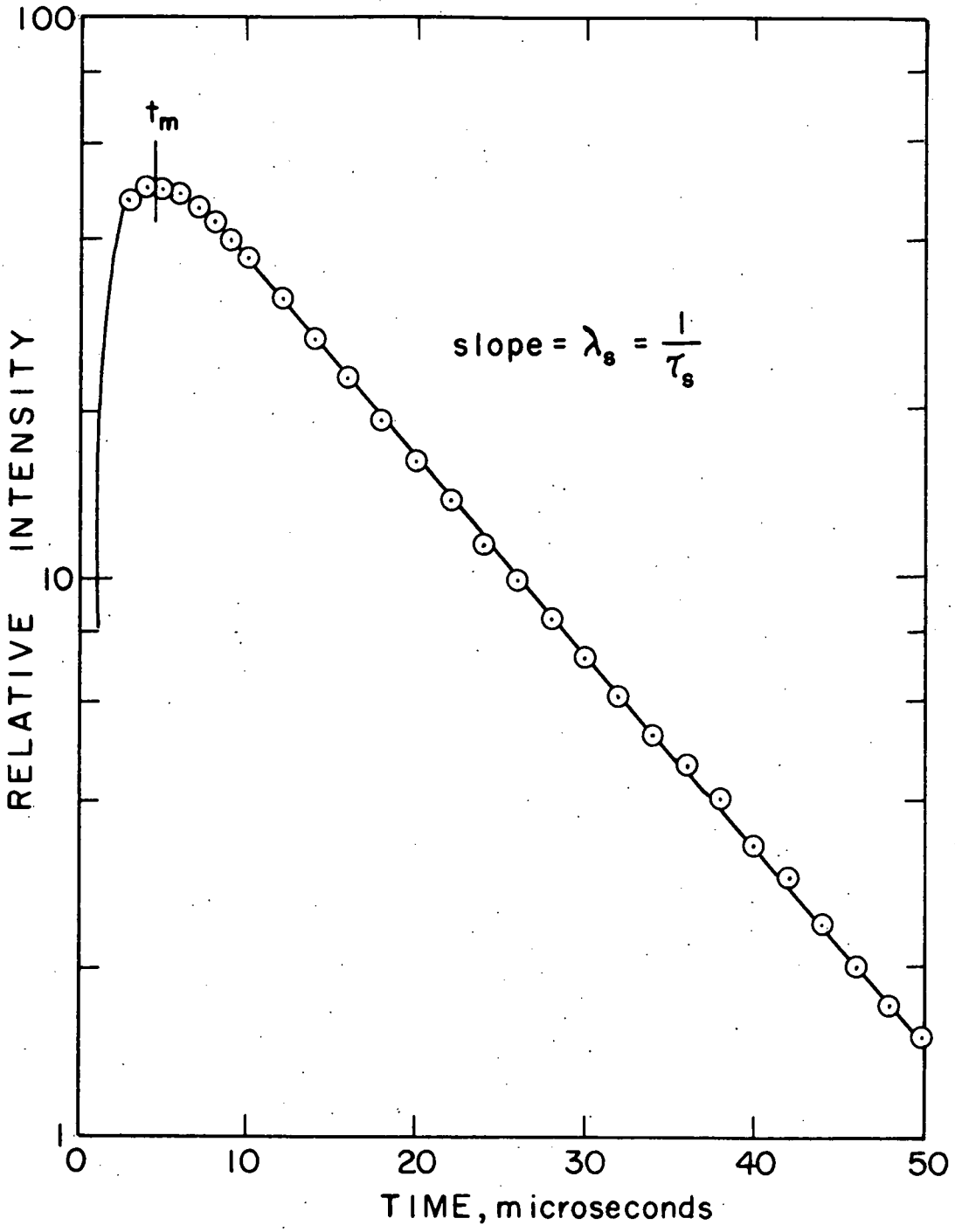

Fig. 3.1.3.1.--Semilogarithmic plot of the luminescence decay of $DyB_3 \cdot 2H_2O$ in EMPA at 77°K.

earth chelate, or even to two different chelate species formed by the interaction of some of the chelate molecules with trace contaminants in the organic glasses. The mathematical analyses of these curved semilogarithmic decays are discussed in Appendix 5.3.

The luminescence decay curves of the chelated rare earth ions are indicative of a two step, first order, exponential decay mechanism shown schematically in Fig. 3.1.3.2. For this decay mechanism a nonradiative decay step with a rate constant λ_1, is followed by a radiative decay step with a rate constant λ_2. The intensity of radiation, I, emitted during the second decay step as a function of time is given by the equation

$$I = (\text{const.})\left(\frac{\lambda_1}{\lambda_2 - \lambda_1}\right)\left(e^{-\lambda_1 t} - e^{-\lambda_2 t}\right) \qquad 3.1.3.1.$$

The population of the emitting state is assumed to be zero at zero time for the derivation of this equation (29). At the time t_m for which the curve reaches a maximum, the following relationship holds:

$$\frac{\lambda_2}{\lambda_1} = e^{(\lambda_2 - \lambda_1)t_m} \qquad 3.1.3.2$$

As can be deduced from equation 3.1.3.1., the rate constant λ_s for the slower of the two steps may be obtained by measuring the slope of the linear region of the plot of lnI *versus* t. A measure of λ_s and t_m may then be used *via* equation 3.1.3.2. to calculate the rate constant λ_f for the faster of the two steps. Because of the symmetry of the two

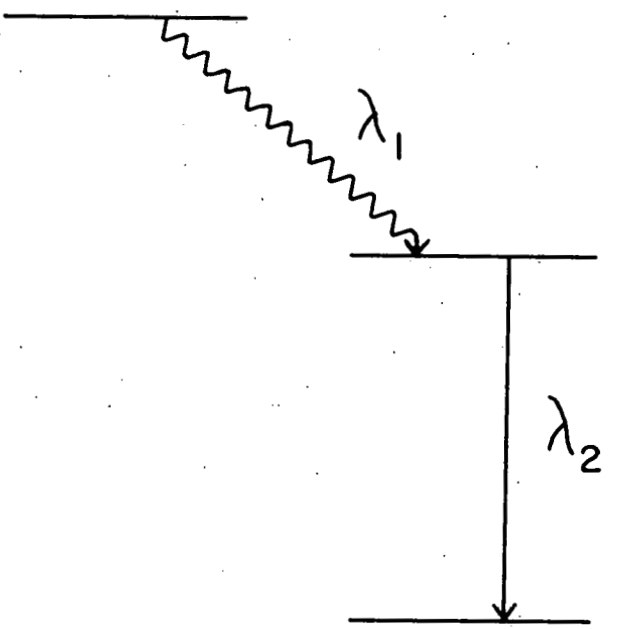

Fig. 3.1.3.2.--Schematic energy level diagram showing a two step, first order, exponential decay mechanism.

∿∿∿∿ nonradiative decay

——→ radiative decay

equations with respect to λ_1, and λ_2, one may assign λ_1 to λ_f and λ_2 to λ_s or vice versa. Additional experimental information is necessary to make the correspondence unique.

The mean lifetimes τ_s and τ_f (reciprocals of the rate constants) of the long-lived state giving rise to the slow decay step and the short-lived state giving rise to the fast decay step respectively, as calculated from the luminescence decay curves of the rare earth chelates, are summarized in Table 3.1.3.1. Included in this table are the data on the crystalline hydrated rare earth chlorides reported by Dieke and Hall (30). It should be pointed out that in the case of the rare earth chlorides, the rare earth ion was excited directly by absorption of the near ultraviolet light, while in the case of the rare earth chelates, the ion was excited via intramolecular energy transfer from the organic ligand.

As can be seen in Table 3.1.3.1., there is a rough correspondence between the radiative lifetimes of the ions in the inorganic salts and τ_s, the lifetimes calculated for the slow step of the luminescence decay of the chelated rare earth ion. The lifetime for the slow step is therefore assigned to the second radiative step of the two step mechanism ($\tau_s = 1/\lambda_2$), while the lifetime of the fast step is assigned to the initial nonradiative decay step of the mechanism ($\tau_f = 1/\lambda_1$).

3.1.4. Determination of the Lower Limit of the Rate of Intramolecular Energy Transfer in Rare Earth Chelates

Now that a unique correspondence has been made between the two mean lifetimes calculated from the luminescence decay

TABLE 3.1.3.1.

MEAN LIFETIMES CALCULATED FROM THE LUMINESCENCE DECAY CURVES OF CHELATED RARE EARTH IONS

Rare Earth Ion	Transition Observed	Mean Lifetime in Microseconds[a]						
		$MB_3 \cdot 2H_2O$ in EMPA at 77°K		MD_3 in EMPA at 77°K		$MA_3 \cdot H_2O$ in EMPA at 77°K		$MCl_3 \cdot 6H_2O$ Solid at 77°K
		τ_f	τ_s	τ_f	τ_s	τ_f	τ_s	τ
Tb^{3+}	$^5D_4 \longrightarrow {}^7F_5$	2	630	2	464[b]	2	901	487[c]
Eu^{3+}	$^5D_0 \longrightarrow {}^7F_2$	2	430	1	361	2	564	120[c]
Sm^{3+}	$^4F_{5/2} \longrightarrow {}^6H_{9/2}$	3	14.1	2	20.1	-	-[e]	~10[c]
Dy^{3+}	$? \longrightarrow {}^6H_{13/2}$	2	12.3	-	-[d]	-	-[e]	~10[c]

[a]Probable error ± 10 %.

[b]Semilogarithmic plot is initially curved; τ_s calculated from the linear region of the curve at longer times.

[c]Dieke and Hall (30).

[d]No Dy^{3+} emission observed from this chelate.

[e]Rare earth ion emission observed, but intensity of emission was too weak for lifetime measurements.

curves with the lifetimes of the two step, first order, exponential decay mechanism, this two step mechanism may be related to the possible paths of energy migration in rare earth chelates. These paths are indicated in the detailed energy level diagram shown in Fig. 3.1.4.1. This diagram is essentially the same as that shown in Fig. 3.1.1.2. except that vibrational levels have been added to the electronic levels of the complex and known rate constants (expressed in reciprocal seconds) are indicated. If the complex is raised to an excited vibrational level of an excited electronic state, it very rapidly loses its excess vibrational energy to the surrounding lattice. The rate constant, K_{IC} corresponding to this loss of vibrational energy is believed to be on the order of 10^{13} sec.$^{-1}$ (20,31). Once the complex reaches the zeroth vibrational level of the excited singlet state S_1, it may combine radiatively with the ground state yielding short-lived ($K_f \sim 10^8$ sec.$^{-1}$) molecular fluorescence. Because intersystem crossing (radiationless conversion from S_1 to T_1) competes favorably with fluorescence for the depopulation of the excited singlet state (18,22), the rate constant, K_{IS}, associated with intersystem crossing must be on the order of, or greater than the rate constant associated with fluorescence. For this reason, the magnitude of the intersystem crossing rate constant is placed at greater than or equal to 10^7 sec.$^{-1}$. Since the decay of the flash lamp is on the order of two microseconds, the rate constant, K_L, associated with the pumping of the singlet state is given a value of 5×10^5 sec.$^{-1}$. The rate

Fig. 3.1.4.1.--Energy level diagram showing possible paths of energy migration in rare earth chelates.

(Rate constants are expressed in units of reciprocal seconds.)

- - - - ➤ transitions via absorption of radiation

——➤ transitions via emission of radiation

∿∿∿➤ radiationless transitions

——●—— denotes resonance level of the rare earth ion

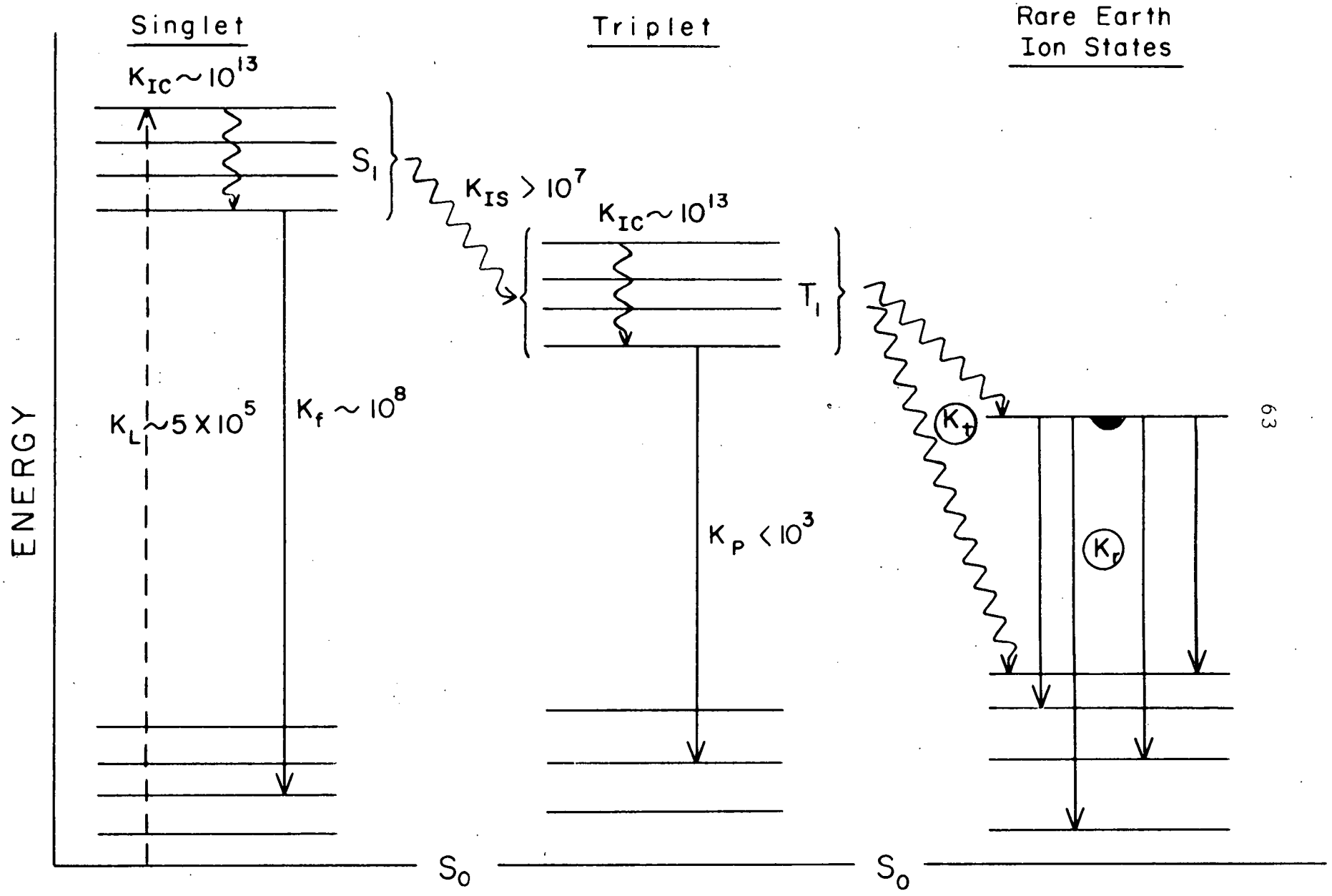
Singlet
Triplet
Rare Earth Ion States
$K_{IC} \sim 10^{13}$
S_1
$K_{IS} > 10^7$
$K_{IC} \sim 10^{13}$
T_1
$K_L \sim 5 \times 10^5$
$K_f \sim 10^8$
$K_P < 10^3$
K_t
K_r
ENERGY
S_0
S_0

constant K_t is associated with intramolecular energy transfer, and the rate constant K_r is associated with the decay of the resonance level of the rare earth ion. The rate constant, K_p, associated with the spin-forbidden radiative combinations between the zeroth vibrational level of the triplet state and the ground state is usually much less than 10^3 $sec.^{-1}$.

The experimentally determined decay time τ_s has already been assigned to the radiative step of the two step mechanism. It must, therefore, represent the mean lifetime of the resonance level of the rare earth ion. The negative reciprocal of τ_s is thus equal to the rate constant K_r of Fig. 3.1.4.1. The remaining lifetime, τ_f, which is calculated to be two microseconds for all the samples reported and which is associated with the initial step of the two step mechanism, must be assigned to some preceding energy transfer step in the chain of events leading to the population of the resonance level of the ion. There are three such steps to be considered: (a) pumping of the singlet state by the flash lamp, (b) intersystem crossing, and (c) intramolecular energy transfer from the triplet state of the complex to the resonance level of the ion.

Because the rate constant of the intersystem crossing step is greater than or equal to 10^7 $sec.^{-1}$, the mean lifetime associated with this rate constant is less than or equal to 0.1 microsecond. Intersystem crossing occurs much too fast to account for the nonradiative energy transfer process. For all the compounds studied, λ_f (which is equal to $1/\tau_f$) was

found to be 5 X 10^5 sec.$^{-1}$. This coincides with the rate constant K_L associated with the decay of the flash lamp. Step (a), the rate of pumping of the singlet state, is the step determing the rate of population of the resonance level of the rare earth ion. This immediately implies that the transfer of energy from the triplet system occurs at a rate faster than the decay of the flash lamp; i.e. the rate constant, K_t, associated with intramolecular energy transfer in rare earth chelates is greater than or equal to 5 X 10^5 sec.$^{-1}$. In view of the long lifetimes associated with the resonance levels of the chelated rare earth ions (the τ_s values of Table 3.1.3.1.), it may also be concluded that intramolecular energy transfer in rare earth chelates occurs at a rate much too fast to be controlling the rate of decay of the rare earth ion resonance levels.

3.2. Nature of the Excited States from Which Intramolecular Energy Transfer Occurs

3.2.1. Triplet State Energy Requirements for Intramolecular Energy Transfer

From the data obtained by Whan (22), it was concluded that whenever the emitting triplet state of the chelate is below a resonance level of a rare earth ion, no line emission is observed in the emission spectra. Therefore, Whan postulated that a necessary condition for intramolecular energy transfer from the excited electronic states of the chelate molecule to the electronic states of the chelated rare earth ion, resulting

in line emission by the ion, is that the emitting triplet state of the molecule must possess an energy which is greater than or at least close to the energy of the resonance level of the ion.

It is generally accepted (31) that the emitting level of an electronic system of a given spin multiplicity is the zeroth vibrational level of the lowest electronic state of that multiplicity. It is for this reason that Crosby and co-workers (18) have replaced the term "emitting level of the triplet state" with "lowest triplet state of the complex." From a careful analysis of the spectroscopic data, these workers concluded that intramolecular energy transfer did not involve the simple transfer from the zeroth vibrational level of the triplet state to the ion resonance level. This conclusion was based principally on the observations that the population of Dy^{3+} and Tm^{3+} resonance levels <u>via</u> intramolecular energy transfer from the triplet state of the tristribenzoylmethide chelates occurred even though a measure of the phosphorescence band of the chelates placed the emitting level of the triplet state below the resonance levels of the two ions. Thus it was concluded that, while radiative depopulation of the triplet state was assumed to originate at the zeroth vibrational level of the lowest triplet state, intramolecular energy transfer could originate from some slightly higher level of the triplet system.

An estimate of just how much above the lowest triplet level the transferring level may be can be obtained from the

following data. DyD_3 exhibits no line emission characteristic of dysprosium. The resonance level of Dy^{3+} is placed at 20,958 $cm.^{-1}$ (32) while the triplet state of the complex is placed at 20,520 $cm.^{-1}$ (18). Dysprosium tristribenzoylmethide, however, does exhibit emission characteristic of dysprosium. The triplet state of this complex is placed at 20,833 $cm.^{-1}$ (18). These data would indicate that transfer from an upper level of a triplet system 430 $cm.^{-1}$ above the emitting level is improbable, but that transfer from an upper level of the triplet system only 125 $cm.^{-1}$ above the emitting level is probable. As the position of the emitting triplet level can only be estimated to within $\pm$50 $cm.^{-1}$, and since the position of the resonance level of Dy^{3+} is derived from spectroscopic data on the hydrated chloride crystals, not too much faith can be placed on the accuracy of the above calculations.

The question as to whether intramolecular energy transfer does occur from some higher components of the triplet state or from the lowest triplet level may be resolved through considerations of both the lifetime of the emitting triplet state and the rate of intramolecular energy transfer. For, whichever mechanism is proposed, it must be compatible with the depopulation rate of the triplet system by both phosphorescence and intramolecular energy transfer processes.

3.2.2. Molecular Phosphorescence Decay Times of Rare Earth Chelates

Lifetimes of the lowest excited triplet states of the

rare earth complexes were determined by measuring the phosphorescence decay times of the complexes. (See Appendix 5.4. for details.) An attempt was made to measure phosphorescence decay times of benzoylacetonate complexes of La^{3+}, Lu^{3+}, Gd^{3+}, Sm^{3+}, Dy^{3+}, Pr^{3+}, Nd^{3+}, Tm^{3+}, Er^{3+}, and Yb^{3+}. With the exception of the first three ions mentioned, the phosphorescences exhibited by the chelates dissolved in EMPA glasses at 77°K were too weak to obtain reliable phosphorescence decay measurements. The results on the lanthanium, lutetium, and gadolinium complexes are summarized in Table 3.2.2.1. The data are compared with those given by Yuster and Weissmann (33) for the phosphorescence decays of dibenzoylmethide complexes of the same ions.

The phosphorescence decay times of the chelates of La^{3+} and Lu^{3+} are almost fifty times longer than the phosphorescence decay times of the Gd^{3+} complexes. These differences cannot be attributed to variations in competing intramolecular energy transfer processes because these three ions have no low-lying 4f electronic states. The lanthanum ion possesses no 4f electrons, and the lutetium ion possesses a closed shell of fourteen 4f electrons. The first excited electronic state of the gadolinium ion, placed at 32,000 $cm.^{-1}$ (34), is much too high to be populated <u>via</u> intramolecular energy transfer. Yuster and Weissman (33) attributed the short lifetime of the gadolinium complexes to interactions between the highly paramagnetic Gd^{3+} ions and the electrons of the ligand. The comclusion drawn by the authors was that the higher the para-

TABLE 3.2.2.1.

PHOSPHORESCENCE DECAY TIMES OF β-DIKETONE COMPLEXES OF LANTHANUM, LUTETIUM, AND GADOLINIUM DISSOLVED IN EMPA GLASSES AT 77°K

Rare Earth Ion	Decay Time, milliseconds	
	$MB_3 \cdot 2H_2O$	MD_3[a]
La^{3+}	70	90
Gd^{3+}	2	2[b]
Lu^{3+}	90	120

[a]Data reported by Yuster and Weissman (33).

[b]Complex was dissolved in an absolute ethanol glass at 77°K.

magnetism of the complexing ion, the greater is the probability for radiative combinations between the first excited triplet state and the singlet ground state. The postulated increase in radiative transition probability would result in a decreased lifetime for the triplet state.

It should not be concluded that the phosphorescence lifetimes exhibited by the gadolinium chelates represent the shortest phosphorescence lifetimes possible for rare earth complexes. There are two other rare earth ions which have even more paramagnetic ground states (35). They are Ho^{3+} and Dy^{3+}, each possessing a paramagnetic moment of $\sim$10.5 Bohr magnetons as compared to the 8.0 Bohr magnetons of the ground state of Gd^{3+}. Since the phosphorescence lifetimes of the complexes decreased by a factor of $\sim$50 on changing the complexed ion from diamagnetic La^{3+} or Lu^{3+} ions to the Gd^{3+} ion possessing a paramagnetic ground state of 8.0 Bohr magnetons, the phosphorescence lifetimes could probably be decreased by as much as a factor of 100 by forming complexes with the more paramagnetic Ho^{3+} or Dy^{3+} ions with ground states of 10.5 Bohr magnetons; i.e., the phosphorescence lifetimes of the chelates of Ho^{3+} or Dy^{3+} could be as small as one millisecond. Thus, if one accepts the reasoning of Yuster and Weissman, it can be estimated that in the absence of intramolecular energy transfer, the triplet state lifetimes of rare earth trisbenzoylacetonate or trisdibenzoylmethide chelates are greater than or equal to one millisecond.

Measurements of phosphorescence decay times of such chelates as $SmB_3 \cdot 2H_2O$, $DyB_3 \cdot 2H_2O$ or SmD_3, in which intra-

molecular energy transfer processes could possibly be competing with phosphorescence for depopulation of the triplet state, could not be made due to the low intensities of the phosphorescences. Estimates of the minimum phosphorescence lifetimes of these chelates can be obtained from the spectroscopic data presented by Whan and Crosby (20). These data show that although the chelates EuD_3, SmD_3, $SmB_3 \cdot 2H_2O$, $DyB_3 \cdot 2H_2O$, $HoB_3 \cdot 2H_2O$, and HoD_3 all exhibit rare earth line emission arising from intramolecular energy transfer in the chelates, a weak phosphorescence band is recorded in the emission spectrum of each of them. As the phosphoroscope resolution time was 100 microseconds, any sample emission recorded in the phosphorescence spectrum must have had a decay time of not less than twenty microseconds. (It is assumed that the intensity of sample emission beyond five mean lives of decay is much too weak to be recorded by the spectrograph.) It is concluded that the shortest possible lifetime of the triplet state of a rare earth chelate, in which intramolecular energy transfer could be vying with radiative decay for the depopulation of the triplet level, is twenty microseconds.

3.2.3. Elimination of the Emitting Level of the Triplet State as the Energy Transferring Level

Two possible paths for intramolecular energy transfer from the triplet system of the complex to the 4f electronic levels of the rare earth ion are shown in Fig. 3.2.3.1. As indicated in the energy level diagrams, energy may be trans-

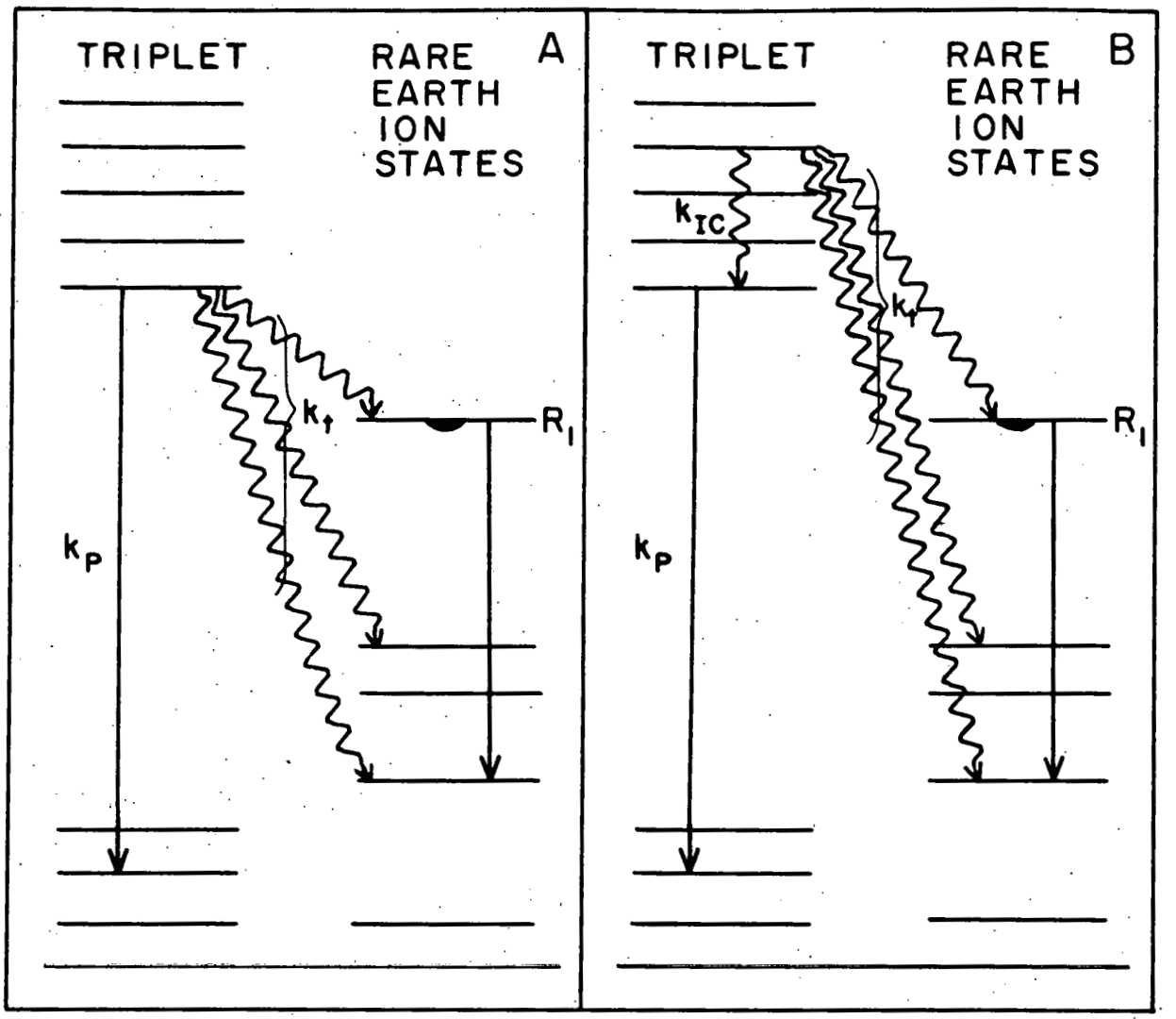

Fig. 3.2.3.1.--Possible paths for intramolecular energy transfer in rare earth chelates. (For definitions of symbols see 3.1.4.1.)

A) transfer occurs from the lowest triplet level

B) transfer occurs from a vibrational (or electronic) level above the lowest triplet level

ferred to the resonance level and to the lower lying levels of the ion. The rate constant K_t measures the rate of depopulation of the triplet level by intramolecular energy transfer to all possible rare earth ion states, not just the rate of depopulation to the resonance level of the ion only. On the basis of experimentally determined rate constants a choice may now be made between the two proposed mechanisms of Fig. 3.2.3.1.

If the mechanism of energy transfer shown in Fig. 3.2.-3.1.A is operative in rare earth chelates, then the lifetime of the triplet state is a function of both the radiative transition constant, K_p, and the energy transfer constant, K_t. The measured mean lifetime of the triplet state in this case is given by the expression

$$\tau = \frac{1}{K_p + K_t} \qquad 3.2.3.1.$$

The lifetime, τ, of the triplet state of chelates in which energy transfer could be competing with radiative decay for the depopulation of the triplet level was shown in the last section to be greater than or equal to twenty microseconds, while the experimentally determined rate constant for energy transfer is $\geqq 5 \times 10^5$ sec.$^{-1}$. Substituting these values into equation 3.2.3.1. and solving for K_p, the radiative decay constant of the triplet state, a value of -4.5×10^5 sec.$^{-1}$ is obtained. This number is an absurdity since it would predict a spontaneous population of the triplet state from the ground state. Thus experimental observations eliminate the possibility that intramolecular energy transfer occurs from the emitting level of the triplet state. Because the emitting level of the

triplet system is believed to be the zeroth vibrational level of the lowest triplet state, intramolecular energy transfer in rare earth chelates must occur from some component of the triplet system energetically higher than the zeroth vibrational level of the lowest triplet state of the complex. Such a transfer process is shown in the energy level diagram of Fig. 3.2.3.1.B.

3.2.4. Intramolecular Energy Transfer Rate Constants for Transfer from Upper Levels of the Triplet State

If intramolecular energy transfer occurs from some higher component of the triplet system, then the transfer mechanism must compete with whatever mechanisms exist for the internal conversion of these upper levels to the emitting level of the triplet state. Not only must the energy transfer mechanism compete with the internal conversion mechanisms, but it must compete efficiently, for Whan (22) has shown that whenever energy transfer does occur in the rare earth chelates, only weak phosphorescence is observed in the emission spectra of the complexes.

The energy transfer may occur from either an excited vibrational level of the lowest triplet state or possibly from other nearby electronic components of the lowest triplet state or from other nearby higher triplet levels. Internal conversion between vibrational states of the same electronic level or between electronic states of the same spin multiplicity is believed to occur at a very fast rate corresponding to a first

order rate constant of $\sim 10^{13}$ sec.$^{-1}$. This places the rate constant for the competing transfer processes in the neighborhood of 10^{13} sec.$^{-1}$. It is therefore concluded that not only is the rate constant for intramolecular energy transfer definitely greater than or equal to 5×10^{5} sec.$^{-1}$, but that the rate constant could be as high as 10^{13} sec.$^{-1}$.

It should be emphasized at this point that the arguments presented in these last two sections are based entirely on the assumption that weak phosphorescences observed in the spectra of those rare earth chelates which exhibit rare earth line emission arise from the same molecular species in which intramolecular energy transfer to the rare earth ion is occurring. It could be argued that these weak molecular emissions arise from some dissociative product or trace contaminant in which the molecular emission occurs completely independently of the energy transfer process. An inspection of the emission spectra presented by Whan and Crosby (20) reveals, however, that the positions and structures of these weak phosphorescences are the same or very similar to the strong phosphorescences exhibited by the gadolinium complexes, thus supporting the contention that they do indeed arise from the same species in which intramolecular energy transfer processes are occurring.

3.3. Quenching of Electronic States of Complexed Rare Earth Ions

The arguments presented in the previous sections of this discussion have been devoted entirely to the problem of intramolecular transfer of electronic energy in rare earth

chelates. Little emphasis was placed on the relative magnitudes of the lifetimes of the resonance levels of the chelated rare earth ions other than that the lifetimes were of the same order of magnitude as the decay times of the rare earth ions in the hydrated inorganic chloride crystals. Attention will now be focused on the magnitudes of the decay times of the rare earth ions.

The data presented in Table 3.1.3.1. indicate that the measured lifetimes γ_s of the resonance levels of the chelated rare earth ions are in general longer than the lifetimes of the ion in the hydrated chlorides, at least at 77°K. It has been demonstrated that the intramolecular energy transfer process occurs at a rate much too fast to control the rate of decay of the resonance levels of the rare earth ion. Thus, the increased lifetimes of the resonance levels of the chelated rare earth ions must be due to a decrease in the probability for depopulation of the electronic level.

There are two general mechanisms available for the depopulation of an electronic state: (a) loss of electronic energy via the emission of radiation and (b) radiationless transitions (quenching of the electronic state) via the conversion of electronic energy to vibrational or translational energy of the system. The data on the rare earth chelates dissolved in EMPA glasses at 77°K were insufficient for determining which of these two mechanisms predominates during the depopulation of the resonance levels of the ions. In order to determine the relative efficiency of each of these mechanisms for the depopulation of the excited electronic states of

complexed rare earth ions, a study of the absorption spectra, emission spectra, and luminescence decay times of complexed rare earth ions was undertaken. These studies were conducted on solvated rare earth chlorides, rare earth oxides dissolved in metaphosphate glasses, and microcrystalline β-diketone chelates.

3.3.1. The Existence of Quenching

3.3.1.1. Relationship Between Absorption Strengths and Luminescence Decay Times. -- The possible paths for the depopulation of an excited electronic state of a complexed rare earth ion are shown schematically in Fig. 3.3.1.1.1. The depopulation mechanisms involve both radiative combinations between the resonance level, R, and lower electronic states, L_i, as well as the nonradiative combinations between these states. The probability constants for the former transitions are denoted by the K_{r_i}, while the probability constants for the latter transitions are denoted by the K_{q_i}. The mean lifetime, τ, of the electronic state is given by the reciprocal of the sum of all the transition probabilities.

$$\tau = \frac{1}{\sum_i \left(K_{r_i} + K_{q_i}\right)} \qquad 3.3.1.1.1.$$

An increase in the lifetime of the electronic state of an ion due to a change of environment can be due to a decrease in the total probability for radiative transitions, $\sum K_{r_i}$, or a decrease in the total probability for radiative transitions,

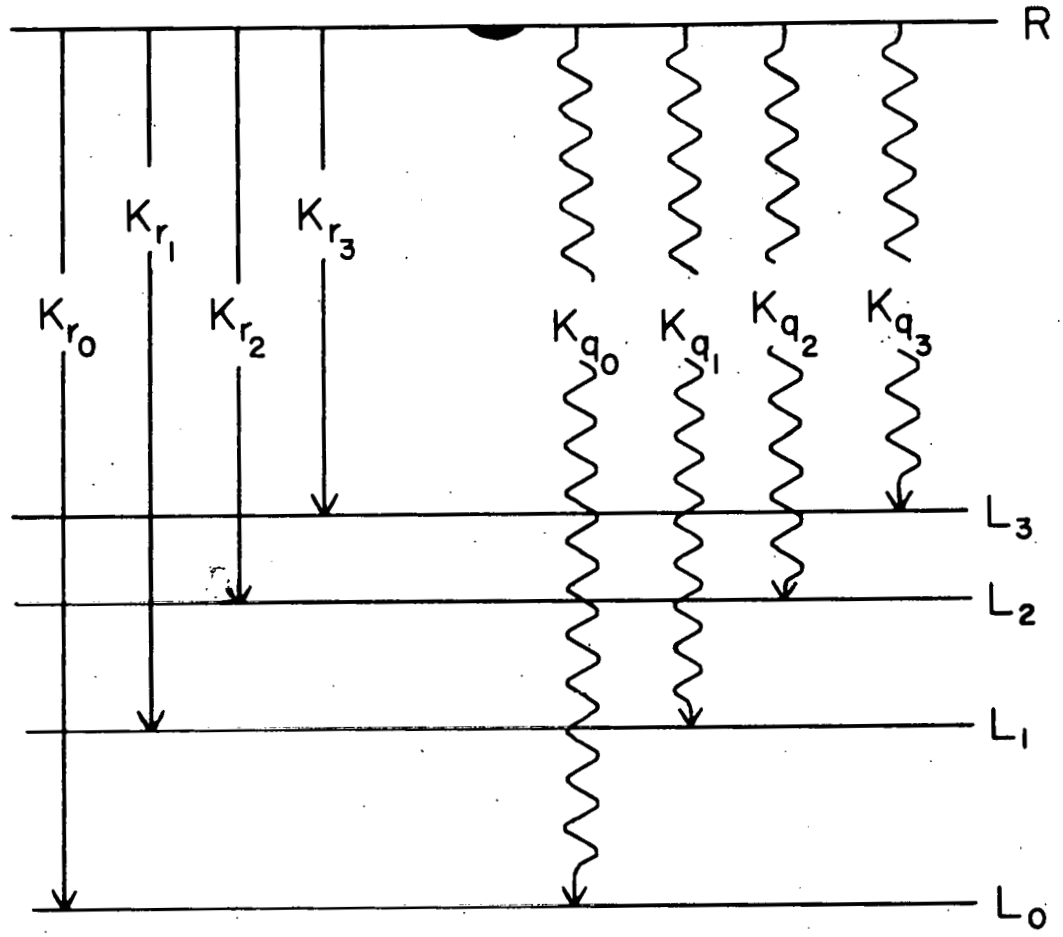

Fig. 3.3.1.1.1.--Paths available for the depopulation of an excited electronic state of a complexed rare earth ion.

⟶ radiative transitions

∿∿∿ radiationless transitions

$\sum K_{q_i}$, or a combination of the two effects. There are no simple methods available for the direct experimental determination of the total nonradiative transition probability; but the magnitude of the radiative transition probability of one particular transition can be calculated from the absorption spectrum of the transition.

According to Barrow (36), the spontaneous radiative transition probability, $A_{g\rightarrow h}$, for radiative transitions between an upper electronic state g and a lower electronic state h is related to the absorption strength of the transition by the relationship:

$$A_{g\rightarrow h} = \frac{8\pi(1000)c(\bar{\nu}_{gh})^2}{N}\int \alpha(\bar{\nu})d\bar{\nu} \qquad 3.3.1.1.2.$$

where c is the speed of light,

N is Avogadro's number,

$\bar{\nu}_{gh}$ is the frequency of the transition in wave numbers,

$\alpha(\bar{\nu})$ is the molar extinction coefficient of the transition at frequency $\bar{\nu}$,

and integration is performed over the region of the absorption spectrum attributable to the transition $g\rightarrow h$.

In the derivation of this equation, $\alpha(\bar{\nu})$ is defined by the equation:

$$\alpha(\bar{\nu}) = \frac{1}{cl}\ln(I_o/I) \qquad 3.3.1.1.3.$$

where c, l, I_o, and I are the same quantities defined in Section 2.3.

Substituting the molar extinction coefficient $\alpha(\bar{\nu})$ with the

molar extinction coefficient $\epsilon(\bar{\nu})$ defined in Section 2.3. ($\alpha(\bar{\nu}) = 2.303\ \epsilon(\bar{\nu})$), replacing the $A_{g\rightarrow h}$ with K_{r_i}, and introducing numerical values for the constants in equation 3.3.1.1.2. reduces the relationship to the following:

$$K_{r_i} = 2.88 \times 10^{-9} (\bar{\nu}_{r_i})^2 \int \epsilon(\bar{\nu}) d\bar{\nu} \quad . \qquad 3.3.1.1.4.$$

The total radiative transition probability for the upper electronic state is given by the relationship:

$$K_r = \sum_i K_{r_i}$$

$$= 2.88 \times 10^{-9} \sum_i (\bar{\nu}_{r_i})^2 \int_{\text{ith band}} \epsilon(\bar{\nu}) d\bar{\nu} \quad . \qquad 3.3.1.1.5.$$

Thus, variations of the lifetimes of electronic states of the rare earth ions, which are due primarily to changes of the radiative transition probabilities, could be readily detected through variations of the absorption strengths of the complexed rare earth ion. Any increase of the radiative transition probability, K_{r_i}, would be accompanied by an increase in the integrated absorption strength $\int \epsilon(\bar{\nu}) d\bar{\nu}$.

3.3.1.2. Absorption Strengths of Complexed Rare Earth Ions. -- In order to determine whether the increases in the decay times of the chelated rare earth ions over those of the ions in the hydrated chlorides were due to a decrease in the radiative transition probabilities, a study of the absorption spectra of the very weak $(4f)^n \rightarrow (4f)^n$ electronic transitions of the complexed rare earth ions was undertaken. The spectra

were measured using concentrated solutions of rare earth chelates or rare earth chlorides in liquid solutions at room temperature. Solvents were selected so that the environment of the ions in the solutions approximated the environment of the rare earth ion in the glasses or crystals used for luminescence studies. Identical solvent systems could not be used for the rare earth chelates, however, because the solubility of the chelates in EMPA was not high enough to detect the weak transitions to be measured. Although the absorption spectra of large, single, optically clear crystals of the hydrated rare earth chlorides would have been most desirable, such crystals were not available and solutions were used. It can be reasonably assumed, however, that the immediate environment of the ion in the concentrated aqueous solutions cannot be too much different from that of the ion in the crystalline material. The visible absorption spectra of complexed Eu^{3+}, Sm^{3+}, and Dy^{3+} ions are presented in Fig. 3.3.1.2.1. through Fig. 3.3.1.2.5.

The absorption spectra presented in these figures arise from transitions from the ground electronic state of the ion to upper electronic levels. Transitions are labeled according to the quantum number designations of the parent atomic states of the rare earth ion. Assignments are made on the basis of energy differences determined from the energy level diagram of Fig. 3.1.2.2. Absorption spectra of the ions in the near infrared and infrared region of the spectrum, which correspond to transitions between the ground state and low lying electronic states of the ion, are not shown. As the electronic

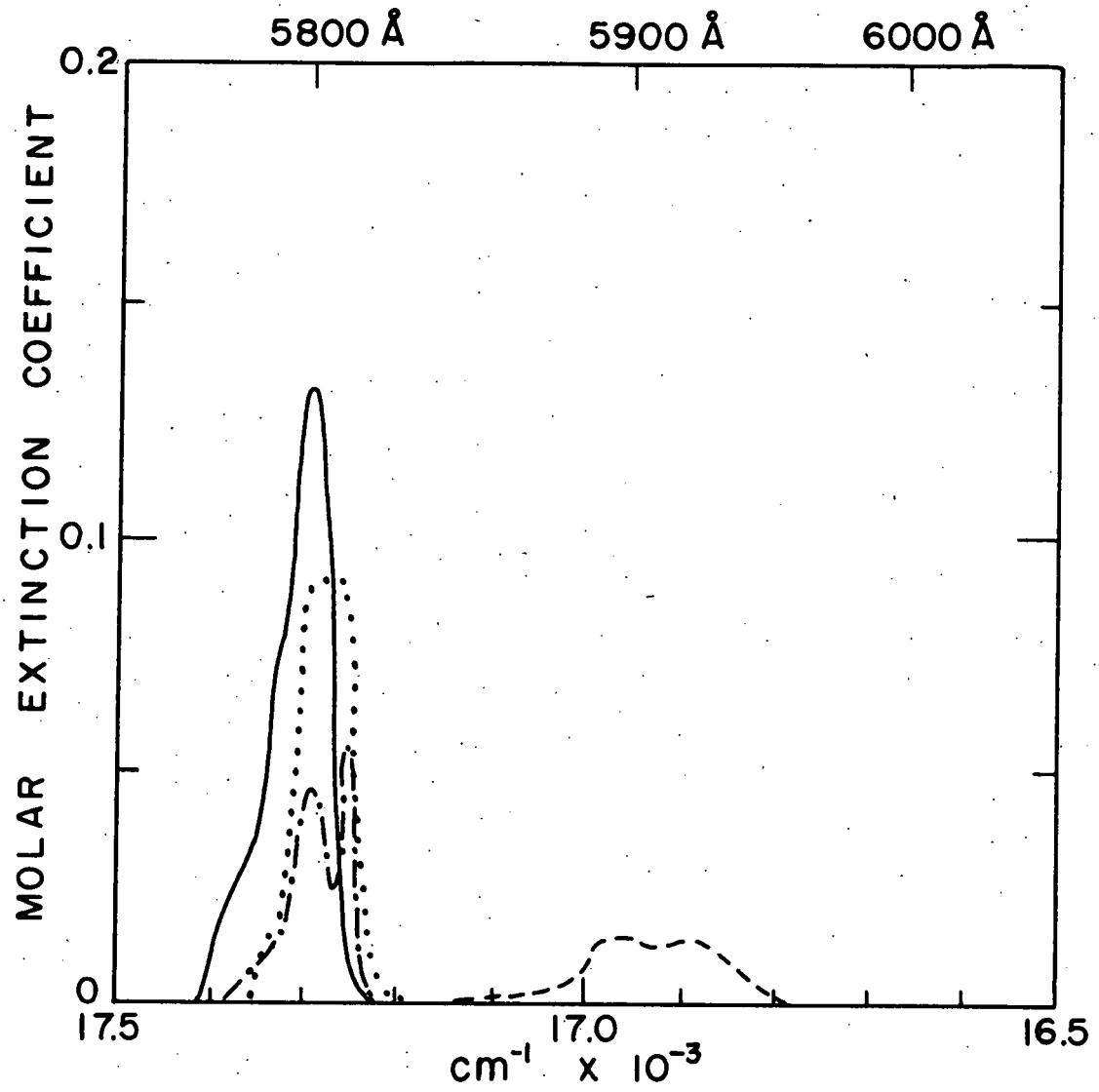

Fig. 3.3.1.2.1.--The $^7F_0 \rightarrow {}^5D_0$ transition of the Eu^{3+} ion in various environments at 25° C.

----- 0.21 M $EuCl_3$ in water

——— 0.01 M EuD_3 in benzene

····· 0.01 M $EuB_3 \cdot 2H_2O$ in acetone

-·-·-·- 0.01 M $EuA_3 \cdot H_2O$ in acetone

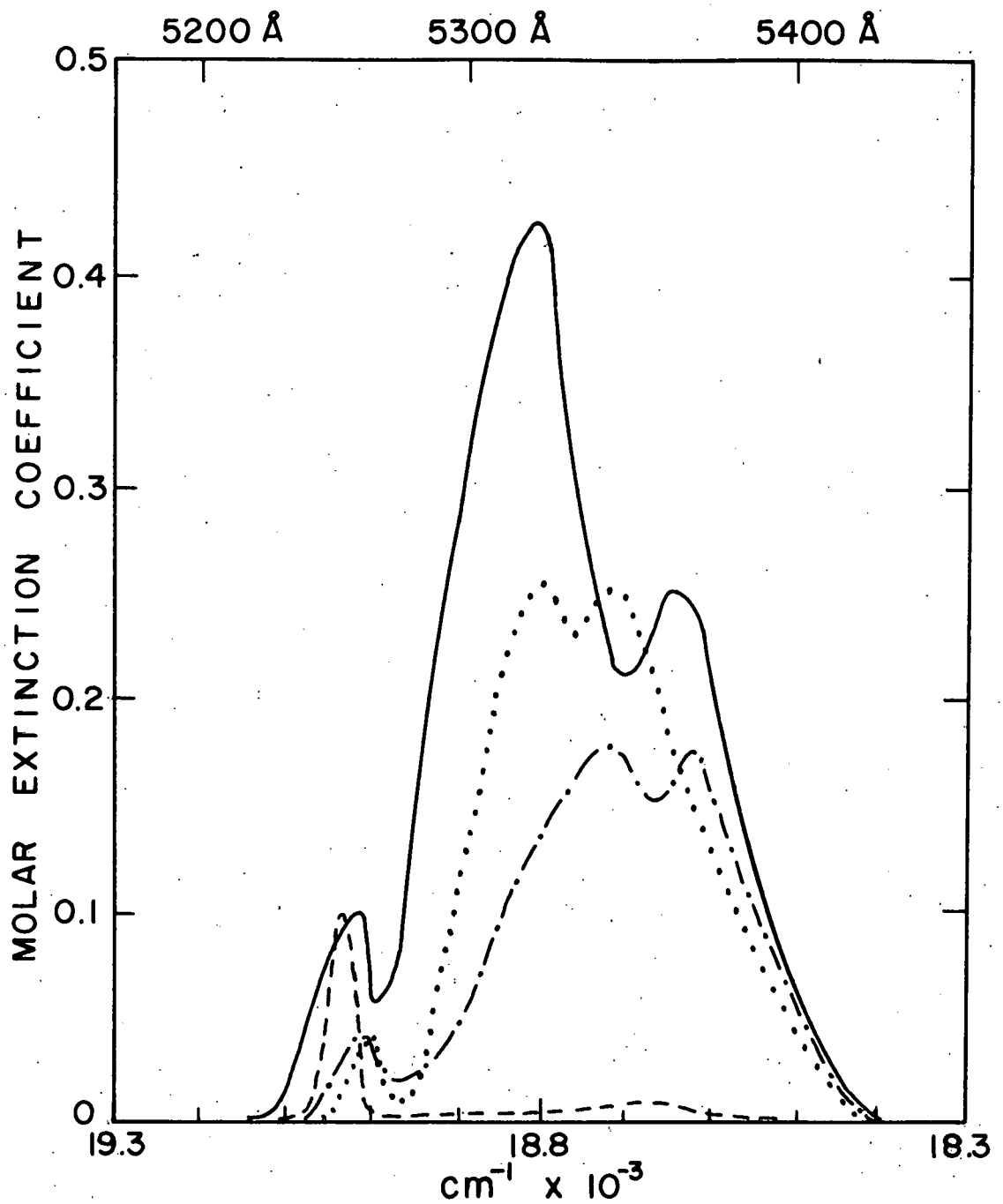

Fig. 3.3.1.2.2.--The $^7F_0 \longrightarrow {}^5D_1$ transition of the Eu^{3+} ion in various environments at 25°C.

------ 0.21 M $EuCl_3$ in water

——— 0.01 M EuD_3 in benzene

····· 0.01 M $EuB_3 \cdot 2H_2O$ in acetone

-·-·-·- 0.01 M $EuA_3 \cdot H_2O$ in acetone

Fig. 3.3.1.2.3.--The $^7F_0 \longrightarrow {}^5D_2$ transition of the Eu^{3+} ion in various environments at 25°C.

------ 0.21 M $EuCl_3$ in water. Measured extinction coefficients for this solution have been multiplied by a factor of ten in order that the absorption curve be visible on the figure

——— 0.01 M EuD_3 in benzene

····· 0.01 M $EuB_3 \cdot 2H_2O$ in acetone

-·-·-·- 0.01 M $EuA_3 \cdot H_2O$ in acetone

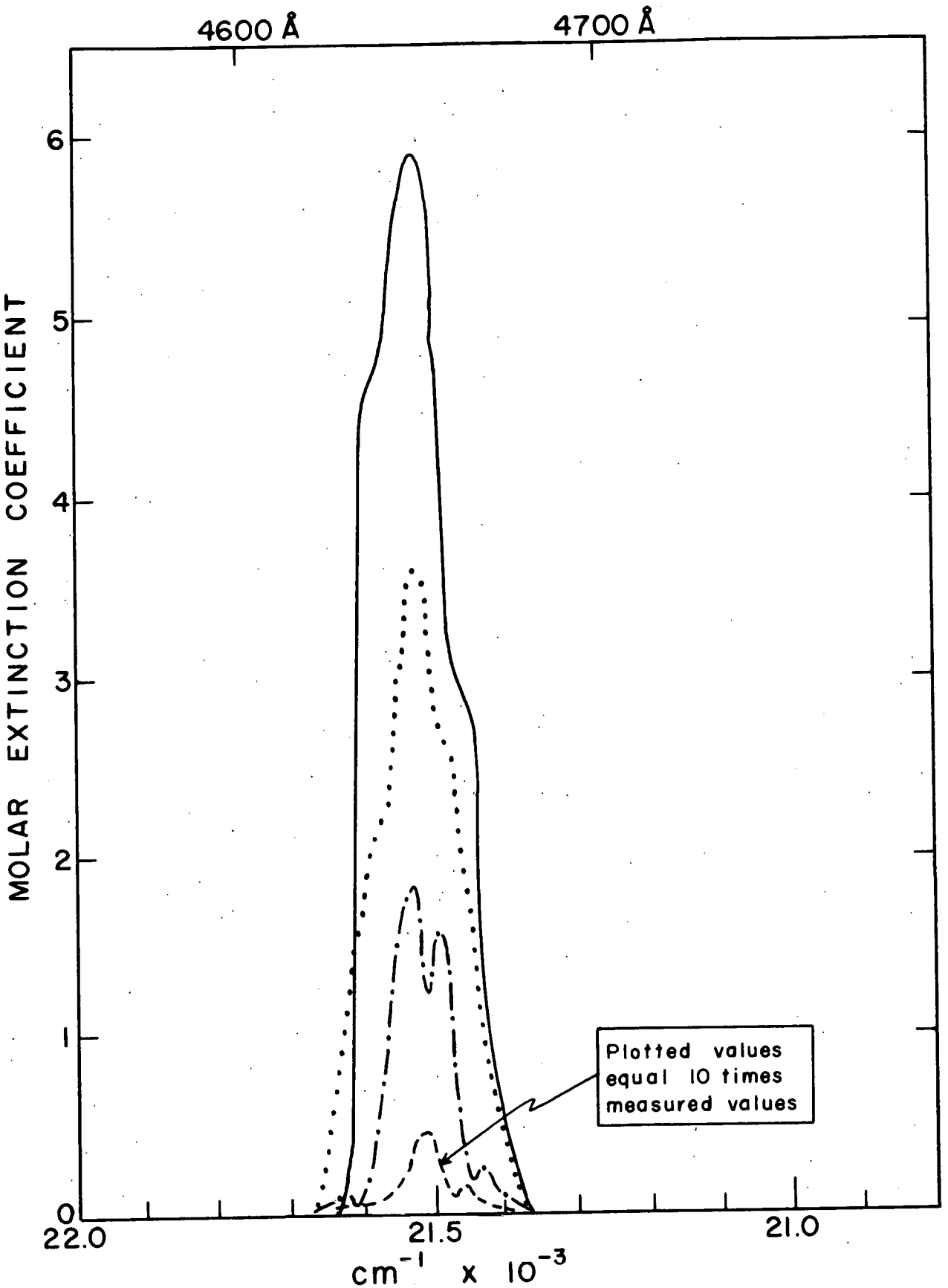
4600 Å
4700 Å
MOLAR EXTINCTION COEFFICIENT
0
1
2
3
4
5
6
22.0
21.5
21.0
cm⁻¹ x 10⁻³
Plotted values
equal 10 times
measured values

Fig. 3.3.1.2.4.--Visible absorption spectrum of the Sm^{3+} ion in various environments at 25°C.

- - - - - 0.24 M $SmCl_3$ in water

——— ~ 0.01 M SmD_3 in acetone

····· 0.01 M $SmB_3 \cdot 2H_2O$ in acetone

—·—·—·— resolution of SmD_3 spectrum into two J-J transitions

⌐——⌐ probable J-J transitions

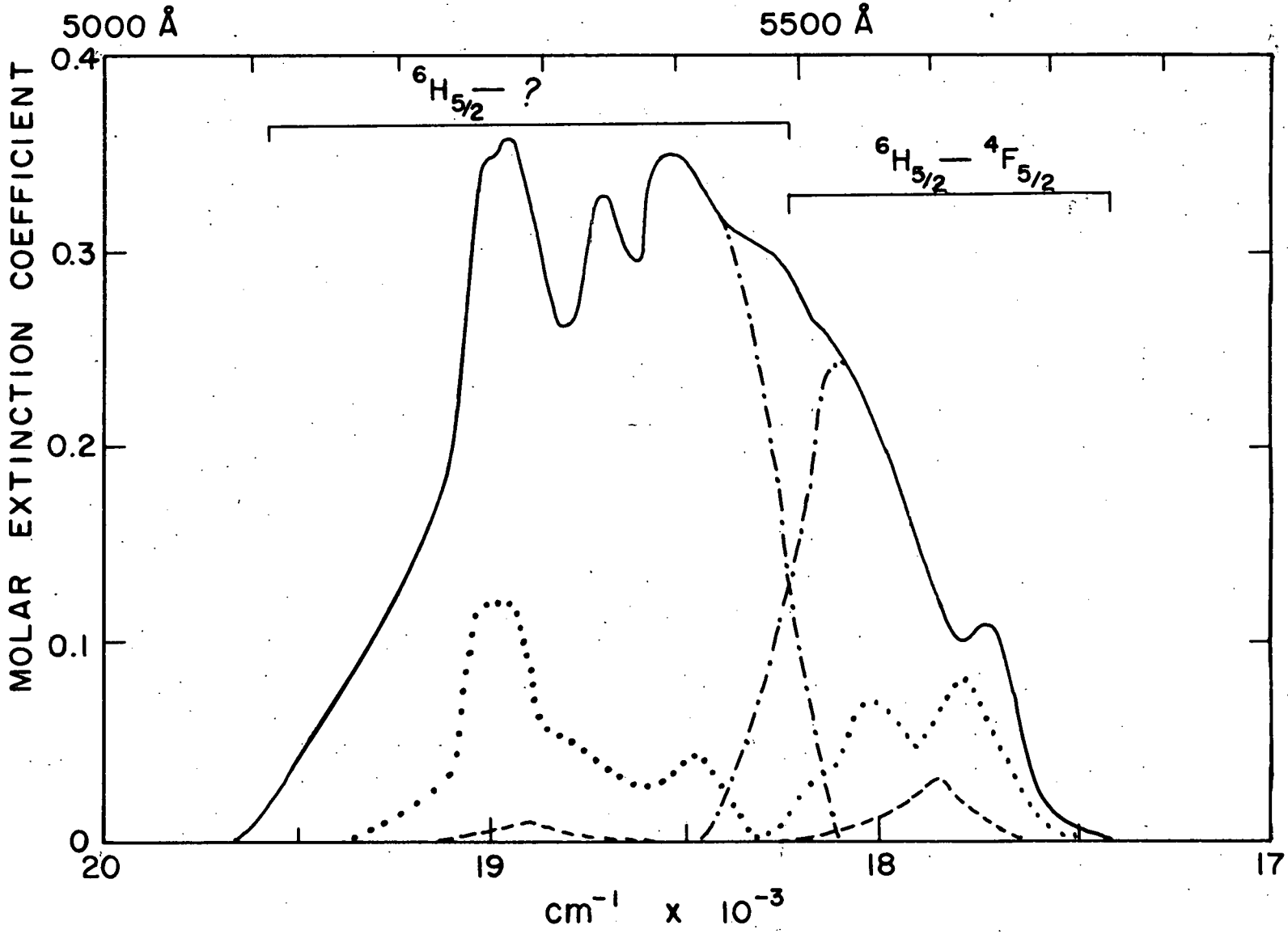
5000 Å
5500 Å
MOLAR EXTINCTION COEFFICIENT
0.4
0.3
0.2
0.1
0
$^6H_{5/2}$ — ?
$^6H_{5/2}$ — $^4F_{5/2}$
20
19
18
17
cm^{-1} x 10^{-3}

Fig. 3.3.1.2.5.--Visible absorption spectrum of the Dy^{3+} ion in various environments at 25°C.

– – – – – 0.21 M $DyCl_3$ in water

····· 0.01 M $DyB_3 \cdot 2H_2O$ in acetone

–·–·–· 0.01 M $DyA_3 \cdot H_2O$ in acetone

┌──────┐ probable J-J transition

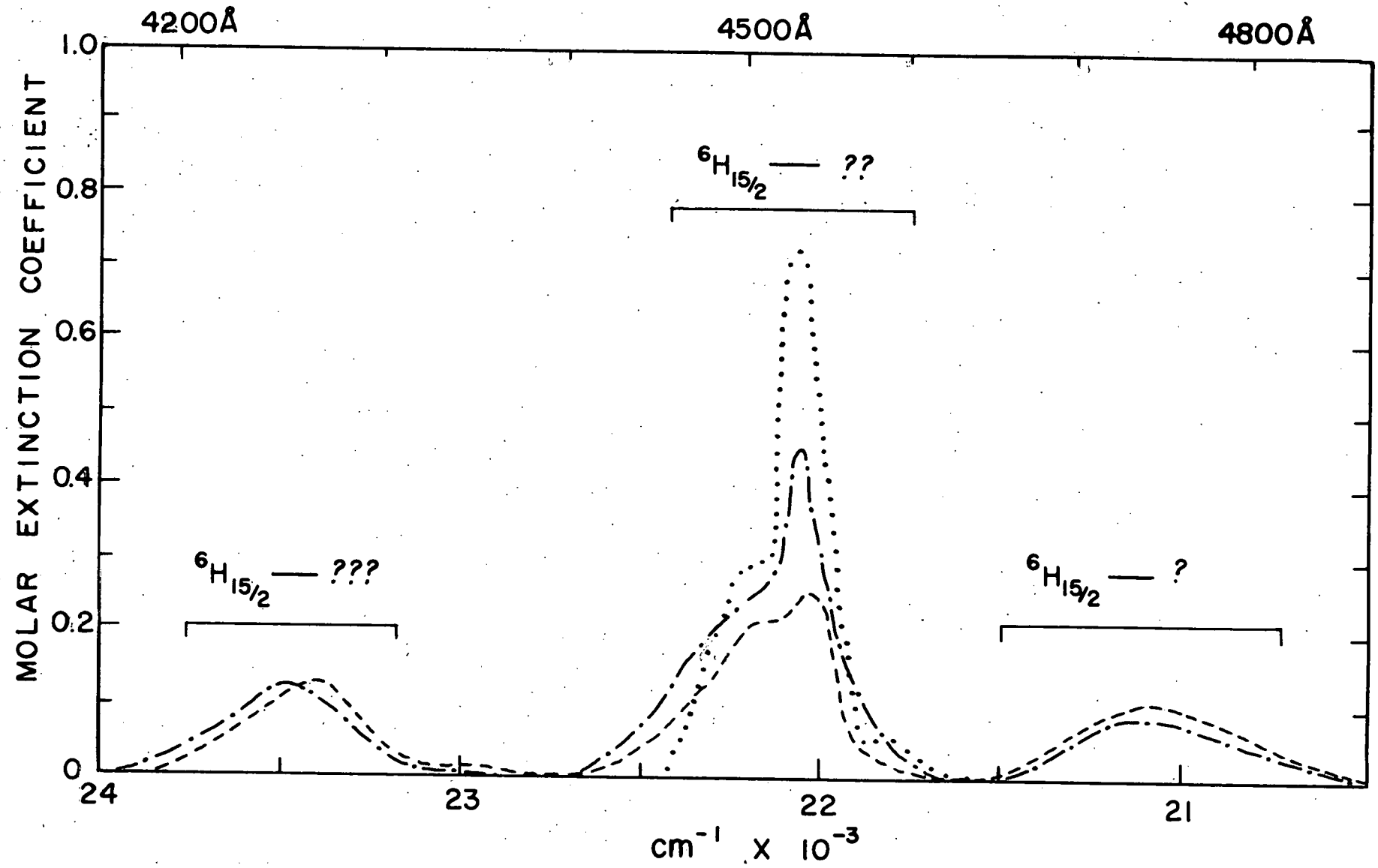
4200Å
4500Å
4800Å
1.0
0.8
0.6
0.4
0.2
0
MOLAR EXTINCTION COEFFICIENT
$^6H_{15/2}$ — ??
$^6H_{15/2}$ — ???
$^6H_{15/2}$ — ?
24
23
22
21
cm^{-1} X 10^{-3}

states of the ion lying just above the ground state are too high in energy to be thermally populated at room temperature, absorption bands corresponding to transitions between these low lying states and the upper resonance levels could not be recorded.

Three distinct transitions are observed in the visible absorption spectrum of the Eu^{3+} ion. They are shown in the first three figures. These transitions occur between the $^7F_0$ ground state of the ion and the first three upper ^5D states. For Sm^{3+} the absorption bands corresponding to the transitions between the ground state ($^6H_{5/2}$) and the first two upper states ($^4F_{5/2}$ and ?) are shown in Fig. 3.3.1.2.4. while the transitions between the ground state and the first three upper levels of the Dy^{3+} ion are shown in Fig. 3.3.1.2.5.

As can be seen in Fig. 3.3.1.2.1., the $^7F_0 \rightarrow {}^5D_0$ transition of $EuCl_3$ appears a few hundred wave numbers to the low frequency side of the same transition in the chelated Eu^{3+} ion. Because each of the electronic levels involved in this transition is nondegenerate (J = O, for both states), only one electronic band should be observed in absorption spectra for this transition. The appearance of the $EuCl_3$ absorption band at lower frequencies than the chelates must be attributed to a significant difference in the local environment of the europium ion. Miller, Sayre, and Freed (37) report that for $EuCl_3$ dissolved in a water-alcohol mixture, a weak absorption band at $\sim$17,000 $cm.^{-1}$ was readily discernible, while for $EuCl_3$ dissolved in anhydrous methanol, two absorption bands were re-

corded, one at ~17,300 cm.$^{-1}$ and the other at ~17,000 cm.$^{-1}$. It would appear that in the case of $EuCl_3$ in anhydrous methanol, two entirely different Eu^{3+} species were being formed, each giving rise to a separate $^7F_0 \rightarrow {}^5D_0$ transition in the absorption spectrum. If this is true, the appearance of $^7F_0 \rightarrow {}^5D_0$ absorption bands in different regions of the absorption spectrum of such dissimilar species as chelated Eu^{3+} and hydrated Eu^{3+} is not surprising. The appearance of additional "fine structure" in the absorption bands shown in Fig. 3.3.1.2.1. is probably due to instrumental error. This instrumental error arises from the fact that the measured absorption intensities were about 0.01 absorbance units or less. Such low absorption intensities are almost in the range of normal instrumental noise. The possibility still exists, however, that this fine structure could be attributed to vibrational interactions.

Transitions between the nondegenerate $^7F_0$ and the threefold degenerate $^5D_1$ state (degenerate in the free ion) shown in Fig. 3.3.1.2.2. are characterized by three absorption peaks in the chelate spectra while only a sharp peak at ~19,000 cm.$^{-1}$ plus a hint of a band around 18,700 cm.$^{-1}$ are found in the chloride absorption spectrum. The appearance of three absorption peaks in the chelated Eu^{3+} ion absorption spectra indicates that the ligand field of the β-diketone chelates completely removes the electronic degeneracy of the $^5D_1$ state. This latter result may be used to obtain information about the symmetry of the ligand field perturbing the chelated Eu^{3+}

ion.

An inspection of the symmetry group correlation tables presented by Prather (38) indicates that the ligand field of Eu^{3+} chelates may belong to any one of a number of symmetry point groups and still completely remove the threefold electronic degeneracy of the $^5D_1$ state. The range of choice may be narrowed, however, by considering only point groups consistent with the structural model illustrated in Fig. 3.1.1.1. The ligand field may arise from an octahedral arrangement of oxygen atoms about the Eu^{3+} ion and thus belong to the O_h point group, or it may arise from a trigonally distorted octahedral arrangement of oxygen atoms and belong to the D_3 group. If solvent molecules (water of hydration, etc.) are located on the three fold axis of the system, the field may be reduced to the C_3 point group. An inspection of Prather's tables indicates that ligand fields belonging to the C_3 group completely remove the electronic degeneracy of the $^5D_1$ state; while fields belonging to the D_3 group split the J = 1 level into two states, and fields belonging to the O_h group do not split the J = 1 level. It is therefore concluded that the ligand field perturbing the chelated europium ion belongs to the C_3 symmetry point group. This would mean that other atoms besides the six oxygen atoms of the three ligands are contributing to the ligand field.

The exact symmetry of the ligand field perturbing the hydrated rare earth ion in aqueous solutions cannot be deduced from the absorption spectrum since little is known about the

arrangement of the water molecules about the Eu^{3+} ion. Nevertheless, it can be stated that, because the $^7F_0 \rightarrow {}^5D_1$ transition of hydrated Eu^{3+} is characterized by two bands, the ligand field cannot possess octahedral symmetry. If the field did possess such a high degree of symmetry, it would not split the triply degenerate $^5D_1$ state of the ion.

An analysis of the $^7F_0 \rightarrow {}^5D_2$ absorption bands shown in Fig. 3.3.1.2.3. cannot be made due to poor resolution of the peaks. Because there is so little known about the J quantum numbers of the upper electronic levels of the Sm^{3+} and Dy^{3+} ions, information about the crystal field splitting of the electronic states of these ions could not be obtained from the absorption spectra. Probable J-J assignments of absorption bands are indicated in the figures.

3.3.1.3. Experimental Evidence for Quenching of the Electronic States of Rare Earth Ions. -- A survey of the absorption spectra presented in the last section reveals that the absorption strengths of the chelated rare earth ions are in general much greater than the absorption strengths of the rare earth ions in aqueous solution. The increased absorption strengths arise from a lowering of the symmetry of the electrostatic field surrounding the complexed rare earth ion. Radiative transitions between the 4f electronic states of the rare earth ion involving the emission or absorption of electric dipole radiation are strictly forbidden when the ion is in an electrostatic environment which possesses an inversion center of symmetry. The electrostatic field due to the six

water molecules surrounding the rare earth ion in aqueous solutions possesses such a center of symmetry (37). The electrostatic field of the trigonally distorted octahedral arrangement of chelate oxygen atoms about the rare earth ion would not possess this inversion center of symmetry. Transitions involving strong electric dipole radiation would be allowed in this situation thus accounting for the increased absorption strengths of the chelated rare earth ions.

Spontaneous radiative transition probabilities of the transitions identified in the absorption spectra are listed in Table 3.3.1.3.1. The transition probabilities were computed according to equation 3.3.1.1.4 in which the frequency of the strongest absorption peak of the transition was taken as the average frequency of the transition. With the exception of SmD_3, the absorption bands belonging to different J-J transitions were clearly separated so that no difficulties were encountered in the integration of the absorption strengths. Integration of the molar extinction coefficients over a given absorption band was done by the technique of "counting squares." In the case of SmD_3, there is no distinct division in the absorption spectrum between the different J-J transitions. On the other hand, the absorption spectra of $SmCl_3$ and $SmB_3 \cdot 2H_2O$ are clearly divided into two distinct transitions. By comparing the spectrum of SmD_3 with the spectra of the latter two complexes, the absorption band of SmD_3 was resolved into two bands--one corresponding to each of the J-J transitions observed in the spectra of the other two samarium complexes.

TABLE 3.3.1.3.1.

RADIATIVE TRANSITION PROBABILITIES FOR ELECTRONIC TRANSITIONS IN COMPEXED RARE EARTH IONS

Ion	Transition[c]	Average Frequency of Transition, $cm.^{-1}$	Spontaneous Radiative Transition Probability in units of $sec.^{-1}$ [a]			
			$MCl_3 \cdot nH_2O$	$MA_3 \cdot H_2O$	$MB_3 \cdot 2H_2O$	MD_3
Eu^{3+}	(R) $^5D_0 \rightarrow {}^7F_0$	17,300	0.026	0.042	0.090	0.12
	(R) $^5D_1 \rightarrow {}^7F_0$	18,800	0.016	2.0	3.2	4.0
	$^5D_2 \rightarrow {}^7F_0$	21,550	0.032	6.4	13	29
Sm^{3+}	(R) $^4F_{5/2} \rightarrow {}^6H_{5/2}$	18,000	0.23	--[b]	1.3	4.9
	? $\rightarrow {}^6H_{5/2}$	18,900	0.80	--	1.5	7.4
Dy^{3+}	(R) ? $\rightarrow {}^6H_{15/2}$	21,000	17.	14	~0	--[b]
	?? $\rightarrow {}^6H_{15/2}$	22,100	38.	69	85	--
	??? $\rightarrow {}^6H_{15/2}$	23,400	17.	17	~0	--

(a) Accuracy of results is about ± 35 %.

(b) Absorption spectra of these compounds not taken.

(c) (R) denotes transitions originating from a resonance level of the chelated rare earth ion.

Joos and Hellwege (39) report a value of 0.0276 sec.$^{-1}$ for the radiative transition probability of the $^5D_0 \rightarrow {}^7F_0$ transition of Eu^{3+} in the microcrystalline hydrated chloride. The value of 0.026 sec.$^{-1}$ calculated here from the absorption spectrum of the Eu^{3+} ion in an aqueous solution indicates that for these two different physical systems there is little difference in the local environment of the Eu^{3+} ion. The data presented in Table 3.3.1.3.1. also show that the probabilities for radiative transitions in chelated rare earth ions are, in general, equal to or greater than the probabilities for radiative transitions in hydrated rare earth chlorides. It is reasonable to assume that there is also a corresponding change in the radiative transition probabilities for transitions between the emitting level (R) and the electronic levels lying just above the ground state of the ion--transitions which could not be seen in the absorption spectrum of the ion. In view of these results, it can be concluded that variations in the radiative transition probabilities are not causing the observed differences between the decay times of the hydrated rare earth ions and the chelated rare earth ions. If the depopulation of the electronic states of the ion occurred only through emission of radiation, the data in Table 3.3.1.3.1. would indicate that the lifetimes of the chelated ions should be shorter than the lifetimes of the hydrated chlorides. The observed increase in lifetimes going from the hydrated chloride environment to the chelate environment can only mean that radiative transitions play a minor role in the depopulation of the

resonance levels of the hydrated ion while nonradiative quenching processes play a major role. The observed increases in the lifetimes are controlled by changes of the nonradiative transition probabilities.

From studies of the emission spectra and luminescence decay times of hydrated europium and terbium salts, both Rinck (10) and Geisler and Hellwege (11) have concluded that during the depopulation of the lowest resonance levels of these ions, about 2 % of the decays occurred via radiative transitions while ~98% of the decays occurred via radiationless processes. These authors concluded that if decays of the resonance levels of the Tb^{3+} and Eu^{3+} ion in the hydrated salts, $Eu(SO_4)_3 \cdot 8H_2O$ and $Tb(BrO_3)_3 \cdot 9H_2O$, were to occur via radiative processes only, the lifetimes of the resonance levels would be as long as fourteen milliseconds. The longest lifetime of any of the chelated rare earth ions (see Table 3.1.3.1.) is the 0.9 millisecond lifetime reported for the $TbA_3 \cdot H_2O$ complex. This is still short of the fourteen millisecond limit indicating that, even in the rare earth chelates, a considerable amount of quenching of the resonance levels of the rare earth ions is still occurring.

It is doubtful that the intrinsic radiative decay times of the lowest resonance levels of the Sm^{3+} and Dy^{3+} ions are as high as the fourteen millisecond limit computed for the Tb^{3+} and Eu^{3+} ions. Not only are the radiative transition probabilities larger in the Sm^{3+} and Dy^{3+} ions (see Table 3.3.1.3.1.), but there are more possibilities for radiative

combinations with lower lying electronic states. (Both Eu^{3+} and Tb^{3+} possess seven electronic states below the lowest resonance level while Dy^{3+} and Sm^{3+} possess ten and twelve respectively.) In spite of the increased probability for radiative transitions in the Sm^{3+} and Dy^{3+} ions, it is doubtful that the approximately ten microsecond decay times of these two ions can be attributed to radiative transitions alone. Quenching, in all probability, also plays a large role in the decay of the resonance levels of the two ions.

3.3.2. Nature of the Quenching Process in Complexed Rare Earth Ions

3.3.2.1. Possible Quenching Mechanisms. -- There are two general mechanisms postulated for the conversion of electronic energy of an atom or molecule to kinetic energy of nuclear motion (30). The conversion may occur by random collisions of the second kind, or it may occur through vibrational-electronic (vibronic) coupling of the atom or molecule to the surrounding matrix. In the former process, a random collision between an electronicly excited atom or molecule and another molecule converts the electronic energy of the former into translational or vibrational energy of the collision partners. Interactions need occur between the collision partners only during the collision.

Quenching of the electronic energy of an ion through vibronic coupling of the ion to the surrounding lattice arises from the fact that the electrons of the ion interact electro-

statically with the adjacent atoms or molecules. The surrounding atoms and molecules are not static, but rather they are moving according to the vibrational modes of the crystal. The electrostatic interactions between the electrons of the ion and the dynamic lattice couples the electronic energy of the ion to vibrational motion of the lattice. In effect, vibrational energy levels are superimposed upon the pure electronic levels of the ion. The spacing between levels is dependent upon the frequency of the vibrational modes of the surrounding lattice.

The results of these vibronic interactions are twofold: (a) electronic energy of the ion may be converted completely to vibrational energy of the lattice (vibronic quenching), and (b) radiative combinations between electronic states accompanied by simultaneous transitions between vibrational states of the lattice result in the appearance in the spectra of vibrational satellites next to the spectral line corresponding to the pure electronic transition. The vibrational satellites may appear as distinct lines or they many manifest themselves as line broadening.

Van Uitert (40,41,42,43) has observed a third type of quenching which is dependent upon the concentration of the rare earth ion. From his studies of the luminescences of the alkali tungstates or molybdates doped with Tb^{3+}, Eu^{3+}, Er^{3+}, or Dy^{3+} ions he reported that for high concentrations of the rare earth ions in the crystalline materials the luminescence intensity showed a marked decrease. The author considered the

concentration quenching effect to arise from either rare earth ion-rare earth ion interactions or changes of the crystal structure of the material. Either of these effects are believed to ultimately increase the efficiency of vibronic quenching of the rare earth ion states. Concentration quenching thus appears to be, in some respects, a more complicated case of vibronic quenching.

3.3.2.2. Correlation Between the Quenching Efficiency and the Electronic Structure of the Rare Earth Ions. -- When reporting the luminescence decay times of the microcrystalline rare earth chlorides, Dieke and Hall (30) observed that the rare earth ions possessing the longest decay times also possessed the largest energy gap between the lowest resonance level of the ion and the next lowest electronic state of the ion. In Table 3.3.2.2.1. this energy gap between electronic states is compared with both Dieke and Hall's data on rare earth chlorides and the data on rare earth chelates taken from Table 3.1.3.1. The data reveal that this relationship between the energy gap and the magnitude of the decay time of the rare earth ion holds for the chelated rare earth ions as well as for the solvated rare earth ions in the chloride salts. Since efficient quenching of the ion levels is associated with a short lifetime, it can be concluded that the most efficient quenching is associated with those rare earth ions possessing the smallest energy gap between the resonance level and the next lower electronic state.

This last conclusion is almost a rewording of the

TABLE 3.3.2.2.1.

A COMPARISON OF THE LUMINESCENCE DECAY TIMES OF COMPLEXED RARE EARTH IONS WITH THE ENERGY GAPS BETWEEN THE ELECTRONIC STATES OF THE RARE EARTH IONS

Ion	Energy Gap Between Resonance Level and Next Lower Electronic Level in $cm.^{-1}$ [a]	Mean Lifetime of Resonance Level in Microseconds			
		$MCl_3 \cdot 6H_2O$ [a] Solid at 77°K	$MB_3 \cdot 2H_2O$ in EMPA at 77°K	MD_3 in EMPA at 77°K	$MA_3 \cdot H_2O$ in EMPA at 77°K
Gd^{3+}	32,100	7800	--[b]	--[b]	--[b]
Tb^{3+}	16,400	487	630	464	901
Eu^{3+}	12,200	120	430	361	564
Sm^{3+}	7,300	~10	14.1	20.1	--[c]
Dy^{3+}	6,500	~10	12.3	--[b]	--[c]

[a] Taken from data reported by Dieke and Hall (30).

[b] Rare earth ion emission not observed from these chelates.

[c] Rare earth ion emission observed, but too weak to record.

general law governing collisions of the second kind (35), i.e., the quenching efficiency is greater the less the energy which needs to be converted to kinetic energy of nuclear motion. This is not evidence, however, for discarding vibronic quenching of the electronic states. Gouterman (44) has also predicted that quenching arising from vibronic coupling becomes forbidden if there is too much electronic energy to be converted to vibrational energy of the lattice. Regardless of the quenching mechanism, it is apparent from the data of Table 3.3.2.2.1., that there is much less quenching of the resonance level of the Gd^{3+} ion than of any other ion studied. In fact, the lifetime of the $GdCl_3 \cdot 6H_2O$ crystals at $77^{o}K$ (30) is almost the same order of magnitude as the fourteen millisecond limit predicted for the Eu^{3+} and Tb^{3+} ions in the absence of quenching.

3.3.2.3. Evidence for Vibronic Coupling as Derived from the Emission Spectra of the Solid Rare Earth Complexes. -- The mechanism of quenching of electronic energy through vibronic interactions is shown in Fig. 3.3.2.3.1. This figure shows representative potential energy curves of the electronic configurations associated with a resonance level, R, and some lower level, L. Associated with each electronic state are lattice vibrational energy levels k. A rare earth ion excited to the k' vibrational level of the excited electronic state R will rapidly lose its excess vibrational energy to the surrounding lattice and fall to a lower vibrational level O' of the level R. At this point the electronic energy of the state R may be completely converted to vibrational energy resulting in the

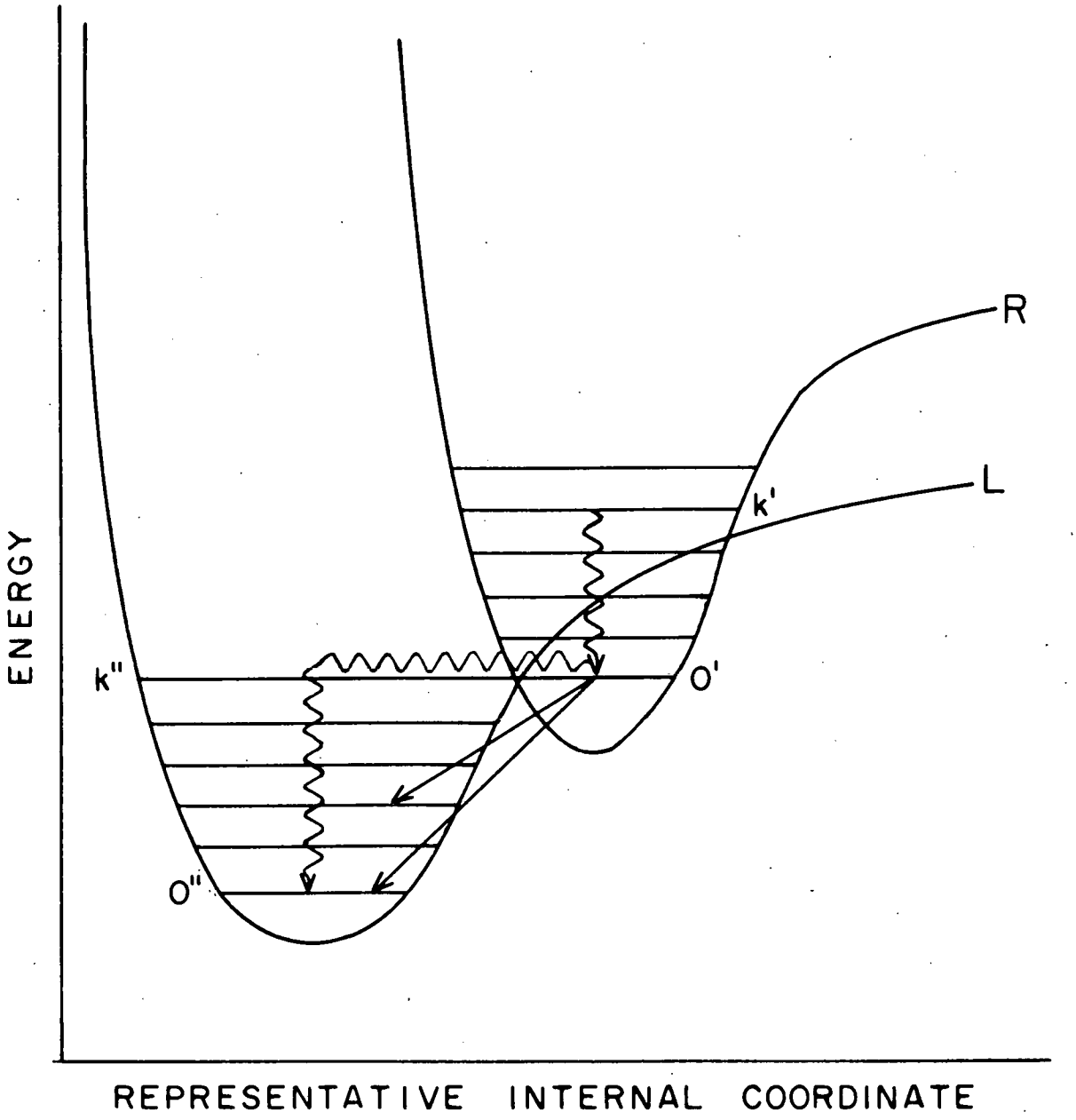

Fig. 3.3.2.3.1.--Energy dissipation via internal conversion, vibrational deactivation, and emission of radiation. (R and L denote potential energy wells of the resonance level and the lower ground state respectively of the complexed rare earth ion. O and k designate vibrational levels of the electronic system.)

⟶ radiative combinations

∿∿∿∿ nonradiative combinations

"crossing" of the system to the k'' vibrational level of the electronic state L. Rapid loss of the excess vibrational energy converts the system to some lower vibrational level O'' of the electronic state L. On the other hand, the system in the lower vibrational state O' of the excited electronic state R may lose its electronic energy via the emission of radiation. Radiative combinations between the electronic state R and the various vibrational levels k'' of the lower electronic state give rise to vibrational satellites in the emission spectra. This process is illustrated in detail in Fig. 3.3.2.3.2.

To determine whether such vibronic coupling occurs in rare earth complexes, a detailed study was made of visible emission spectra of solid rare earth compounds. Rare earth oxides dissolved in sodium metaphosphate glasses, microcrystalline rare earth chlorides solvated either with water or with deuterium oxide, and microcrystalline rare earth chelates were used for the investigation. The emission spectra of these complexes at 77°K are reported in Fig. 3.3.2.3.3. through Fig. 3.3.2.3.7.

Assignments of groups of lines to transitions between particular electronic states of the rare earth ion are indicated in the figures. The simplicity of the emission spectra of complexes of Tb^{3+}, Sm^{3+}, and Dy^{3+} allows unambiguous assignments to be made on the basis of energy differences determined from the energy level diagram of Fig. 3.1.2.2.

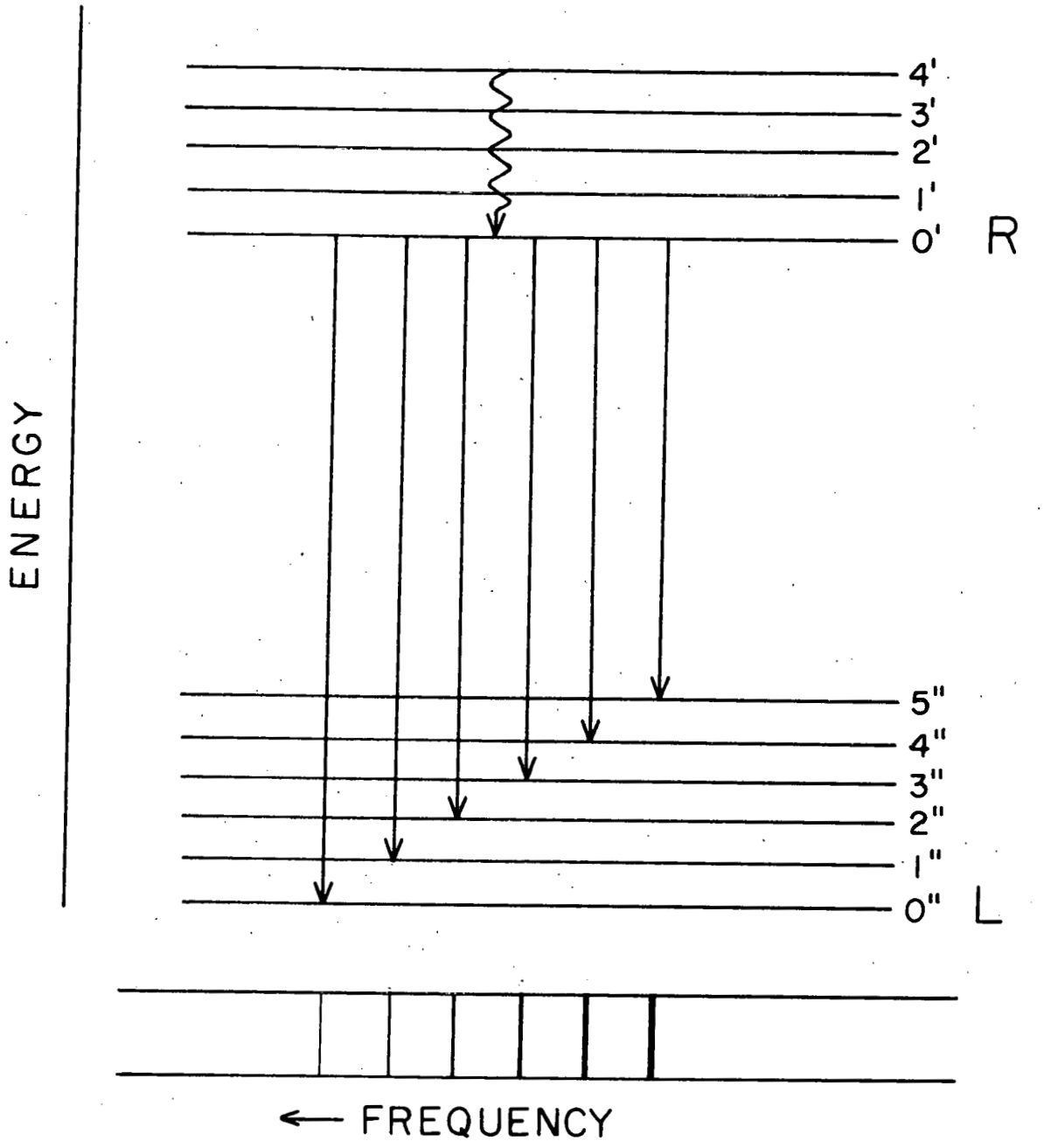

Fig. 3.3.2.3.2.--Schematic diagram illustrating the origin of the vibrational satellites in the emission spectra of complexed rare earth ions. (Upper part of diagram shows a representative energy level diagram for the complexed rare earth ions, while the lower portion represents the emission spectrum which would arise from the indicated transitions.)

Fig. 3.3.2.3.3.--Emission spectra of complexes of samarium. (For definitions of symbols see Fig. 3.1.2.3.)

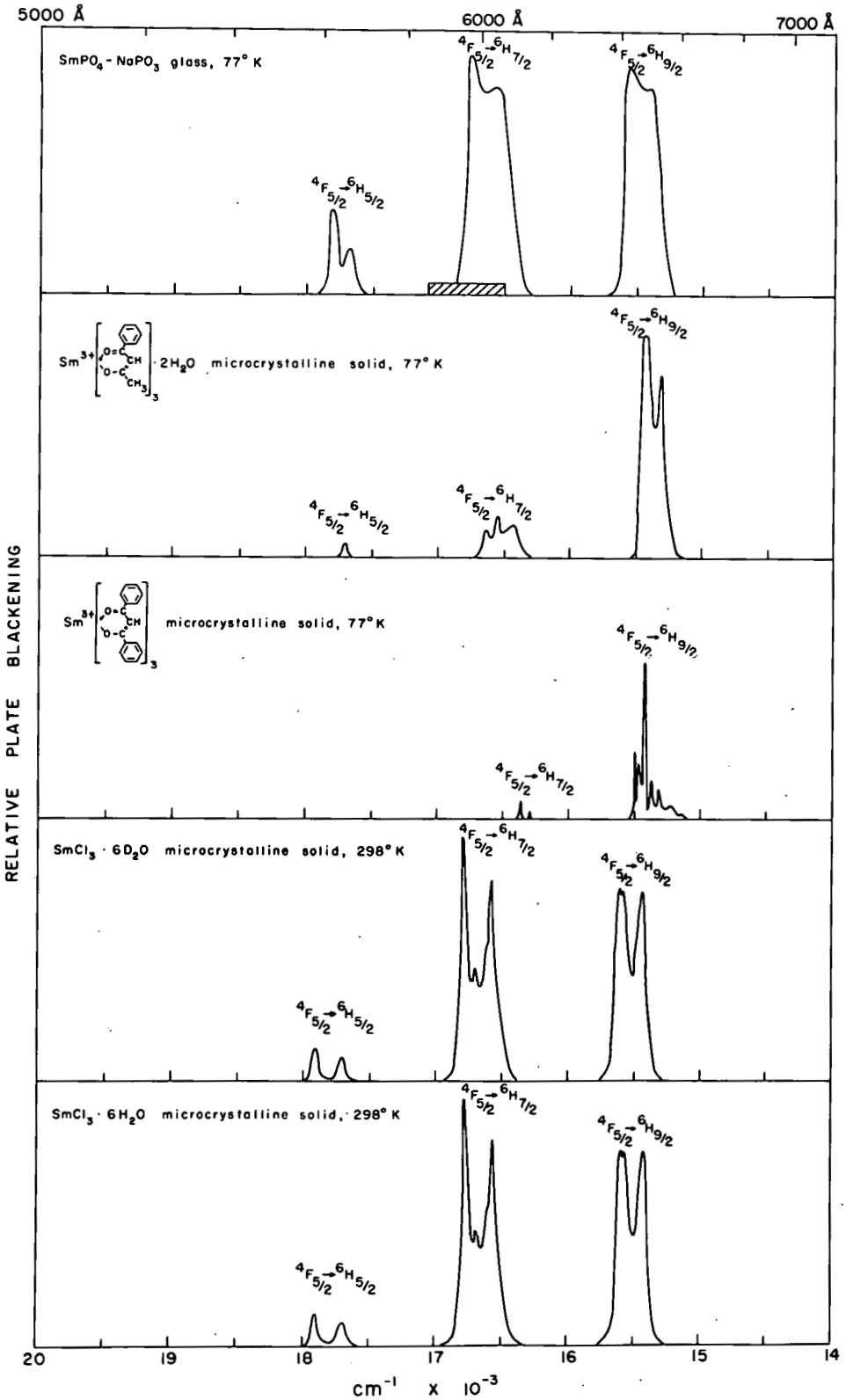
5000 Å
6000 Å
7000 Å
$SmPO_4$ - $NaPO_3$ glass, 77° K
$^4F_{5/2} \rightarrow {}^6H_{5/2}$
$^4F_{5/2} \rightarrow {}^6H_{7/2}$
$^4F_{5/2} \rightarrow {}^6H_{9/2}$
Sm^{3+} $\cdot 2H_2O$ microcrystalline solid, 77° K
microcrystalline solid, 77° K
$SmCl_3 \cdot 6D_2O$ microcrystalline solid, 298° K
$SmCl_3 \cdot 6H_2O$ microcrystalline solid, 298° K
RELATIVE PLATE BLACKENING
20
19
18
17
16
15
14
cm^{-1} x 10^{-3}

Fig. 3.3.2.3.4.--Emission spectra of complexes of dysprosium.

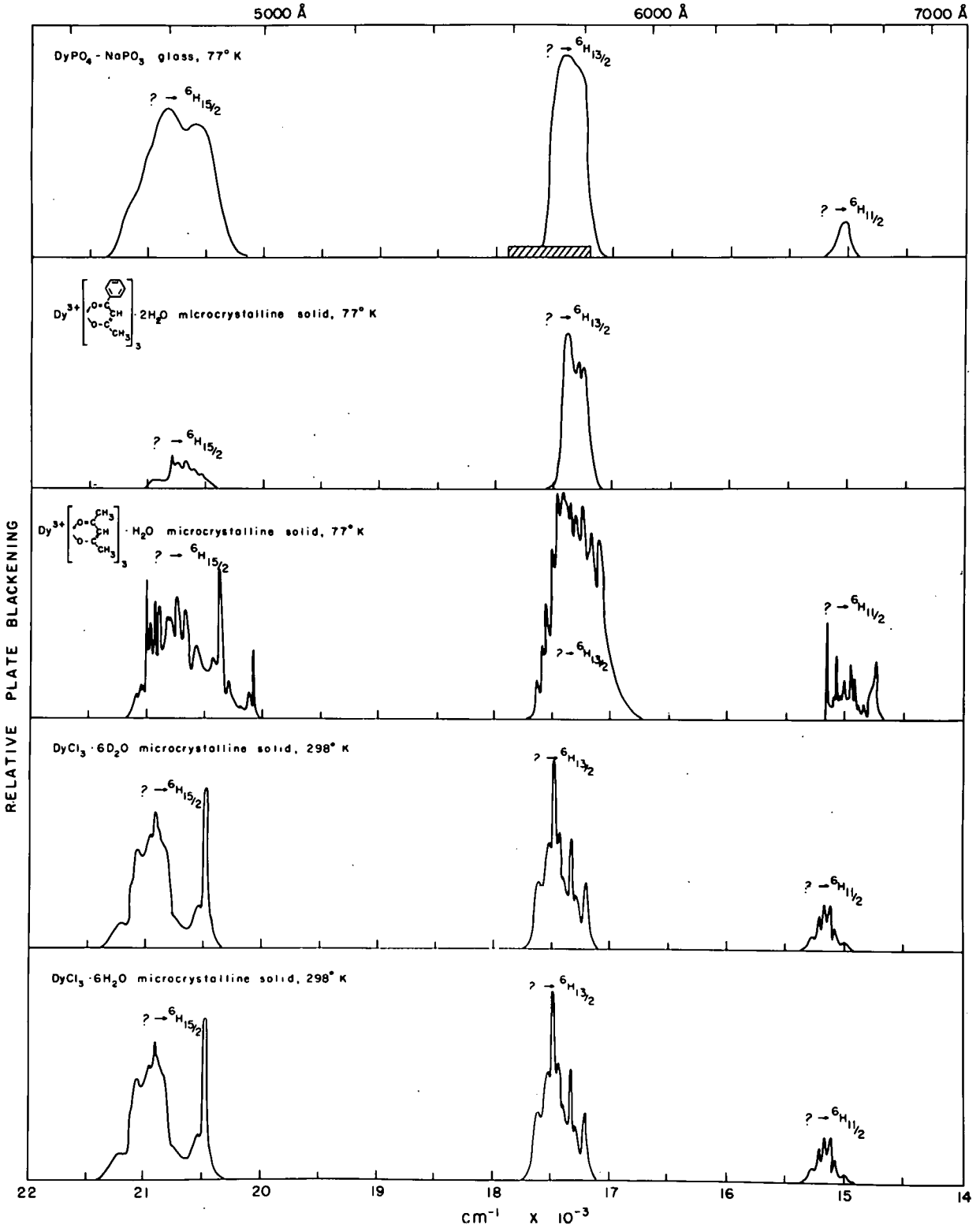
5000 Å
6000 Å
7000 Å
DyPO4 - NaPO3 glass, 77° K
? → 6H15/2
? → 6H13/2
? → 6H11/2
Dy3+ [ ] · 2H2O microcrystalline solid, 77° K
? → 6H15/2
? → 6H13/2
Dy3+ [ ] · H2O microcrystalline solid, 77° K
? → 6H15/2
? → 6H13/2
? → 6H11/2
DyCl3 · 6D2O microcrystalline solid, 298° K
? → 6H15/2
? → 6H13/2
? → 6H11/2
DyCl3 · 6H2O microcrystalline solid, 298° K
? → 6H15/2
? → 6H13/2
? → 6H11/2
RELATIVE PLATE BLACKENING
22
21
20
19
18
17
16
15
14
cm-1 x 10-3

Fig. 3.3.2.3.5.--Emission spectra of complexes of terbium

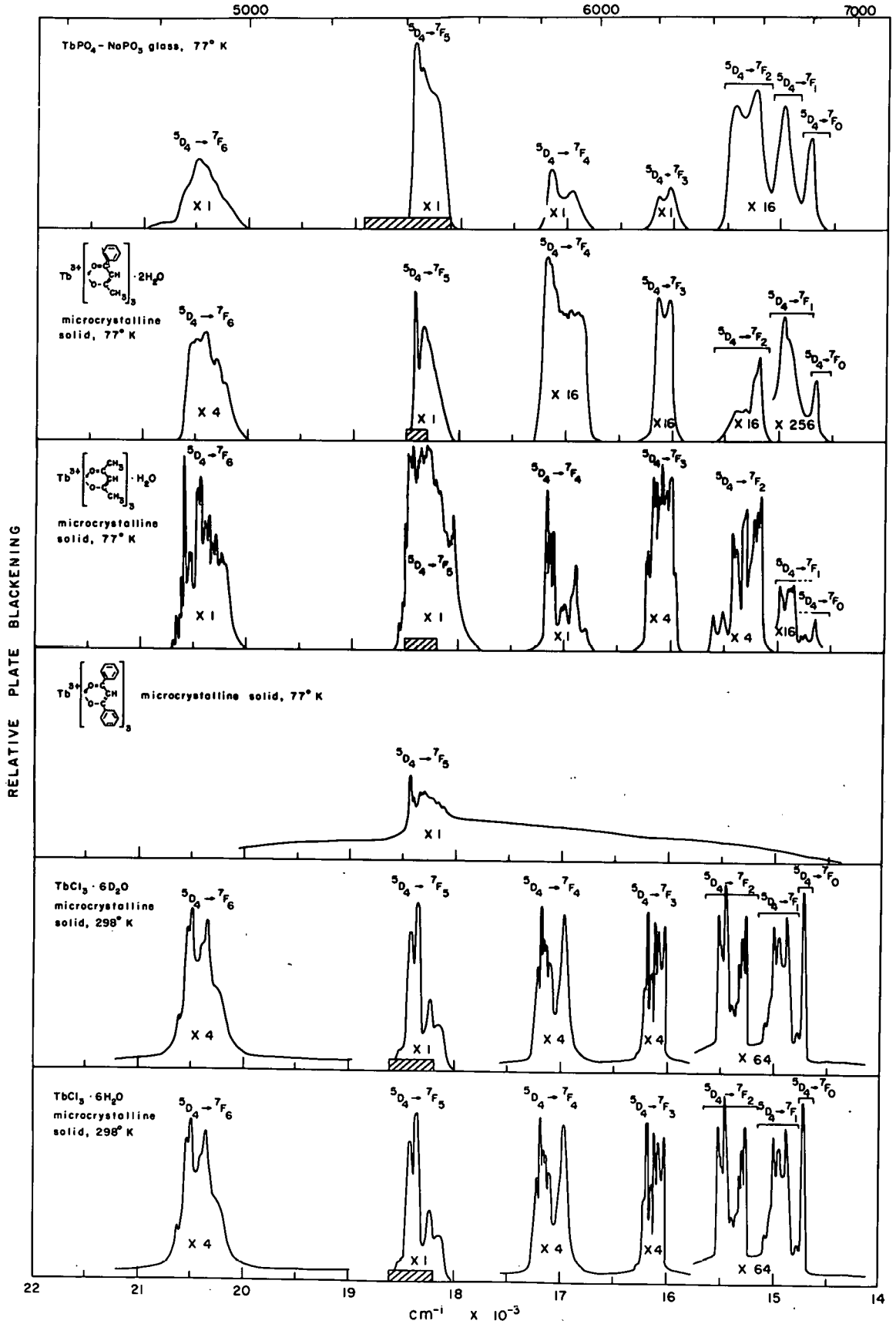
5000
6000
7000
TbPO4 - NaPO3 glass, 77° K
5D4→7F6
5D4→7F5
5D4→7F4
5D4→7F3
5D4→7F2
5D4→7F1
5D4→7F0
X 1
X 1
X 1
X 1
X 16
microcrystalline solid, 77° K
X 4
X 1
X 16
X 1
X 16
X 256
microcrystalline solid, 77° K
X 1
X 1
X 1
X 4
X 4
X16
microcrystalline solid, 77° K
X 1
TbCl3 · 6D2O microcrystalline solid, 298° K
X 4
X 1
X 4
X 4
X 64
TbCl3 · 6H2O microcrystalline solid, 298° K
X 4
X 1
X 4
X4
X 64
RELATIVE PLATE BLACKENING
22
21
20
19
18
17
16
15
14
cm-1 x 10-3

Fig. 3.3.2.3.6.--Emission spectra of $EuPO_4$ in $NaPO_3$ glass at 77°K and microcrystalline $EuB_3 \cdot 2H_2O$ and EuD_3 at 77°K.

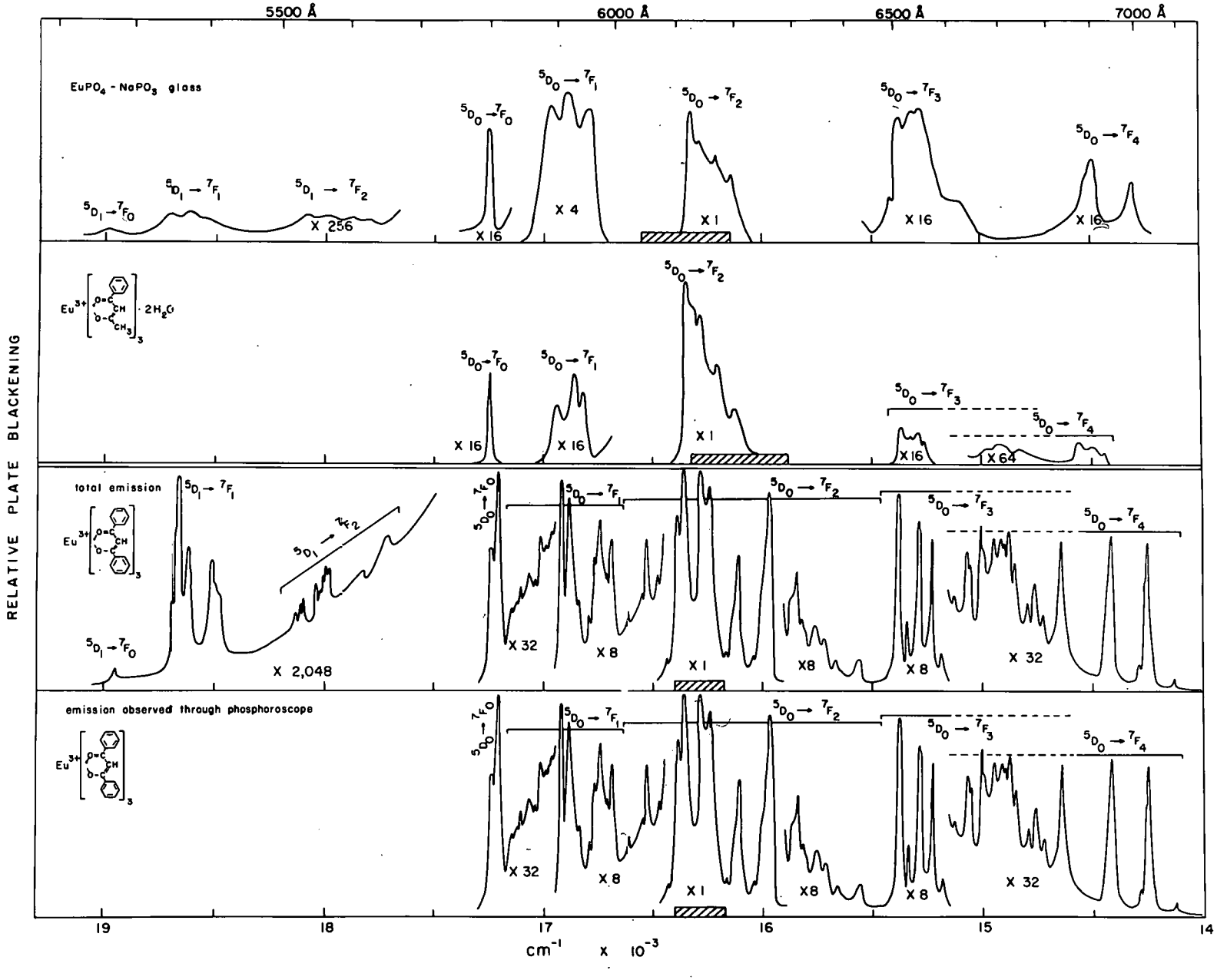
5500 Å
6000 Å
6500 Å
7000 Å
EuPO4 - NaPO3 glass
5D1 → 7F0
5D1 → 7F1
5D1 → 7F2
5D0 → 7F0
5D0 → 7F1
5D0 → 7F2
5D0 → 7F3
5D0 → 7F4
X 256
X 16
X 4
X 1
X 16
X 16
Eu3+ [ ]3 · 2H2O
X 16
X 16
X 1
X 16
X 64
total emission
5D1 → 7F0
5D1 → 7F1
5D1 → 7F2
X 2,048
5D0 → 7F0
X 32
X 8
X 1
X8
X 8
X 32
emission observed through phosphoroscope
X 32
X 8
X 1
X8
X 8
X 32
RELATIVE PLATE BLACKENING
19
18
17
16
15
14
cm-1 x 10-3

Fig. 3.3.2.3.7.--Emission spectra of microcrystalline $EuA_3 \cdot H_2O$ at 77°K and microcrystalline $EuCl_3 \cdot 6D_2O$ and $EuCl_3 \cdot 6H_2O$ at 298°K.

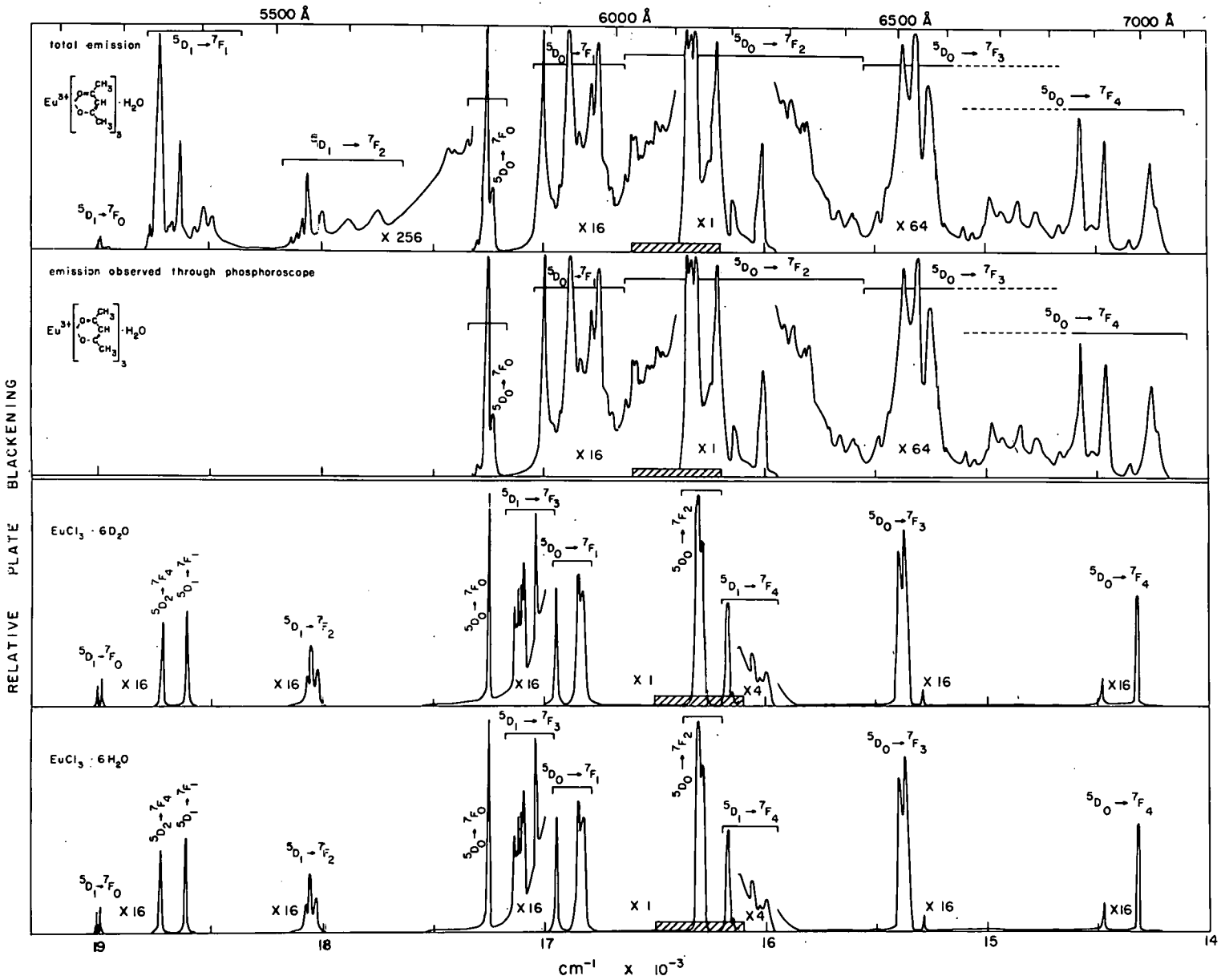
5500 Å
6000 Å
6500 Å
7000 Å
total emission
$Eu^{3+}[O-C(CH_3)=CH-C(CH_3)=O]_3 \cdot H_2O$
$^5D_1 \rightarrow {}^7F_1$
$^5D_1 \rightarrow {}^7F_2$
$^5D_1 \rightarrow {}^7F_0$
$^5D_0 \rightarrow {}^7F_0$
$^5D_0 \rightarrow {}^7F$
$^5D_0 \rightarrow {}^7F_2$
$^5D_0 \rightarrow {}^7F_3$
$^5D_0 \rightarrow {}^7F_4$
X 256
X 16
X 1
X 64
emission observed through phosphoroscope
$Eu^{3+}[O-C(CH_3)=CH-C(CH_3)=O]_3 \cdot H_2O$
$EuCl_3 \cdot 6D_2O$
$EuCl_3 \cdot 6H_2O$
$^5D_2 \rightarrow {}^7F_4$
$^5D_1 \rightarrow {}^7F_1$
$^5D_1 \rightarrow {}^7F_3$
$^5D_0 \rightarrow {}^7F_1$
$^5D_0 \rightarrow {}^7F_2$
$^5D_1 \rightarrow {}^7F_4$
X 4
RELATIVE PLATE BLACKENING
19
18
17
16
15
14
cm^{-1} x 10^{-3}

The assignments of lines in the emission spectra of solvated europium chloride were taken from the work of DeShazer and Dieke (8).

Analysis of the emission spectra of europium chelates was accomplished by comparing the total emission spectra and the emission spectra recorded through the phosphoroscope. (This technique is described in Section 3.1.2.) The only lines in the emission spectra of europium chelates which could be assigned to $^5D_1$ transitions were found in the blue end of the spectrum between 17,000 cm.$^{-1}$ and 19,000 cm.$^{-1}$. While four more groups of lines arising from $^5D_1$ transitions are predicted to lie in the red end of the spectrum, they were evidently so weak that they could not be detected by the above mentioned method. $^5D_1$ lines also appeared in the blue end of the total emission spectrum of $EuB_3 \cdot 2H_2O$, but they were too weak to be readily recorded.

With the exception of one compound, (TbD_3), there were no gross differences between the spectra of microcrystalline rare earth chelates and the spectra of rare earth chelates dissolved in EMPA glasses at 77^{o}K (see Figs. 3.1.2.3. and 3.1.2.4.). While the line emission of the benzoylacetonate complexes was sharper for the chelate in the EMPA glasses than it was from the microcrystalline material, the reverse was found to be true for the dibenzoylmethide and acetylacetonate chelates. The nearly complete absence of Tb^{3+} emission in the emission spectrum of the microcrystalline solid was caused by a shift of the triplet level of the complex on

going from the EMPA glass to the microcrystalline solid. This phenomenon is discussed more fully in the last section of the Discussion.

The diffuse nature of the line emission of the rare earth ions embedded in metaphosphate glasses was due to the completely amorphous nature of the glasses. The lack of regularity in the electrostatic environments of the rare earth ions "smears" the electronic energy levels of the ion. Radiative transitions between such levels result in the observed diffuse bands. The sharpness of the emission spectra of the solvated chlorides and chelates is characteristic of emissions from rare earth ions located in environments possessing uniform symmetry.

Vibronic coupling is clearly visible in the emission spectra of the solid dibenzoylmethide and acetylacetonate complexes. This coupling manifests itself in two ways: (a) the appearance of more spectral lines in a given energy region than are allowed for radiative combinations between pure electronic states, and (b) the appearance of regular vibrational progressions to the side of a sharp electronic transition. In the emission spectra of EuD_3 and $EuA_3 \cdot H_2O$, transitions from the nondegenerative $^5D_0$ state to the nondegenerate $^7F_0$ level, the threefold degenerate $^7F_1$ level, and the fivefold degenerate $^7F_2$ state are all characterized by more spectral lines than are possible for radiative combinations between pure electronic states. The excess lines must arise from transitions between vibrational levels superimposed upon the

electronic levels of the ion. While only one spectral line is predicted for the $^5D_0 \rightarrow {}^7F_0$ transition of Eu^{3+}, both $EuA_3 \cdot H_2O$ and EuD_3 possess more than one line in the spectrum corresponding to this transition. Details of the structure of this transition are shown in Fig. 3.3.2.3.8.

In general, the emission spectra of the dibenzoylmethide or acetylacetonate chelates are much too complex for a unique resolution of the spectra into pure electronic transitions plus vibrational progressions. For a few lines of the $TbA_3 \cdot H_2O$ and $DyA_3 \cdot H_2O$ emissions, however, this identification is possible. Details of these emissions lines are shown in Figs. 3.3.2.3.9 and 3.3.2.3.10. Vibrational progressions are found lying to the short wave length side of the 4856 Å, 5425 Å, and 5446 Å lines of the Tb^{3+} emission; while vibrational progressions are found lying to the short wave length side of the 5726 Å line and to the long wave length side of the 5742 Å line of the Dy^{3+} emission. The wave lengths, frequencies, and frequency differences of these lines are summarized in Table 3.3.2.3.1. The progressions listed here, which vary in frequency from 6 $cm.^{-1}$ to 50 $cm.^{-1}$, are of the same order of magnitude as the 19 $cm.^{-1}$ progression found by Satten (45) in the spectra of the hydrated salts of neodymium and the 40 $cm.^{-1}$ to 60 $cm.^{-1}$ found by Whan (22) in the emission spectra of the rare earth benzoylacetonate and dibenzoylmethide chelates dissolved in EMPA glasses at 77°K.

No vibrational satellites are found in the emission spectra of inorganic salts of the rare earth ions. They are detected, however, in the absorption spectra of very concen-

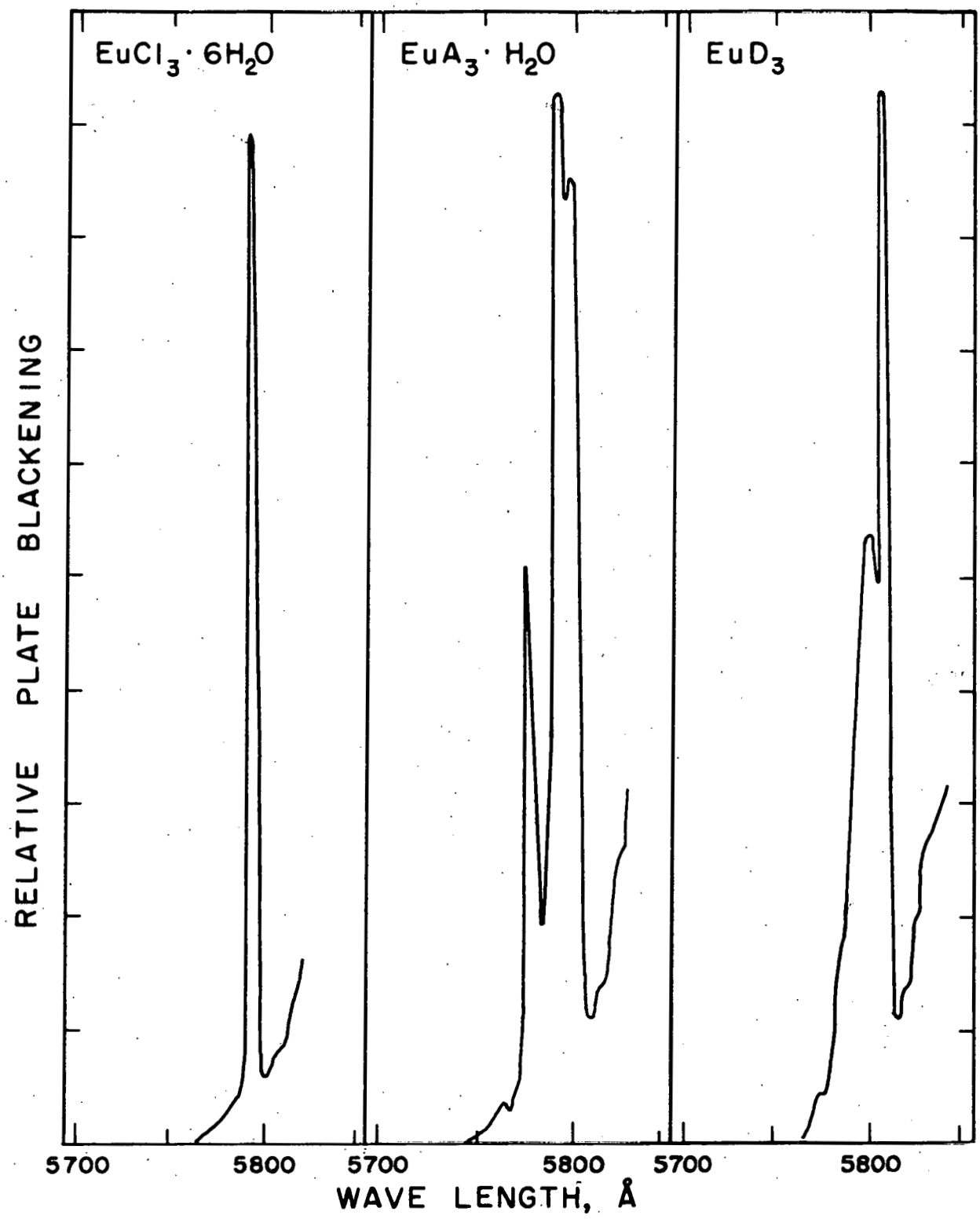

Fig. 3.3.2.3.8.--The $^5D_0 \rightarrow {}^7F_0$ transition observed in the emission spectra of microcrystalline complexes of trivalent europium at 77°K.

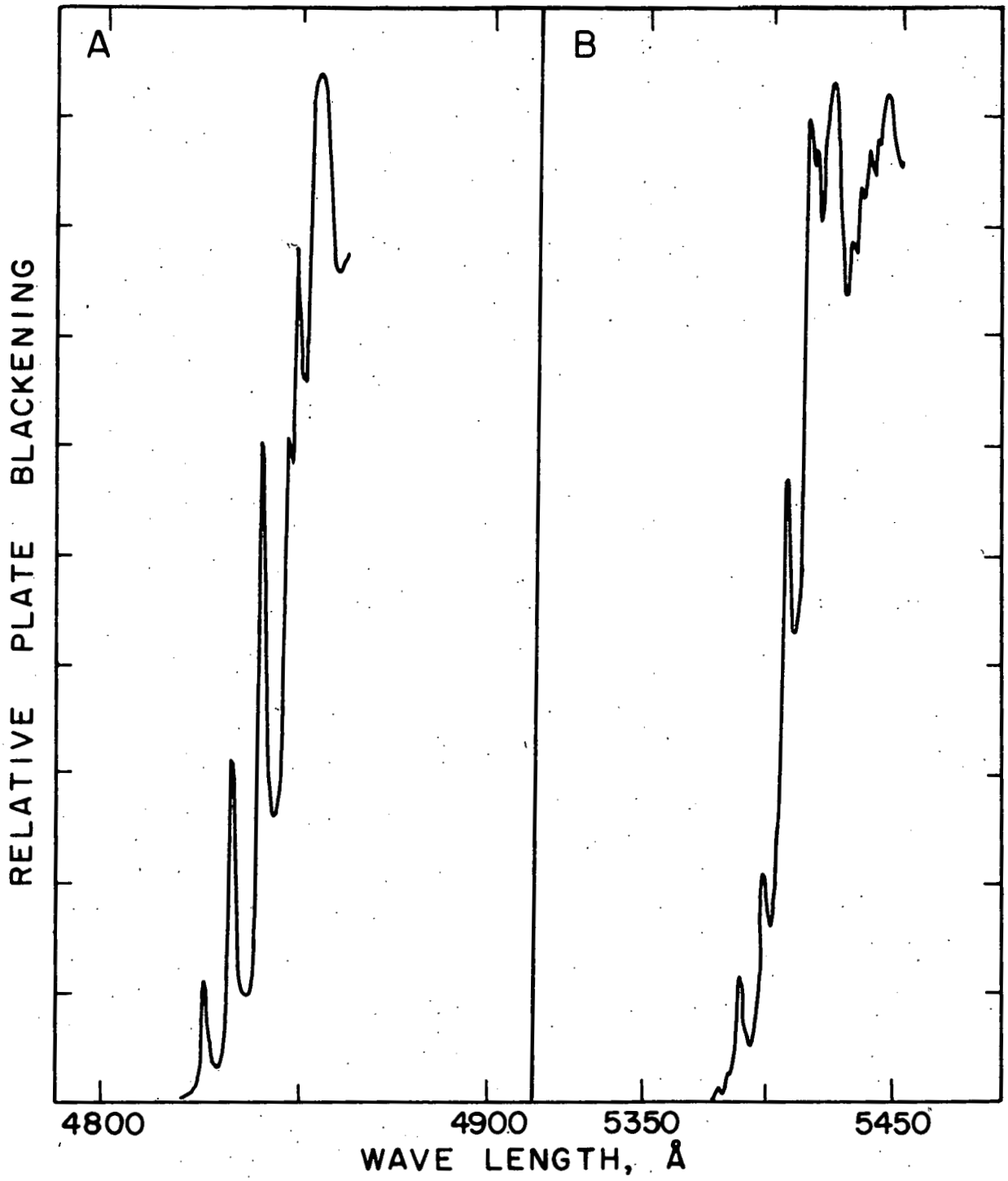

Fig. 3.3.2.3.9.--Fine structure of the emission spectrum of microcrystalline $TbA_3 \cdot H_2O$ at 77°K.

A. Short wave length side of the $^5D_4 \longrightarrow {}^7F_6$ transition

B. Short wave length side of the $^5D_4 \longrightarrow {}^7F_5$ transition

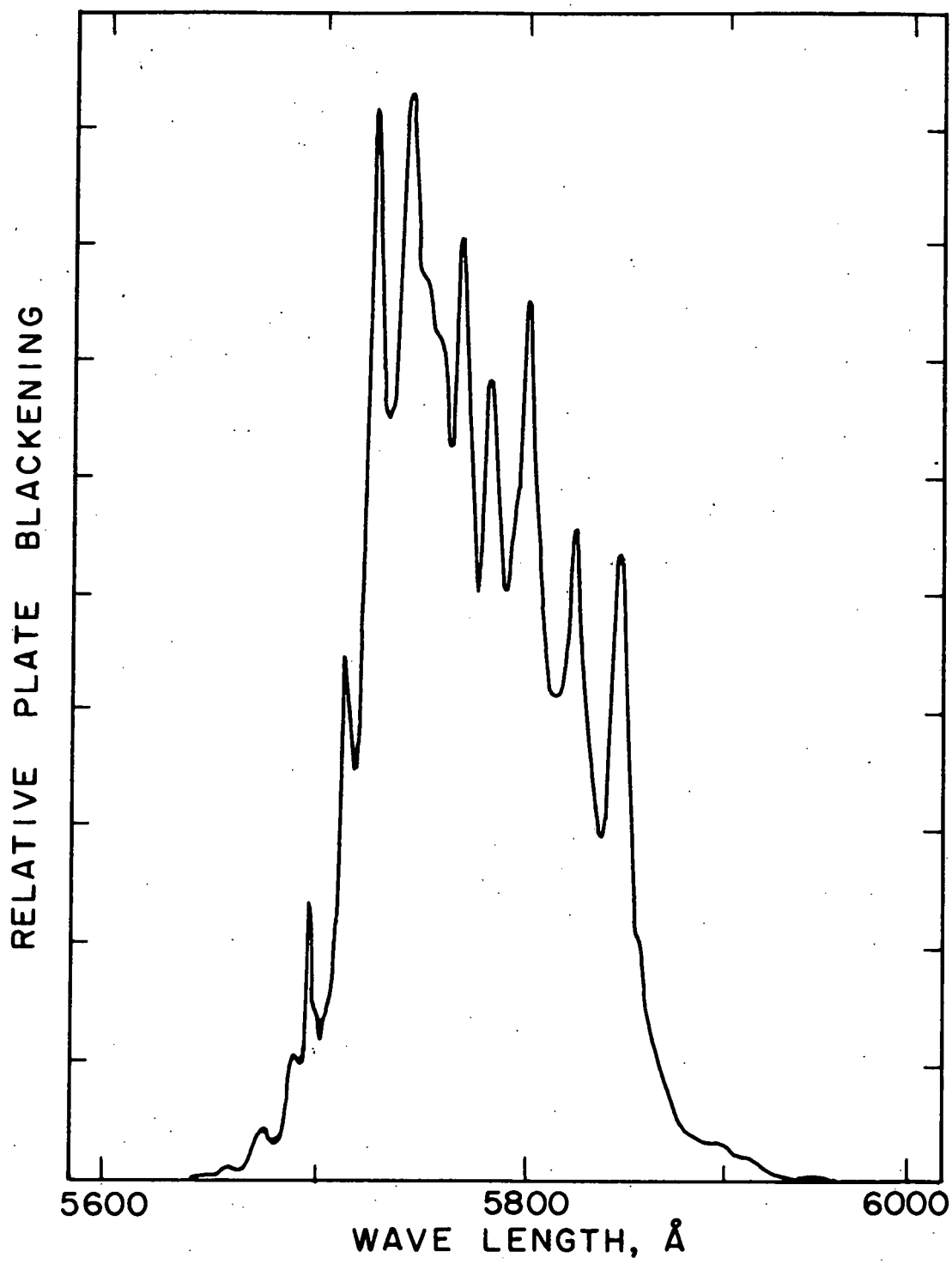

Fig. 3.3.2.3.10.--Fine structure of the ? $\longrightarrow {}^{6}H_{13/2}$ transition observed in the emission spectrum of microcrystalline $DyA_3 \cdot H_2O$ at 77°K.

TABLE 3.3.2.3.1.

LINE PROGRESSIONS IN THE EMISSION SPECTRA OF MICROCRYSTALLINE RARE EARTH CHELATES AT 77°K

Compound	Transition	Wave Length, Å	Frequency, $cm.^{-1}$	Frequency Differences, $cm.^{-1}$
$EuA_3 \cdot H_2O$	$^5D_0 \rightarrow {}^7F_0$	5780	17,296	
				50
		5797	17,246	
				12
		5801	17,234	
EuD_3	$^5D_0 \rightarrow {}^7F_0$	5800	17,237	
				30
		5810	17,207	
$TbA_3 \cdot H_2O$	$^5D_4 \rightarrow {}^7F_6$	4825	20,720	
				30
		4832	20,690	
				30
		4839	20,660	
				30
		4846	20,630	
				13
		4849	20,617	
				30
		4856	20,587	
$TbA_3 \cdot H_2O$	$^5D_4 \rightarrow {}^7F_5$	5386	18,561	
				34
		5396	18,527	
				31
		5405	18,496	
				31
		5414	18,465	
				6
		5416	18,459	
				28
		5424	18,431	

TABLE 3.3.2.3.1. (Continued)

Compound	Transition	Wave Length, Å	Frequency, $cm.^{-1}$	Frequency Differences, $cm.^{-1}$
		5432	18,404	
				13
		5436	18,391	
				10
		5439	18,381	
				11
		5442	18,370	
				13
		5446	18,357	
$DyA_3 \cdot H_2O$	? $\longrightarrow {}^6H_{13/2}$	5670	17,632	
				50
		5686	17,582	
				25
		5694	17,557	
				52
		5711	17,505	
				46
		5726	17,459	
		5742	17,411	
				24
		5750	17,387	
				22
		5757	17,365	

trated aqueous solutions and single crystals of the salts (45,46). Regardless of whether the vibrational satellites are detected in the emission spectra or the absorption spectra of the ion, the appearance of the vibrational satellites reveals the existence of vibronic coupling of the electronic states of the 4f electrons of the rare earth ion to the vibrational modes of the surrounding atoms or molecules.

The vibrational modes involved in the coupling mechanism must undoubtedly involve motion of atoms or ions close enough to the rare earth ion for significant electrostatic interaction to take place. Whan (22) suggested that low frequency rare earth ion-ketone oxygen vibrations are involved in the quenching. In a discussion by Freed (46), however, it is reported that the vibrational frequencies found in the absorption spectrum of $3Mg(NO_3)_2 \cdot 2Nd(NO_3)_3 \cdot 24H_2O$ were significantly decreased when the water was replaced with deuterium oxide. It would appear that in solvated salts, at least, the vibrational modes must involve motion of the entire water molecule, not just the oxygen atoms alone. Not enough data are presented here to identify the vibrational modes involved in the coupling mechanism. Additional information can be obtained, however, from the luminescence decay data presented in the next two sections.

3.3.2.4. The Efficiency of Quenching as Derived from Luminescence Decay Times of Solid Rare Earth Complexes. -- An investigation of the luminescence decay times of solid rare earth complexes was undertaken to determine the relationship

between quenching efficiency and the nature of the complexing species. The same compounds used in the spectroscopic studies described in Section 3.3.2.3. were also used for the luminescence decay time studies. Light filter combinations were selected to pass sample emission corresponding to the brightest group of lines in the rare earth ion emission spectra which originate from the lowest resonance level of the ion. In the case of the solvated $EuCl_3$ salts, the light filter combination passed a small amount of light originating from the $^5D_1$ state as well as the light originating from the $^5D_0$ state. Because light originating from the $^5D_1$ state was so weak and short lived, however, it did not interfere with decay time measurements of the light originating from the $^5D_0$ level. Spectral regions passed by the light filters are indicated by cross-hatched bars in Fig. 3.3.2.3.3. through Fig. 3.3.2.3.7.

Mean lifetimes of the lowest resonance levels of the solid rare earth complexes are summarized in Table 3.3.2.4.1. With the exception of the sodium metaphosphate glasses, all the data in this table are reported for the complexes in the microcrystalline solid state. Some additional data on hydrated inorganic salts reported by Dieke and Hall (30) are also included in the table for purposes of comparison.

The rare earth compounds listed in this table are grouped according to the ligands believed to be adjacent to the rare earth ion. The inorganic salts are classified according to whether they are solvated with water or with deuterium oxide, for the water molecules are closer to the rare

TABLE 3.3.2.4.1.

LUMINESCENCE DECAY TIMES OF SOLID RARE EARTH COMPLEXES AT $77^{o}K$

Ligand Class	Compound	Mean Lifetime in Microseconds			
		Tb^{3+}	Eu^{3+}	Sm^{3+}	Dy^{3+}
$PO_4^{\equiv}$	MPO_4-$NaPO_3$ glass	3120	3090	⟨2200⟩ (b)	⟨742⟩ (b)
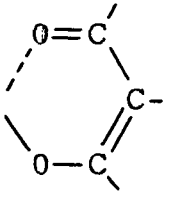	$MA_3 \cdot H_2O$	760	385	--(d)	--(d)
	MD_3	--(e)	460	--(d)	--(d)
	$MB_3 \cdot 2H_2O$	650(c)	466	--(d)	--(d)
D_2O	$MCl_3 \cdot 6D_2O$	721	276	--(d)	--(d)
	$MCl_3 \cdot 6H_2O$	483	122	~10(a)	~10(a)
H_2O	$M(BrO_3)_3 \cdot 9H_2O$	---	120(a)	---	~10(a)
	$M(CH_3CH_2SO_4)_3 \cdot 9H_2O$	430	---	---	~10(a)

(a) Data reported by Dieke and Hall (30).

(b) Semilogarithmic plot is curved. Lifetime represents an average for the curve.

(c) Semilogarithmic plot is curved. Lifetime calculated from long-lived component.

(d) Emission too weak to record.

(e) No emission observed from this compound.

earth ions than are the anions of the salts (47).

The data in Table 3.3.2.4.1. show the following regularities:

(1) For a given ion, a regular decrease in the luminescence decay time is found in the series: phosphates, chelates, D_2O salts, H_2O salts.

(2) For a given ligand class, a regular decrease in the luminescence decay time is found in the series of rare earth ions: Tb^{3+}, Eu^{3+}, Sm^{3+}, Dy^{3+}.

(3) Little differences are found among the luminescence decay times of hydrated inorganic salts of a rare earth ion when the salts differ only by the anion.

(4) Because quenching efficiency is inversely proportional to the luminescence decay time, the quenching efficiency is found to increase according to the series of ligands: phosphates, chelates, D_2O salts, H_2O salts.

The metaphosphate glasses, which exhibit the longest luminescence decay times, have lifetimes approaching the predicted fourteen millisecond intrinsic radiative lifetime limit.

As was pointed out earlier, the efficiency of quenching by collisions of the second kind is inversely proportional to the amount of electronic energy to be dissipated. If the quenching of a complexed rare earth ion were due primarily to collisions of the second kind, then changes in the environment of the ion, which result in major changes in quenching efficiency, must be accompanied by major changes in the

electronic energy to be dissipated. Although environmental changes of the complexed rare earth ion do result in significant changes in quenching efficiency, the emission spectra of the rare earth ion in the various environments indicate that, while small shifts of tens of wave numbers occur in the positions of the electronic levels of the rare earth ion, there are no major changes in the energies of the electronic levels. Second order collisions, therefore, are not the primary cause of quenching of rare earth ion resonance levels. The primary cause of quenching of rare earth ion resonance levels must be vibronic interactions.

Although it is true that the efficiency of vibronic quenching is very low for vibrational frequencies which are too large (44), it is also believed that for a given amount of electronic energy the efficiency of vibronic quenching is proportional to the frequency of the lattice mode which dissipates the energy. The marked increase of the lifetimes of the chlorides solvated with deuterium oxide over those of the hydrated rare earth chlorides must be due to a decrease of quenching efficiency caused by a decrease in the lattice vibrational frequencies. If the vibrational modes do indeed involve the entire water molecule, the required decrease in the frequencies of lattice vibrations must be brought about by the substitution of the H_2O molecules with the heavier D_2O molecules.

If the lattice vibrations were to involve only the vibrations of the adjacent oxygens, one would expect an increase

in quenching on going from the solvated salts to the chelates. This increased quenching efficiency would arise from the higher vibrational frequencies of the metal-oxygen coordinate-covalent bond in the chelates as compared to the lower frequencies of the metal-oxygen coordinate bond in the solvated rare earth salts. The data of Table 3.3.2.4.1. show that the quenching efficiency of the chelates is less, not greater, than the quenching efficiency in the solvated salt systems. Thus lattice vibrations must involve more than just the ketonic oxygen of the chelates.

Although no quantitative measurements of relative luminescence intensity were made, it was observed that the intensity of the ion emission roughly paralleled the magnitude of the luminescence decay times. The metaphosphate glasses, which exhibit quite long lifetimes, also exhibit quite bright emissions, while the hydrated rare earth salts, which exhibit short luminescence decay times, emit very weakly. For a given type of rare earth complex, the long-lived emission of europium or terbium was always brighter than the short-lived emission of dysprosium or samarium. In general, it was observed that those physical or chemical changes of the rare earth ion environment which caused a change in the decay time of the ion luminescence also caused a corresponding change in the intensity of ion emission.

This parallelism between luminescence decay time and luminescence intensity is in perfect agreement with the idea that quenching plays the major role determining the variations

in the luminescence decay times. Any increase in quenching, causing a decrease in luminescence decay times, must also cause a decrease in emission intensity since more of the electronic energy is being converted to nuclear kinetic energy of the lattice and less is being converted to electromagnetic radiation.

3.3.2.5. Temperature Dependence of the Luminescence Decay Times of Complexed Rare Earth Ions. ---The luminescence decay times of a few of the solid rare earth ion complexes were checked at room temperature as well as at low temperature ($77^{o}K$). The luminescence decay times at these two temperatures are compared in Table 3.3.2.5.1. The decay times at $298^{o}K$ could be obtained for only a few complexes as the emission intensities of most of the complexes were too weak to be recorded at this temperature. This was especially true for the rare earth chelates. The data presented in Table 3.3.2.5.1. indicate that, in general, the luminescence decay times of both the metaphosphate glasses and the solvated inorganic salts exhibit no significant temperature dependencies. The luminescence decay times of the chelate compounds exhibited a significant temperature dependence.

The chelates not only showed significant decreases in decay times when the temperature was raised from $77^{o}K$ to $298^{o}K$, but they also exhibited significant decreases in luminescence intensities. The emissions of $TbB_3 \cdot 2H_2O$, $TbA_3 \cdot H_2O$, and $EuA_3 \cdot H_2O$ became so weak that room temperature

TABLE 3.3.2.5.1.

EFFECT OF TEMPERATURE ON THE LUMINESCENCE DECAY TIMES OF COMPLEXED RARE EARTH IONS

Ligand Class	Compound	Luminescence Decay Time, microseconds	
		77°K	298°K
$PO_4^{\equiv}$	$TbPO_4$-$NaPO_3$ glass	3120	3180
	$EuPO_4$-$NaPO_3$ glass	3090	2900
	$SmPO_4$-$NaPO_3$ glass	⟨2250⟩*	⟨2340⟩*
	$DyPO_4$-$NaPO_3$ glass	⟨742⟩*	759
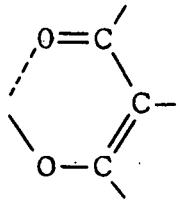	EuD_3 solid	460	80
	$EuB_3 \cdot 2H_2O$ solid	465	311
D_2O	$TbCl_3 \cdot 6D_2O$	721	719
H_2O	$EuCl_3 \cdot 6H_2O$	122	124
	$TbCl_3 \cdot 6H_2O$	483	471

*Semilogarithmic plots are curved. Decay times represent an average over the entire curve.

measurements of the luminescence decays could not be made. A change in the structure of the emission spectra also accompanied the change of the luminescence decay times. While the low temperature emission spectra of the microcrystalline rare earth chelates were quite sharp (especially from the MD_3 and $MA_3 \cdot H_2O$ complexes) the room temperature emission spectra were fuzzy and diffuse.

The extremely long, temperature independent, decay times of the rare earth ions in metaphosphate glasses would indicate that, either a very small amount of temperature independent quenching was occurring, or, more probably, so little quenching was occurring that, even if it were dependent upon temperature, it could not be readily detected through a measurement of the luminescence decay times. The fairly long, temperature dependent, decay times of the chelate systems indicate that a significant amount of quenching of the resonance levels of the ion probably still exists at $77^{o}K$, and that the mechanism is very temperature dependent. The quenching mechanism of the solvated salts appears to be not only quite efficient, but also insensitive to temperature changes over the range from $77^{o}K$ to $298^{o}K$.

The existence of both temperature dependent and temperature independent vibronic quenching mechanisms may be related to the frequency of the lattice vibrations through the results of Gouterman's analysis of the radiationless transition problem.(44).

Gouterman predicted that quenching may occur spontaneously, or it may be induced through interactions between the

ion and the energy density of the surrounding phonon field. According to his analysis spontaneous transitions are temperature independent, and induced transitions are temperature dependent. Through a comparison of the relative magnitudes of the probability constants for the two radiationless transitions, Gouterman drew the following conclusions:

(1) Radiationless transitions via low frequency lattice vibrations are fairly temperature sensitive as induced transitions predominate.

(2) Radiationless quenching via high frequency lattice vibrations are temperature insensitive since spontaneous transitions predominate.

(3) If the temperature of the system is raised high enough, the temperature dependent, induced transitions would eventually overwhelm the temperature independent, spontaneous transitions.

(4) Radiationless transition constants (induced or spontaneous) are proportional to the cube of the lattice frequency.

(5) Radiationless transitions are forbidden for lattice frequencies above an upper limit related to the Debye temperature of the solid.

Using the above conclusions as a basis for the analysis of the luminescence decay times of rare earth complexes, the following conclusions may be drawn about vibronic quenching of resonance levels of complexed rare earth ions:

(1) For rare earth ions in metaphosphate glasses, no

vibronic quenching occurs. Vibrational frequencies of the rigid glass lattice are higher than the upper limit allowed for radiationless transitions.

(2) Vibronic quenching of the rare earth ions in the solvated inorganic salts is most efficient due to the high frequency of the lattice vibrations involved. Because the frequencies involved are large, temperature independent, spontaneous transitions predominate. Temperature dependent, induced transitions would become effective at temperatures above 298°K. Since the lattice vibrations involve the entire solvent molecule (H_2O or D_2O), the quenching is more efficient in salts solvated with H_2O due to the higher frequency of lattice vibrations.

(3) Vibronic quenching of chelated rare earth ions is moderately efficient. Lattice frequencies involved are lower than those involved in the quenching of the ions in the solvated salts. Due to the lower frequencies involved, the radiationless transition probabilities are smaller than those of the hydrated rare earth ion, and the temperature dependent, induced transitions predominate.

Gouterman's approach is not the only theoretical treatment of radiationless transitions to have appeared in the

literature recently. More rigorous quantum mechanical developments of the problem have been presented by Robinson and Frosch (48,49), Orbach (50,51), and Mattuck and Strandberg (52). Gouterman's analysis of radiationless transitions was chosen for the above discussion because of the simplicity of the treatment and the close analogy of his development to that of the problem of radiative transitions in atomic systems presented in standard texts (36,53). In spite of the fact that this analysis of radiationless transitions is based on a rather simple semiclassical model, the theory does yield a quite satisfactory qualitative explanation of the lifetime data on complexed rare earth ions presented in the last two sections.

3.3.2.6. Secondary Environmental Effects on the Rare Earth Ion Luminescences. -- In order to determine the sensitivity of the rare earth ion luminescences to secondary environmental effects such as the physical state of the complexes or the nature of the solvents in which the complexes are dissolved, the luminescence decay times of europium and terbium chelates were measured when the compounds were dissolved both in ether-3-methylpentane (EMP) and in 3-methylpentane (MP) glasses at 77°K. Light filter combinations were chosen so that only light corresponding to the $^5D_0 \rightarrow {}^7F_2$ transitions of Eu^{3+} at approximately 6150 Å or the $^5D_4 \rightarrow {}^7F_5$ transitions of Tb^{3+} around 5400 Å was monitored by the photomultiplier tube of the lifetime apparatus. For these two ions luminescence

decay times of the chelates dissolved in the various organic glasses are reviewed in Table 3.3.2.6.1. (lifetime data for the chelates in EMPA glasses or in the microcrystalline solid state are included for comparative purposes).

No regular variations of the ion decay times with changes in solvent or physical state are apparent for the chelates in the various environments, but the differences observed are significant. It is because of such seemingly unpredictable, but significant, variations in luminescence decay times with changes in physical state, solvent, etc. that no comparisons have been made between the experimental data appearing in this thesis and the luminescence decay times of rare earth chelates published recently by other authors (54, 55,56,57). The majority of the decay times reported to date are for the chelates in entirely different environments than those reported here.

The luminescence decay times of microcrystalline EuD_3 were studied by Rieke and Allison (55) and Nardi and Yatsiv (54). These authors report that they found no temperature dependency for the europium ion luminescence arising from the $^5D_0$ resonance level. The data for this same system, reported in Table 3.3.2.5.1., show a striking temperature dependency. Nardi and Natsiv report in the experimental section of their paper that, when preparing the europium trisdibenzoylmethide chelate, the final product was not subjected to the prolonged vacuum drying at 125° - 150°C that Whan and Crosby (20) have shown is necessary for the removal of an extra mole of che-

TABLE 3.3.2.6.1.

LUMINESCENCE DECAY TIMES OF RARE EARTH CHELATES AT 77°K IN DIFFERENT ENVIRONMENTS

Chelate	Luminescence Decay Time, microseconds			
	microcrystalline solid	EMPA glass	EMP glass	MP glass
$EuB_3 \cdot 2H_2O$	435	430	⟨450⟩ (c)	360
EuD_3	460	361	⟨363⟩ (c)	354
$EuA_3 \cdot H_2O$	385	564	-- (d)	-- (d)
$TbB_3 \cdot 2H_2O$	650	630	754	769
TbD_3	--(a)	464(b)	⟨360⟩ (c)	-- (a)
$TbA_3 \cdot H_2O$	760	903	-- (d)	-- (d)

(a) No rare earth ion emission observed from these samples.

(b) Semilogarithmic plot of decay is curved, decay time is calculated from the linear region of the plot.

(c) Semilogarithmic plot is curved. Decay time represents an average over the entire curve.

(d) Decay times of these systems were not investigated.

lating agent from the product. In order to determine whether the above mentioned discrepancies could be due to an extra mole of chelating agent in the material used by the other authors for their luminescence studies, the luminescence properties of both europium trisdibenzoylmethide (EuD_3) and europium trisdibenzoylmethide solvated with one extra mole of dibenzoylmethane ($EuD_3 \cdot DH$) were extensively studied.

The luminescence decay times of both EuD_3 and $EuD_3 \cdot DH$ in EMPA glasses and the microcrystalline state plus the corresponding data given by the other authors are presented in Table 3.3.2.6.2. As suspected, the luminescence decay times of the Eu^{3+} ion in solid $EuD_3 \cdot DH$ exhibited no temperature dependence, while the decay times of the EuD_3 chelate were very temperature sensitive. The significant differences in the temperature dependencies of the two compounds were also reflected in significant structural changes of the emission spectra of the two complexes in the microcrystalline state at $77^{o}K$ (see Fig. 3.3.2.6.1.) and in the absorption spectra of the compounds dissolved in benzene (Fig. 3.3.2.6.2.). It is clear that the luminescence data reported by Nardi and Yatsiv as well as Rieke and Allison were obtained from the $Eud_3 \cdot DH$ complex, not from the simpler EuD_3 compound.

Differences in the luminescence properties of the EuD_3 and $EuD_3 \cdot DH$ chelates disappear completely when the compounds are dissolved in hydroxylic solvents. Not only are the luminescence decay times of the two compounds the same when dissolved in EMPA glasses (see Table 3.3.2.6.2.), but the emission

TABLE 3.3.2.6.2.

LUMINESCENCE DECAY TIMES OF EUROPIUM TRISDIBENZOYLMETHIDE CHELATES

Complex	Decay time, microseconds	
	77°K	298°K
EuD_3 in EMPA	360	---
$EuD_3 \cdot DH$ in EMPA	370	---
Microcrystalline EuD_3	460	⟨80⟩ ± 30*
Microcrystalline $EuD_3 \cdot DH$	⟨440⟩*	⟨420⟩*
Microcrystalline EuD_3 (reported by Nardi and Yatsiv (54))**	500	500
Microcrystalline EuD_3 (reported by Rieke and Allison (55))**	522	529

*Semilogarithmic plot of decay is curved. Decay time represents average over entire curve.

**Probably $EuD_3 \cdot DH$ (see text, Section 3.3.2.6.).

Fig. 3.3.2.6.1.--Emission spectra of microcrystalline $EuD_3 \cdot DH$ and EuD_3 at 77° K. (Only the strong $^5D_0 \longrightarrow {}^7F$ transitions are shown.)

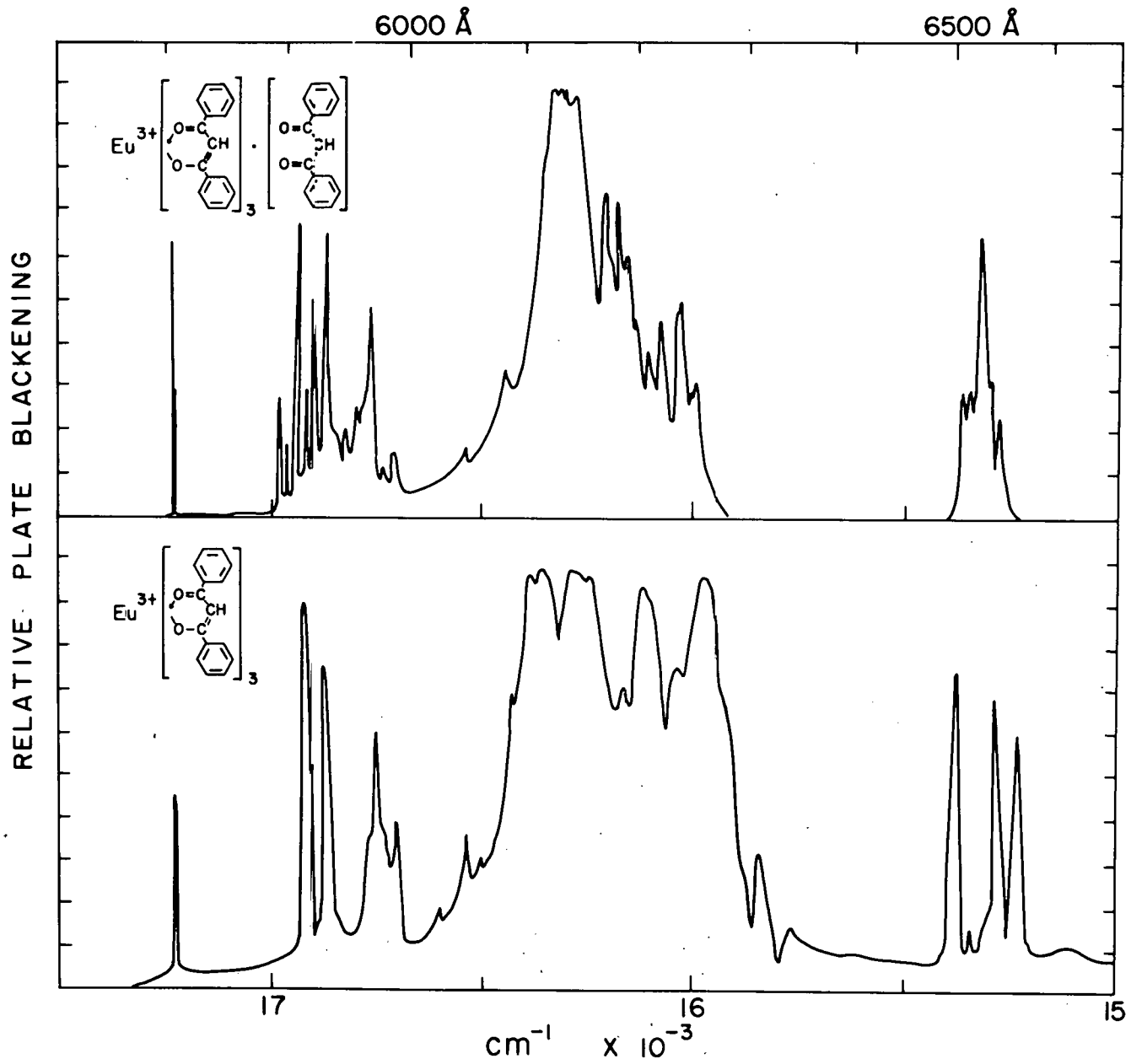
6000 Å
6500 Å
RELATIVE PLATE BLACKENING
17
16
15
cm⁻¹ x 10⁻³

THIS PAGE
WAS INTENTIONALLY
LEFT BLANK

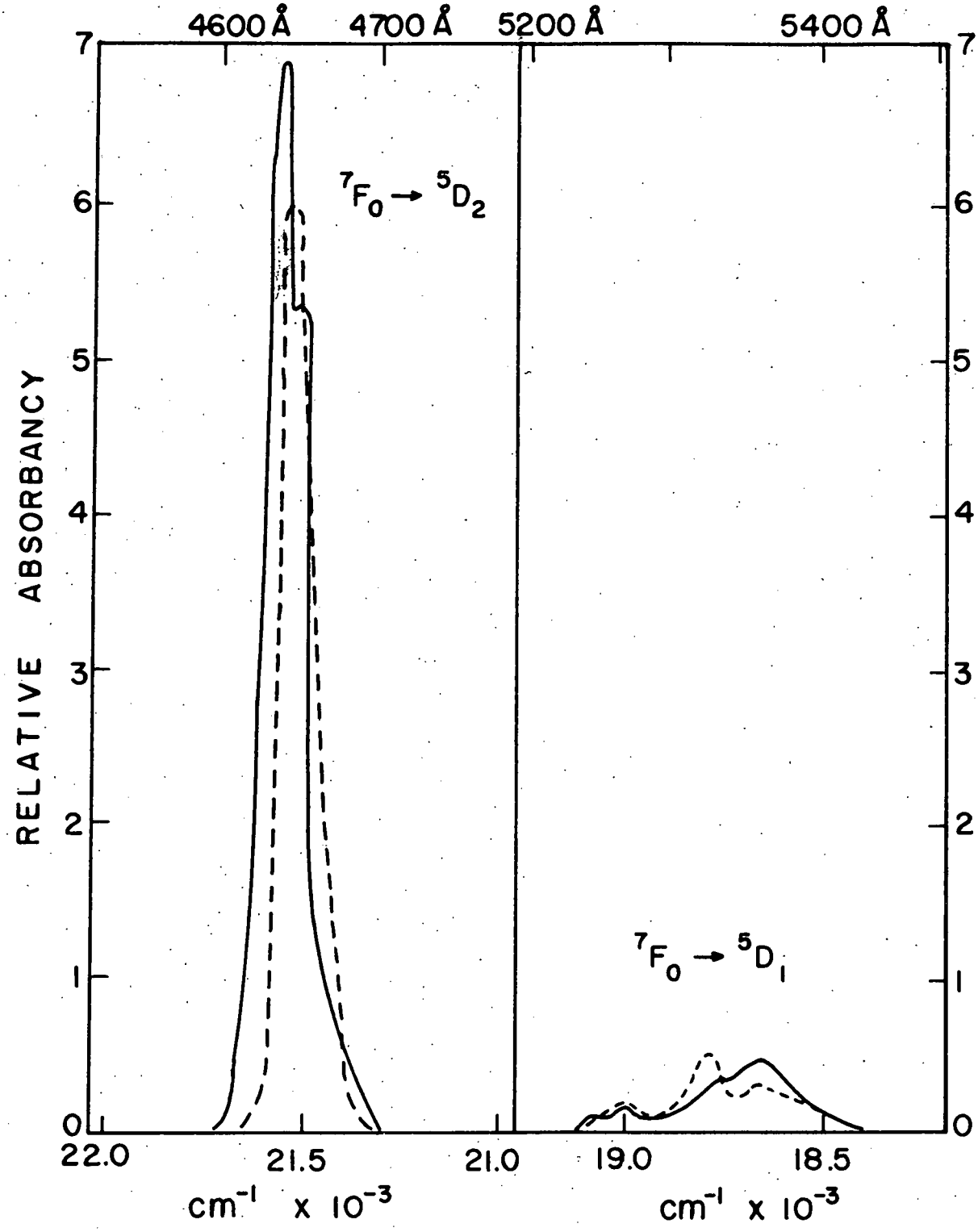

Fig. 3.3.2.6.2.--Absorption spectrum of the Eu^{3+} ion in benzene solutions of EuD_3 and $EuD_3 \cdot DH$.

——— 0.01 M $EuD_3 \cdot DH$

- - - - - 0.01 M EuD_3

spectrum of the spectrum of the $EuD_3 \cdot DH$ complex in an EMPA glass at 77°K is precisely the same as the emission spectrum of EuD_3 in an EMPA glass at 77°K shown in Fig. 3.1.2.1. Furthermore, when both chelates are dissolved in absolute ethanol, no differences could be detected in the structure of the absorption spectrum attributable to the Eu^{3+} ion. These absorption spectra are shown in Fig. 3.3.2.6.3. Removal of the dibenzoylmethane molecule (DH) from the vicinity of the Eu^{3+} ion by the hydroxylic solvent adequately explains why differences in the luminescence properties of the EuD_3 and $EuD_3 \cdot DH$ complexes disappear completely when the chelates are dissolved in hydroxylic media.

A final example of the effect of the environment upon the luminescence properties of chelate systems is found in the case of the TbD_3 chelate. While this chelate exhibits strong luminescence characteristic of the terbium ion when dissolved in EMPA glasses at 77°K, it exhibits only weak ion emission in EMP glasses and practically no ion emission in the MP glass and in the microcrystalline solid state.

The resonance level of the Tb^{3+} ion (see Fig. 3.1.2.2.) is almost coincident with the triplet level of the TbD_3 complex. Studies of rare earth chelates in EMPA glasses (21) reveal that the hydroxylic solvent raises the energy of the triplet level of the complex. This slight shift in triplet state energy of the TbD_3 compound by the alcohol in the EMPA is apparently all that is needed to raise the triplet state of the chelate above the resonance level of the Tb^{3+} ion. In

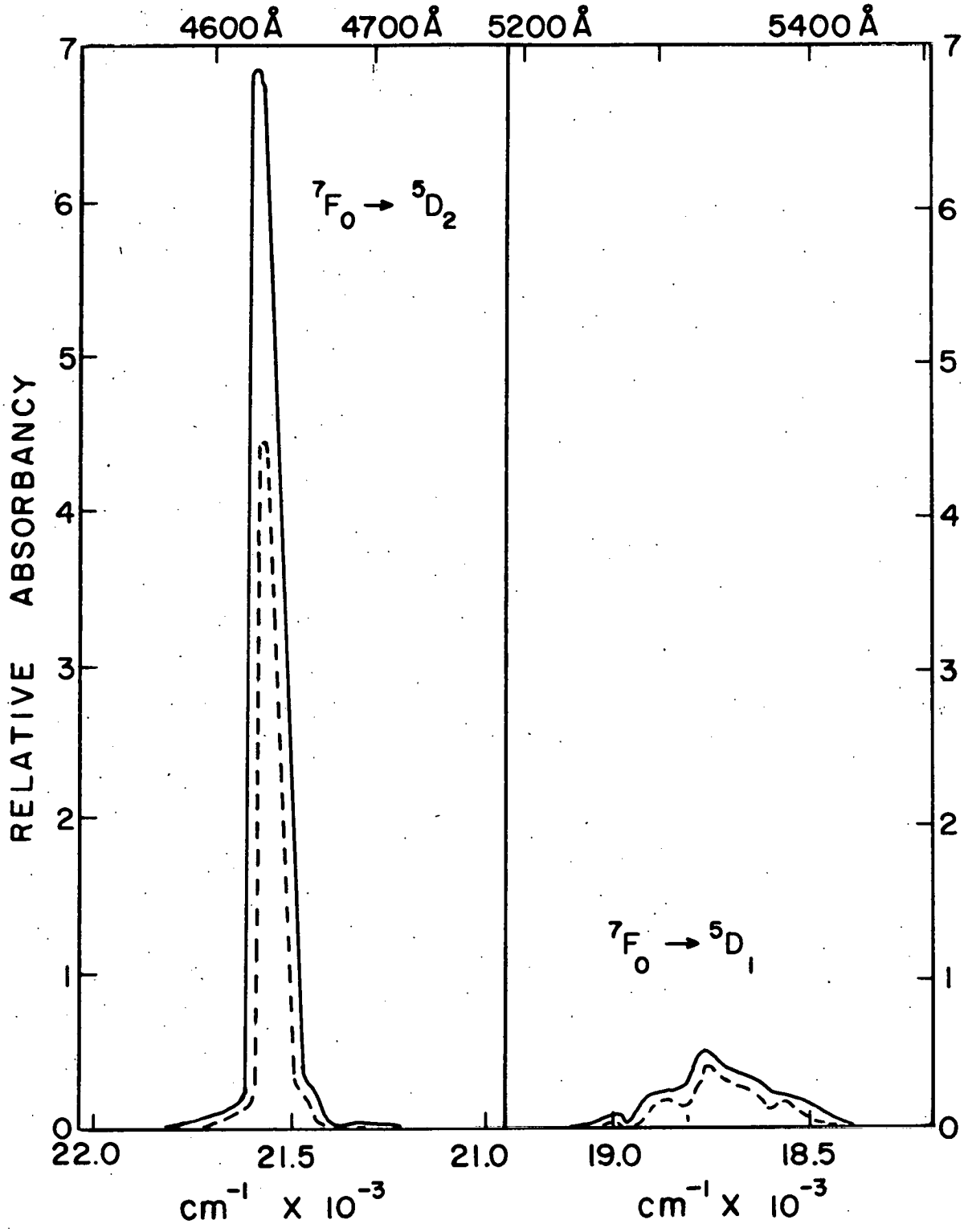

Fig. 3.3.2.6.3.--Absorption spectrum of the Eu^{3+} ion in absolute ethanol solutions of EuD_3 and $EuD_3 \cdot DH$. (Approximately 0.01 molar solutions were used. Complete solution of the EuD_3 in the alcohol was not obtained.)

——— $EuD_3 \cdot DH$

– – – – – EuD_3

non-hydroxylic solvents and in the microcrystalline solid state, the triplet level is too low to efficiently populate the resonance level of the Tb^{+3} ion by intramolecular energy transfer; thus no ion luminescence is observed.

The data presented in this section of the Discussion are too sparse to clarify the effects of solvent or physical state upon the luminescence properties of the rare earth complexes. The data are presented in order to show the possible origins of discrepancies in the luminescence decay times reported by various authors. The data indicate that, due to the sensitivity of the rare earth ion to secondary environmental effects, such factors as method of preparation, physical and chemical nature of the solvent, and the purity of the compound must be carefully considered in an analysis of the luminescence characteristics of complexed rare earth ions.

4. Suggestions for Future Work

Careful measurements of the temperature dependency of the luminescences of complexed rare earth ions are needed. This data would yield useful information about the nature of the quenching mechanisms of rare earth complexes. The luminescence decay time, τ, and the relative intensity of emission, ρ, are related to the transition probabilities by the equations

$$\tau = \frac{1}{K_r + K_q + K_q'(T)} \qquad 4.1.$$

$$\rho = \frac{K_r}{K_r + K_q + K_q'(T)} \qquad 4.2.$$

Where K_r is the spontaneous radiative transition probability,

K_q is the spontaneous radiationless transition probability, and

$K_q'(T)$ is the induced, temperature dependent, radiationless transition probability.

A plot of $1/\tau$ or $1/\rho$ versus temperature, T, would yield the mathematical form of the temperature dependent, radiationless transition probability. From the mathematical relationship, the frequency of the lattice vibrations could

possibly be computed from the following relationship predicted by Gouterman (44):

$$K_q'(T) \propto (e^{\hbar\omega/kT} - 1) \qquad 4.3.$$

where ω is the frequency of the lattice vibration,

$\hbar$ is Planck's constant divided by 2π, and

k is Boltzmann's constant.

Studies of the luminescence properties of chelated rare earth ions have always been hampered by the very poor crystallization properties of the chelate compounds which have prevented the formation of large, optically clear, single crystals. The acetylacetonate chelates prepared for this study appear promising for the preparation of such crystals. Although attempts to grow crystals by vacuum sublimation failed, such techniques as doping colorless aluminum or yttrium trisacetylacetonate crystals (which readily crystallize from acetone solutions) with the rare earth trisacetylacetonates might yield the desired large, single crystals suitable for the luminescence studies.

It would also be of interest to determine the luminescence decay times of rare earth ions embedded in such rigid lattices that very little quenching of the electronic states of the ion could occur. The luminescence decay times of the ions in the metaphosphate glasses are still less than the fourteen millisecond upper limit predicted for some of the rare earth ions. Such systems as the anhydrous rare earth chlorides, in which nearly all the rare earth ions

exhibit luminescence (4), might yield rare earth ion luminescence decay times longer than the three millisecond decay times of the sodium metaphosphate glasses. Of special interest would be the decay time of the Gd^{3+} ion in the anhydrous chloride. The decay time of this ion in such a rigid lattice might be equal to or even greater than the fourteen millisecond upper limit.

Laser action has been reported for the emission of numerous rare earth ions (57-70). With the exception of one ion (Eu^{3+}), the laser action has been confined to emission in the near infrared or infrared region of the spectrum. Laser action of europium ion at $\sim$ 6100 Å from the europium benzoylacetonate chelate has been reported by Lempicke and Samelson (57). The rare earth oxide-sodium metaphosphate glasses appear to be excellent candidates for exhibiting laser action in the visible region of the spectrum. Not only do these glasses exhibit the desirable properties of bright, long-lived, visible emission (indicating very efficient population inversion of the upper resonance levels), but the glasses also exhibit such desirable properties as chemical and mechanical stability, optical clarity, and ease of preparation.

5. Appendix

5.1. Wave Length Calibration for Measurement of Emission Spectra

The emission from a low pressure argon discharge tube, operated at ~2500 V, was recorded with the Steinheil spectrograph, and a densitometer trace of the photographic plate was made with the Jarrell-Ash microphotometer. The wave lengths of the argon lines were assigned using the argon emission wave length table in the Handbook of Chemistry and Physics (71). The distances on the densitometer trace from an arbitrary starting point to each of the argon lines of known wave length were measured. A calibration curve was constructed from these data in which the wave length in Å of the argon line was plotted against distance in inches of the densitometer trace.

Once the sample emission had been photographed with the spectrograph, the argon emission spectrum was superimposed over a narrow region of the sample emission spectrum. Densitometer traces were made of the sample emission alone and then of the sample emission plus the argon line emission. The positions of the argon lines in the latter densitometer trace were determined by comparing the two traces. The distances from at least two different argon lines to the sample peak or

line were measured, and the wave length of the sample emission determined from the calibration curve of wave length versus distance. For spectrograph settings yielding a dispersion of 17 Å/mm. on the photographic plate at 5000 Å, the average error in determining the wave lengths of sample emission was about ± 2 Å.

5.2. Construction and Calibration of the Apparatus used to Measure the Luminescence Decay Times

A block diagram of the apparatus used to measure luminescence decay times has already been given in Fig. 2.5.1.1. A detailed description of each of the components in this diagram is given below.

5.2.1. Spark Source

The circuitry of this unit is given in Fig. 5.2.1.1. The unit, which delivers a twenty kilovolt pulse to the triggered spark gap, is activated by an input pulse of $\sim$40 V. The one second pulse from the time mark generator was usually used for this purpose. RG 58/U coaxial cable was employed for both the input and output leads.

5.2.2. Flash Lamp Power Supply

A schematic diagram of this unit is given in Fig. 5.2.2.1. The components of the power supply were mounted in a lucite chassis made of $\frac{1}{4}$" thick material. Heavy duty, RG 8/U coaxial cable connected this unit with the triggered spark gap. The power supply delivers from 50 to 10,000 volts DC.

5.2.3. Triggered Spark Gap

The circuitry of this portion of the apparatus is given

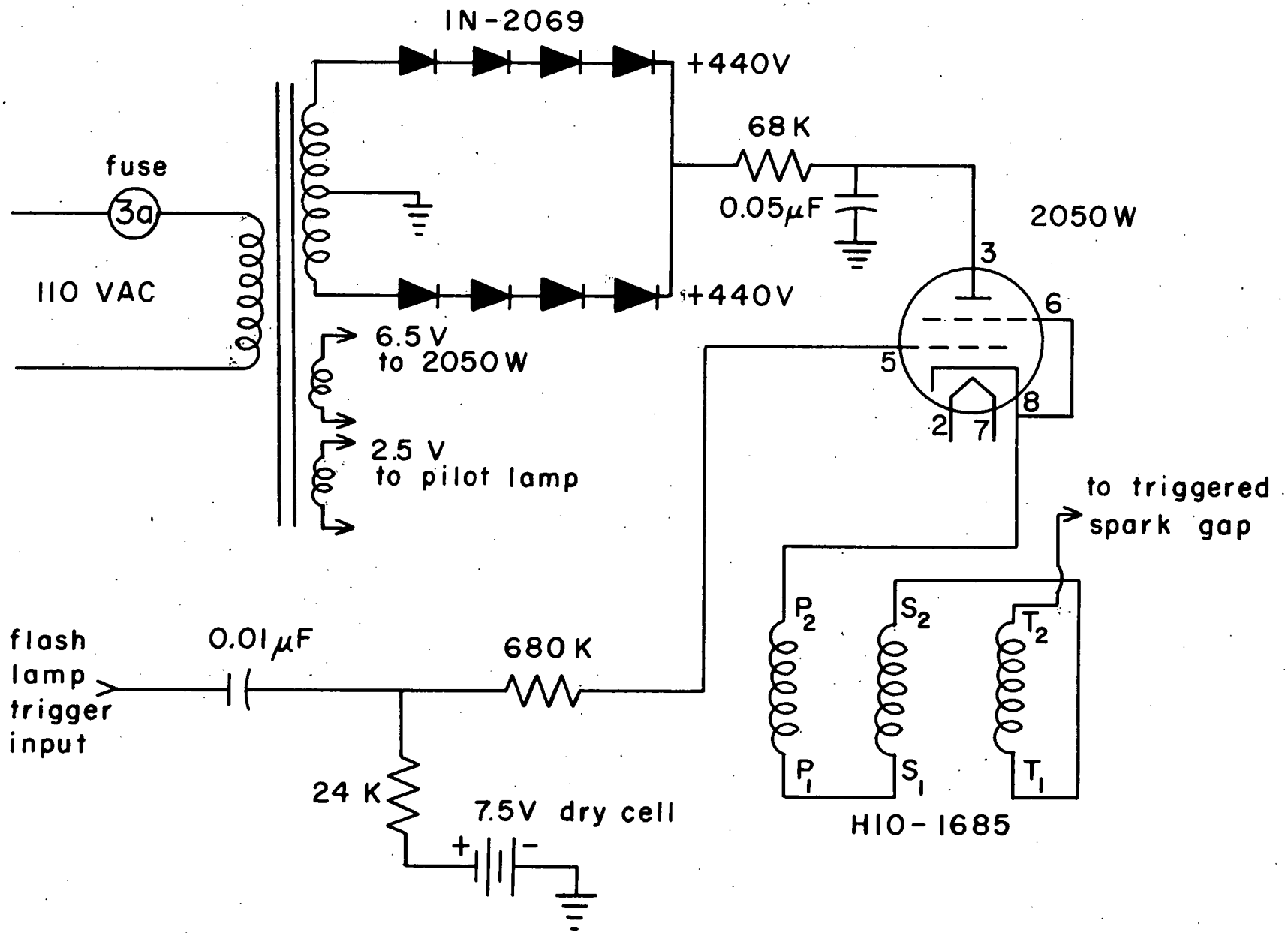

Fig. 5.2.1.1.--Spark source circuit.

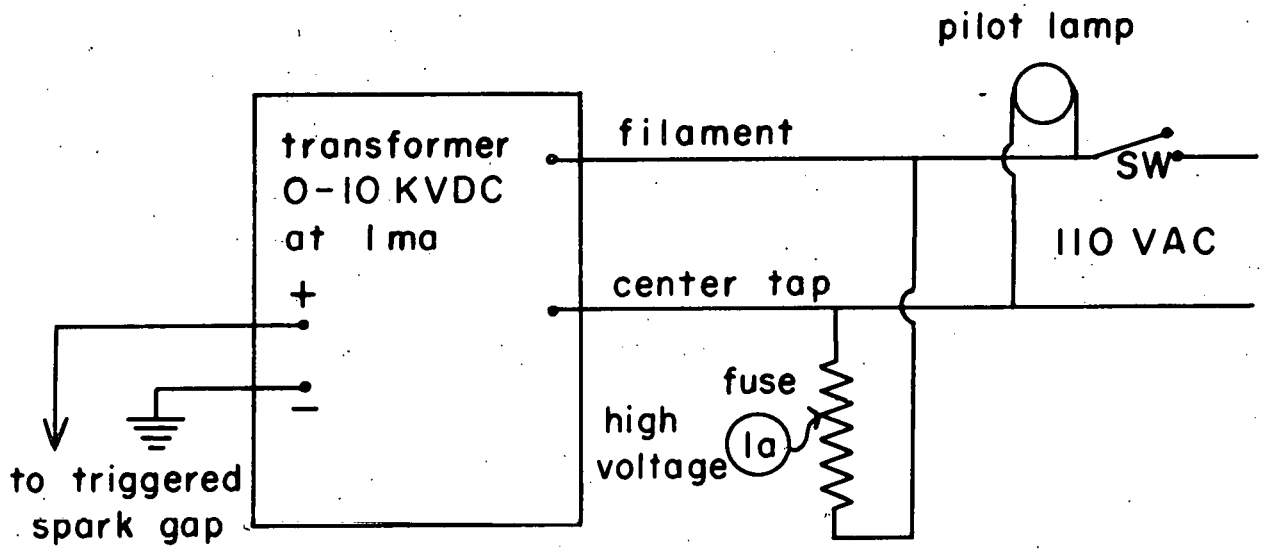

Fig. 5.2.2.1.--Flash lamp power supply circuit.

in Fig. 5.2.3.1. Details on the construction of the spark gap are given in Fig. 5.2.3.2. All components were mounted in a lucite chassis, and heavy duty RG 8/U coaxial cable connected the leads to the flash lamp. When operating this unit, the metal poles of the spark gap were adjusted so that a spontaneous discharge occurred at approximately 400 volts above the desired operating potential of the lamp. The unit was then run at the desired operating voltage at which no spontaneous discharge of the lamp occurred. When the spark source delivered a high voltage pulse to the spark gap, a spark jumped from the end of the wire inside the metal toroid to the toroid itself. This spark ionized the air within the gap and allowed the air gap to discharge the capacitors through the flash lamp. The lifetime of the lamp operated in this fashion was on the order of two to three microseconds. The lamp intensity as a function of time is shown in Fig. 5.2.3.3.

5.2.4. Photomultiplier Tube Power Supply

A bank of heavy duty 90 volt storage batteries (RCA #VS-058) was used for the photomultiplier power supply. The batteries were connected to the photomultiplier via a fourteen strand shielded cable. A Cannon, 15 pin connector was used to connect the cables to the photomultiplier.

This type of power supply was preferred over the more common commercial, electronicly regulated power supplies because it was found to be highly stable (within $\pm$ 0.01 %) and unaffected by the high intensity electromagnetic fields generated

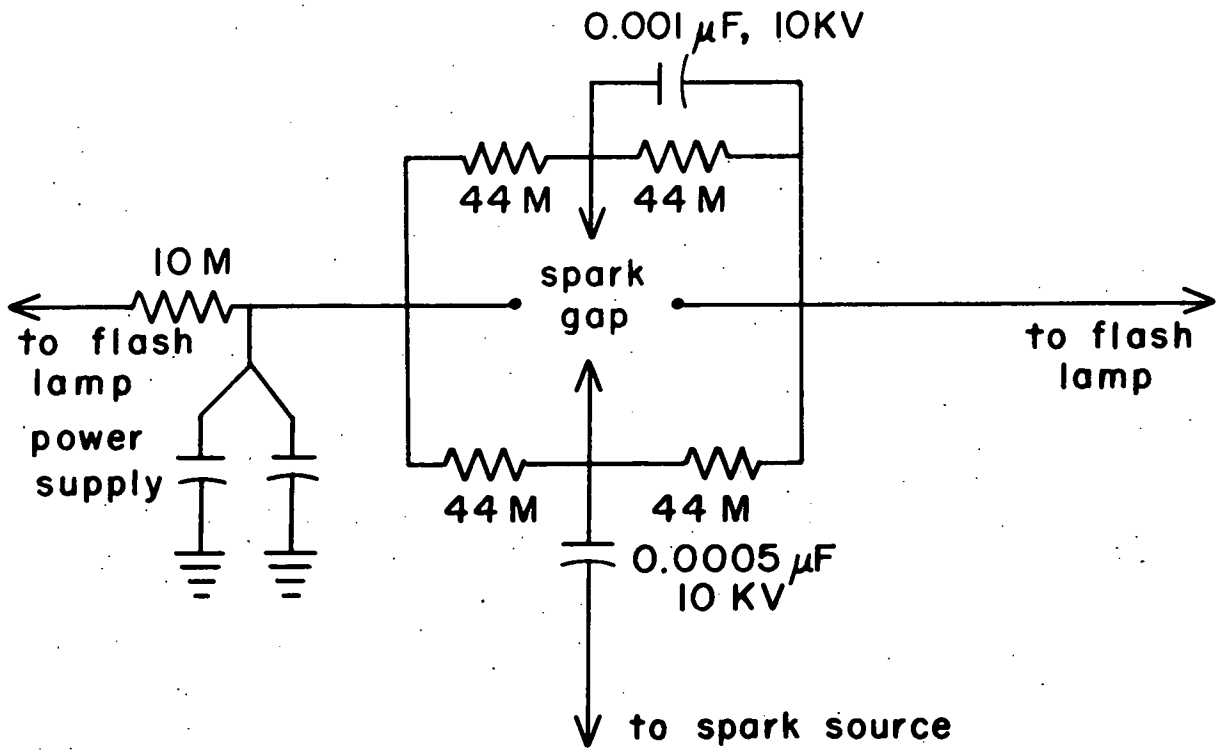

Fig. 5.2.3.1.--Triggered spark gap circuit.

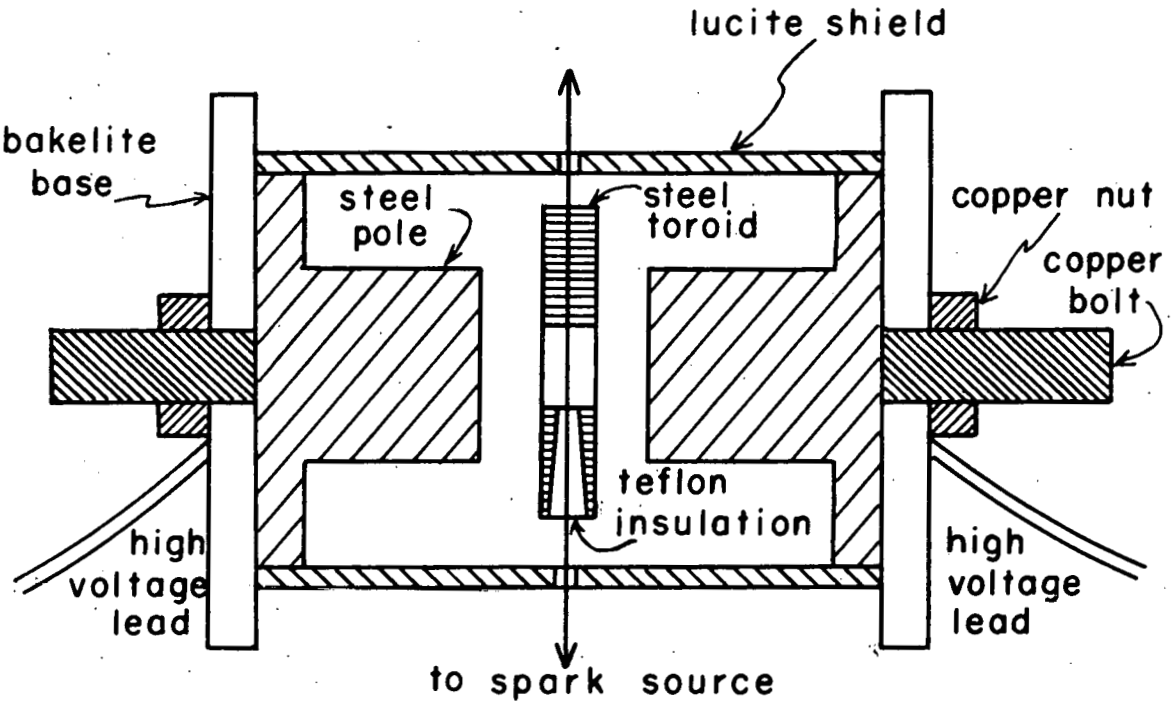

Fig. 5.2.3.2.--Cross sectional drawing of the cylindrical triggered spark gap.

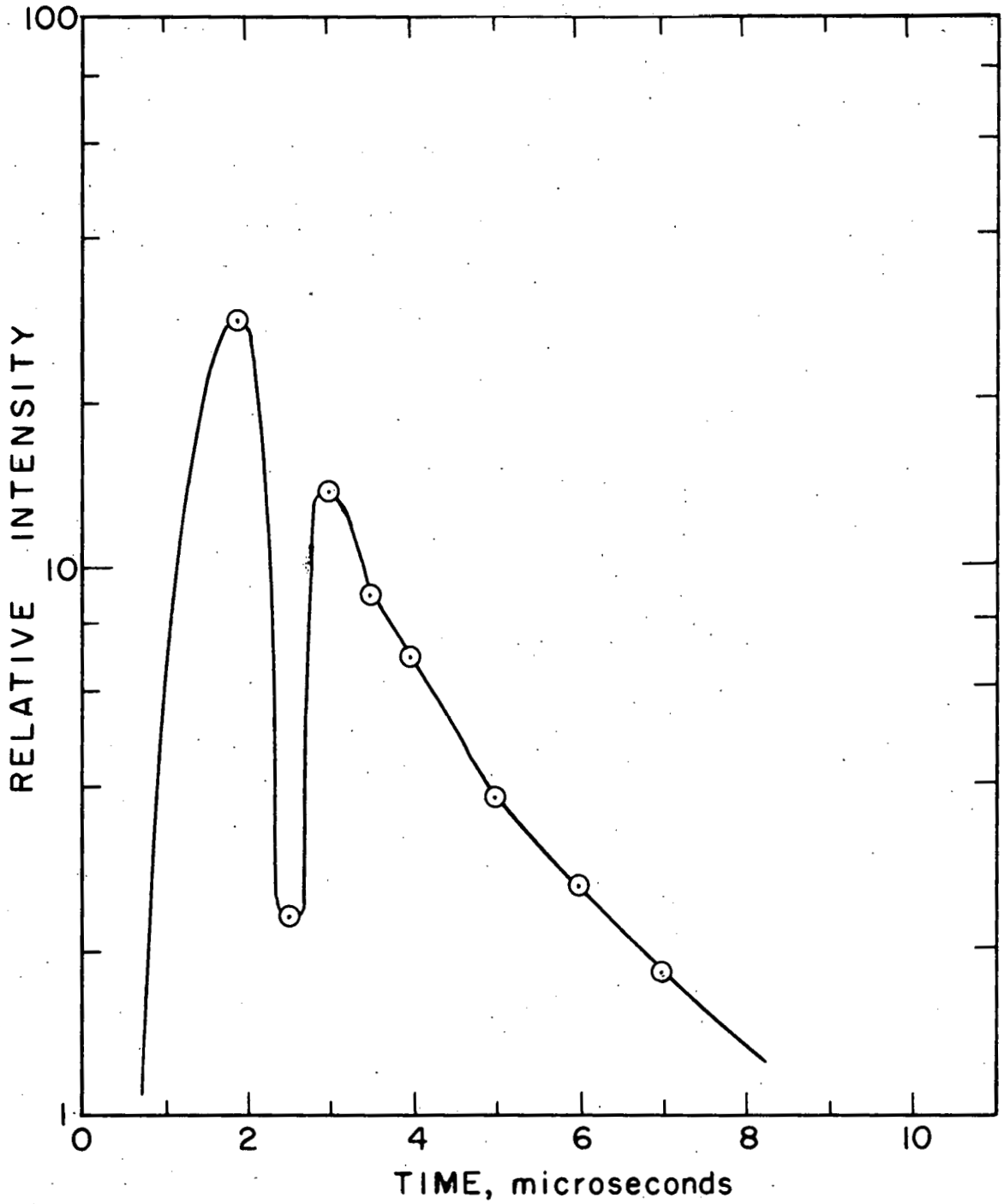

Fig. 5.2.3.3.--Decay of the FX-12 xenon flash lamp operated at one joule per discharge.

during the discharge of the flash lamp.

5.2.5. Photomultiplier Tubes and Photomultiplier Tube Housing

Either of two end-on, ten-stage amplification photomultiplier tubes was used to detect the intensity of sample emission. For sample emission in the visible region of the spectrum, a RCA-2020 photomultiplier with a S-11 response was used. For sample emission in the deep red end of the visible spectrum, a RCA-7102 tube was employed. The wiring diagrams for the photomultiplier tubes are given in Figs. 5.2.5.1. and 5.2.5.2. Each battery in these circuit diagrams represents one of the 90 V storage batteries of the power supply. The photomultipliers were operated at a 1080 volt cathode to anode potential.

Ten different, one half watt, 5 %, carbon resistors, ranging from 2 KΩ to 1.2 MΩ , were employed for the anode to ground load resistance. For load resistances up to 30 KΩ , the response time of the detector circuit was found to be less than one microsecond. At 100 KΩ or larger load resistances, the response time of the detector circuit dropped to more than fifty microseconds. The photomultiplier tubes were usually operated at a 10 KΩ load resistance. Both photodetectors were shielded with a Nicoloi #80802B magnetic shield which was connected to the cathode at -1080 volts.

The signal to ground resistances, photomultiplier, diheptal base, and insulated shield were all mounted within a tubular brass housing which was grounded at + 1080 volts. The

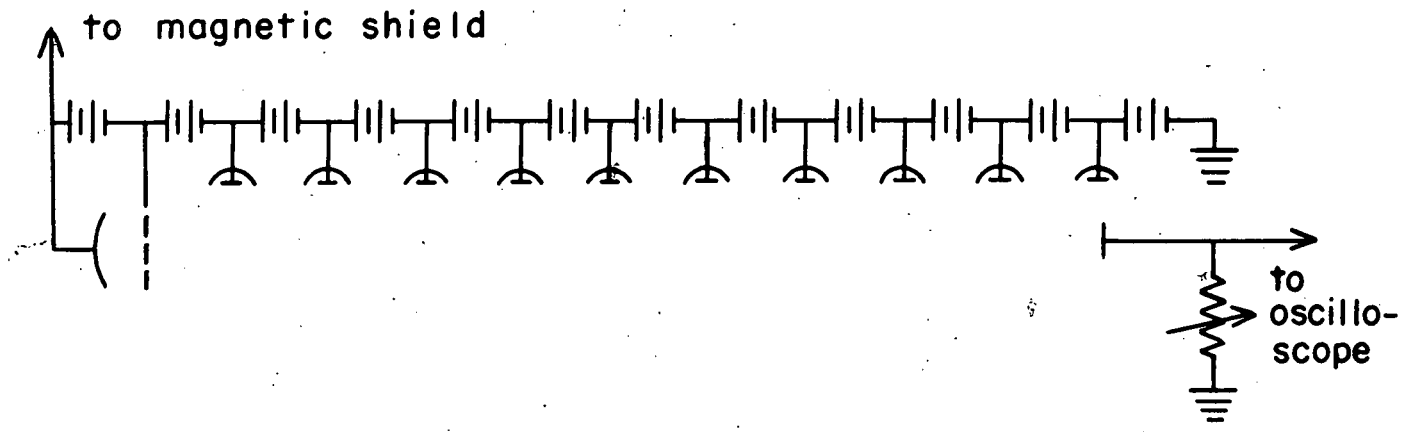

Fig. 5.2.5.1.--Circuit for the RCA-2020 photomultiplier. (All batteries indicated in the circuit are 90 V storage batteries.)

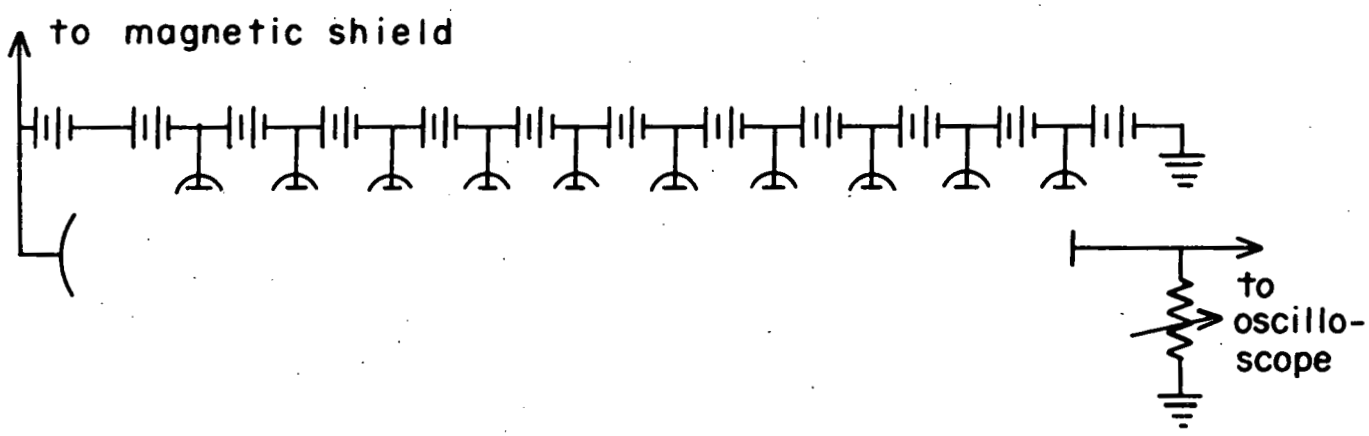

Fig. 5.2.5.2.--Circuit for the RCA-7102 photomultiplier. (All batteries indicated in the circuit are 90 V storage batteries.)

housing was mounted directly against the sample cell for direct observations of luminescence decays, or it was mounted against the exit slit of the monochromator for observations of more selected regions of the sample emission spectrum.

5.2.6. Flash Lamp, Sample Cell, and Light Filters

The relative positions of the flash lamp, sample cell, and light filters are shown schematically in Fig. 5.2.6.1. All the units shown in this figure, with the exception of the monochromator and the photomultiplier tube, were mounted in a black light-tight box which was so baffled that only the properly filtered excitation light reached the sample or subsequently, only filtered emitted light reached the detector. The reflector behind the flash lamp was coated with magnesium oxide for maximum reflection of ultraviolet light.

Descriptions of the remaining components of the apparatus such as the time mark generator, oscilloscope, and camera are found in Section 2.5.1.

5.2.7. Calibration of the Apparatus

There are no primary standards available for calibration of the apparatus used to measure the luminescence decay times. Three criteria must be met by the apparatus, however, if it is to accurately measure luminescence decay times. They are:

(1) the horizontal sweep speed of the apparatus must be accurately calibrated against a time standard,

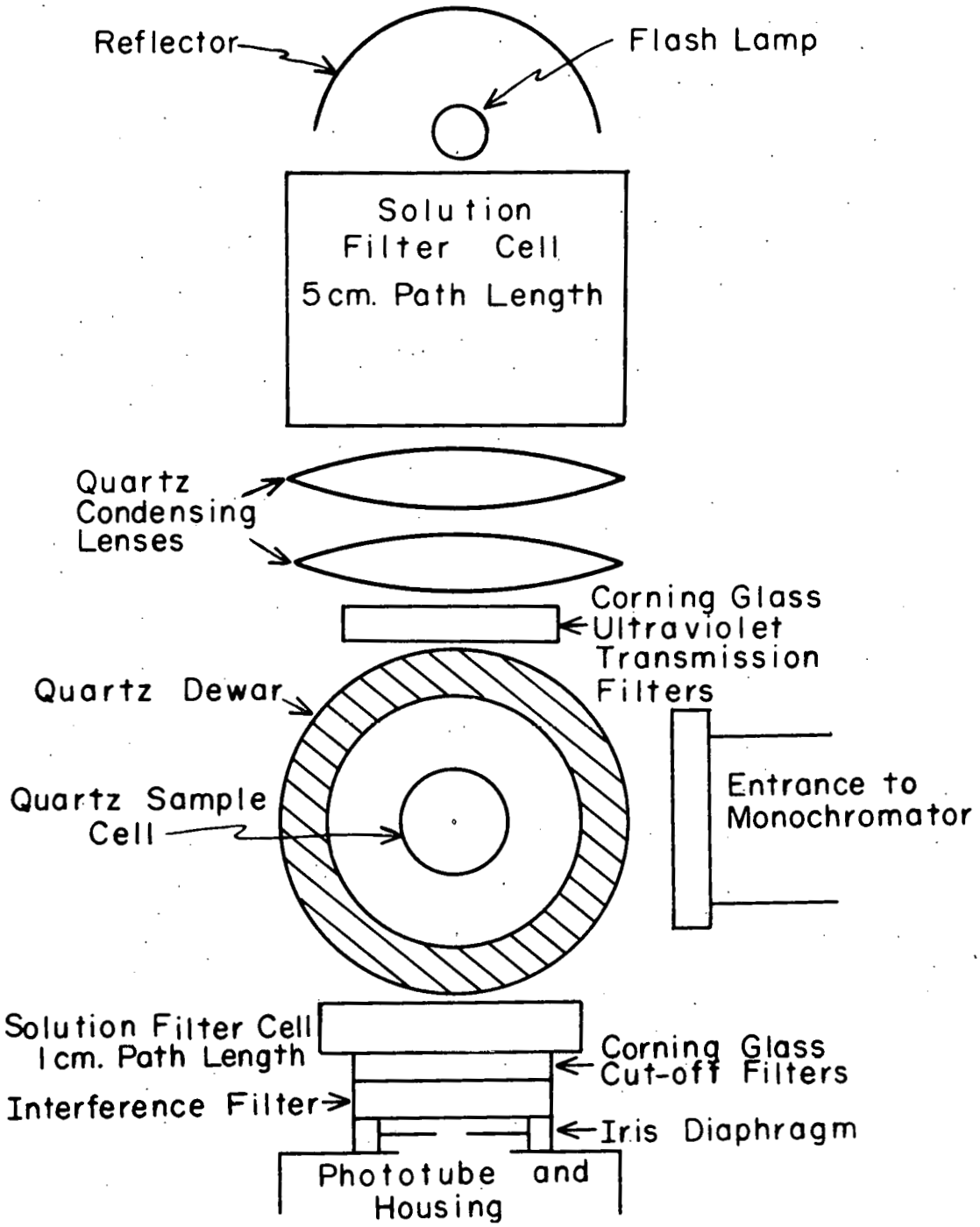

Fig. 5.2.6.1.--Schematic diagram showing relative positions of the flash lamp, sample cell, and light filters.

(2) the response time of the photomultiplier must be sufficiently fast so that the photomultiplier can follow all the light intensity variations of interest, and

(3) the nature of the response of the apparatus to variations of light intensity must be known. (In this instance, the relationship must be linear because of the assumption that vertical distances on the photographs are proportional to relative light intensity.)

The first criterion was met by relying not on the rated sweep speeds of the oscilloscope, but rather by relying on the calibrated time marks signals from the Tektronix Model 180 time mark generator. These time mark signals, appearing on each photograph of the oscilloscope traces, were in turn referenced to the one megacycle standard crystal oscillator of the time mark generator. Frequent checks of the instrument were made to make sure that the instrument remained calibrated against the crystal oscillator.

The response time of the photomultiplier (criterion 2), was checked by observing, with the oscilloscope, the photomultiplier response to a chopped DC light pulse. The chopped light source was obtained by observing the light from a neon pilot lamp through the slots of the whirling Becquerel phosphoroscope. The response time of the phototube, operating at a 10KΩ load resistance, was found to be less than one microsecond--certainly much faster than was needed to respond to

the two to fifteen microsecond rise times and the 10 to 10^6 microsecond decay times encountered in the luminescence decay studies.

The response of the apparatus to light intensity (criterion 3) was checked by measuring the response of the apparatus to a point source of light situated at various distances from the detector. By measuring the distance between the light source and the photomultiplier tube, the relative intensity of light falling on the tube could be computed from the inverse square law. The response of the instrument was found to be linear with light intensity over a region of intensity corresponding to one to one hundred microamperes of photomultiplier output.

A final check on the apparatus was performed by determining how well the data obtained with this instrument agreed with data published previously. In Table 5.2.7.1., the lifetimes of a few compounds calculated from luminescence decay curves obtained with the apparatus are compared with the corresponding lifetimes published in the literature. (Section 5.4. gives the experimental details for the determination of phosphorescence decay times of organic compounds.) As can be seen in the table, the differences between the measured and published results are within experimental error except for the lifetime of α-chloronaphthalene. The shorter measured lifetime of this latter compound could be due to impurities, since stock chemicals were used without further purification for these experiments.

TABLE 5.2.7.1.

COMPARISON BETWEEN MEASURED AND PUBLISHED LUMINESCENCE DECAY TIMES OF A FEW COMPOUNDS AT 77°K

Compound	Measured Decay Times, msec.	Published Decay Times, msec.
acetophenone in EMPA	8.0 ± 0.5	8 ± 2[a]
α-bromonaphthalene in EMPA	17 ± 1	18 ± 2
α-chloronaphthalene in EMPA	21 ± 1	30 ± 4
β-bromonaphthalene in EMPA	21 ± 1	21 ± 1
naphthalene in EMPA	2710 ± 135	2600 ± 200
phenanthrene in EMPA	3350 ± 170	3300 ± 200
$EuCl_3 \cdot 6H_2O$ crystals	0.122 ± 0.005	0.120 ± 0.006[b]
$TbCl_3 \cdot 6H_2O$ crystals	0.483 ± 0.025	0.487 ± 0.024

[a]Data on aromatic compounds taken from McClure (72).

[b]Data on rare earth chlorides taken from Dieke and Hall (30).

5.3. Mathematical Analyses of Luminescence Decay Curves

Four general types of luminescence decay curves encountered in this work are shown in Fig. 5.3.1.

For a simple first order exponential decay, the intensity of emission, I, as a function of time, t, is given by the relationship

$$I = I_o e^{-t/\tau} \qquad 5.3.1.$$

where I_o is the initial intensity of radiation and τ is the mean lifetime of the decaying species. The slope, b, of the linear semilogarithmic plot of I *versus* t is equal to the negative reciprocal of the mean lifetime τ, *i.e.*,

$$b = -1/\tau \qquad 5.3.2.$$

This kind of experimental curve is displayed in Fig. 5.3.1.A.

Fig. 5.3.1.B represents the decay curve for a two step, first order, exponential decay. The analysis of this type of decay curve is discussed in detail in Section 3.1.3.

The decay curves representative of two independently decaying species are shown in Fig. 5.3.1.C. and Fig. 5.3.1.D. The general equation for this kind of decay is given by

$$I = I_1^o e^{-t/\tau_1} + I_2^o e^{-t/\tau_2} \qquad 5.3.3.$$

where τ_1 and τ_2 are the mean lifetimes of the two decaying species, and I_1^o and I_2^o are the initial intensities of the two

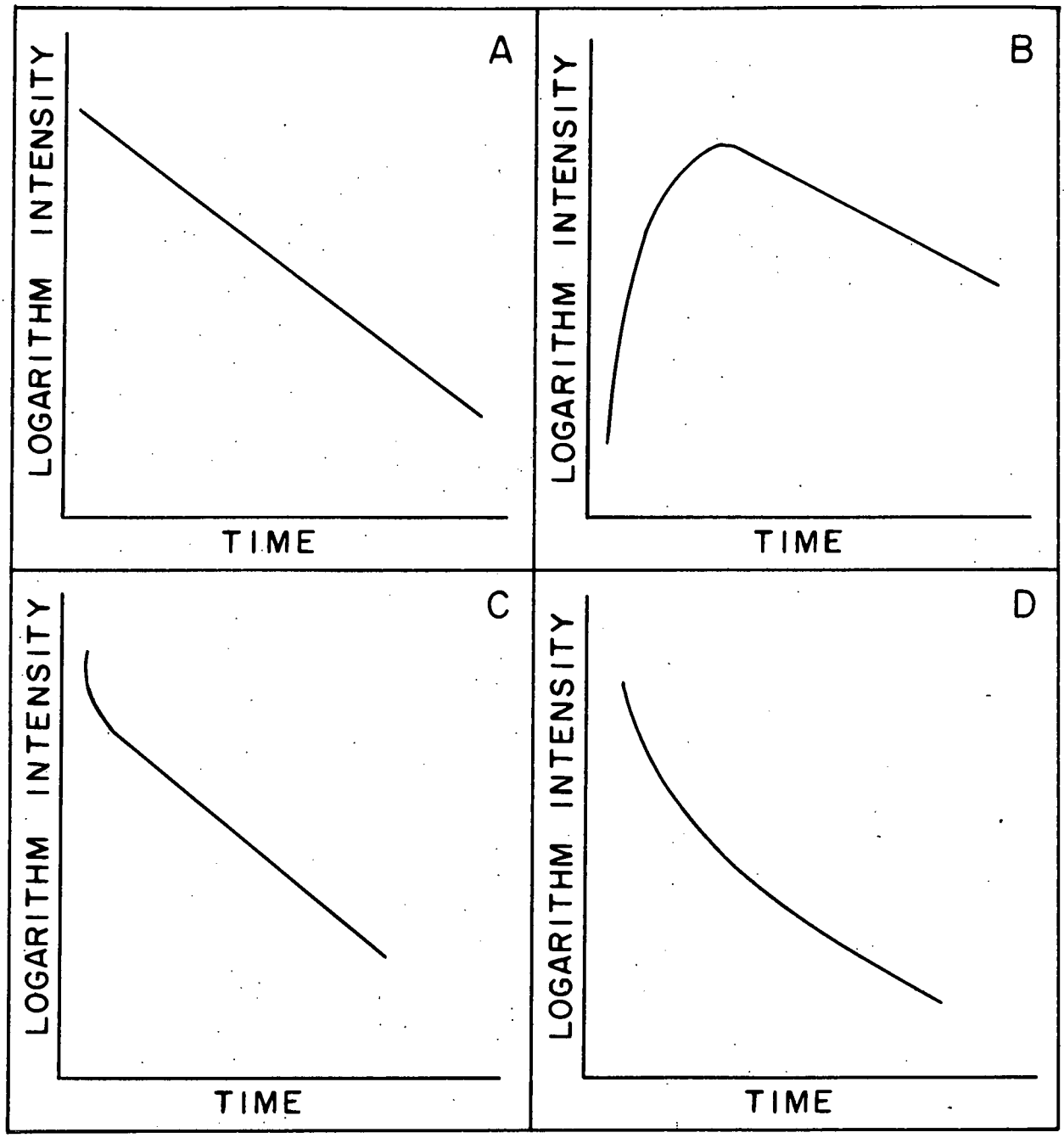

Fig. 5.3.1.--Types of luminescence decay curves.

A. First order, exponential decay.

B. Two step, first order, exponential decay.

C,D. First order, exponential decays arising from two species decaying independently of each other.

components.

In Fig. 5.3.1. C., the shorter-lived component and the longer-lived component have radically different lifetimes. In this case the lifetime of the longer-lived component can be calculated from the slope of the linear region of the curve. The lifetime of the shorter-lived component can be calculated by standard techniques (29). For luminescence decay curves of the kind represented by Fig. 5.3.1.D, there are no simple techniques available for determining the lifetimes of each of the decaying species. The lifetimes of each of the species are different, but they are of the same order of magnitude. When experimental data on chelates yielded such a plot, the curved line of the semilogarithmic plot was treated as a straight line. The negative reciprocal of the slope of the "straight" line, which was determined by statistical methods, was taken as the mean lifetime of both the decaying species. Lifetimes calculated from such curves are subject to considerable error.

The slope of the line, b, and the standard deviation of the slope, s_b, were calculated from experimental data by the statistical least squares methods.* While the slope and the standard deviation were taken as the quantities

$$b - s_b < b < b + s_b, \qquad 5.3.4.$$

the mean lifetimes and their statistical limits were taken

---

*The method used is described in detail in the text on statistical methods of analysis by Snedecor (73).

as the quantity

$$-\frac{1}{b - s_b} < -1/b < -\frac{1}{b + s_b} \qquad 5.3.5.$$

The experimental uncertainty of the data encountered in determining the mean lifetimes from the slope of the linear region of a single luminescence decay curve lead, in general to a random error of less than ± 2 % in the value of the mean lifetime. Lifetimes from luminescence decay curves typified by Fig. 5.3.1.D lead, in general, to an uncertainty as high as ± 10 %.

Repeated investigations of the luminescence decay times of different samples of the same rare earth compound revealed that the experimental errors included other systematic errors and were thus larger than those listed above. The method of preparation, dryness of solvents, and purity of reagents were all found to affect the luminescence decay times to a slight degree. The decay times of the β-diketone chelates were the most susceptible to these effects. When these effects were taken into account in the experimental errors, the accuracy of the measurements was about ± 10% for the lifetimes of rare earth chelates and about ± 5% for the luminescence decay times of the inorganic complexes.

5.4. Decay of Molecular Phosphorescences of Rare Earth Chelates and Organic Compounds

A series of experiments was performed to measure the decay of molecular phosphorescences of both organic compounds and rare earth chelates. The investigations of the molecular phosphorescence of the organic compounds were undertaken in order to determine the accuracy of the lifetime apparatus (See Appendix 5.2.7.). A study of the decays of molecular phosphorescence of rare earth chelates was undertaken as part of the program concerned with determining the rate of intramolecular energy transfer in rare earth chelates.

The decay of phosphorescence emission was determined with the lifetime apparatus described in Section 2.5. and Appendix 5.2. The samples, dissolved in EMPA glasses at 77°K, were irradiated with near ultraviolet light filtered through Corning ultraviolet transmitting filters selected to pass light corresponding to the first strong absorption band of the compound. Corning glass cut-off filters, placed between the sample and the photomultiplier, were selected to pass only emission corresponding to the long-lived phosphorescence of the sample.

Organic compounds selected for study were those compounds listed by McClure (72) which possessed strong (singlet-singlet) absorption bands in the near ultraviolet region of the

spectrum around 3600 Å and intense phosphorescence (triplet-singlet) emission bands between 4500 Å and 6500 Å. The exciting light from the flash lamp was filtered through three Corning #7-54 ultraviolet transmission filters and a saturated aqueous solution of copper sulfate in a 1 cm. long cell. The sample emission was filtered through two Corning #3389 cut-off filters. The phosphorescence decay curves of these compounds are presented in Figs. 5.4.1., 5.4.2., and 5.4.3.

The semilogarithmic plots of most of the decay curves presented here are definitely nonlinear. They are characteristic of first order exponential decays from two or more independently decaying species. Although phosphorescence decay times computed from these curves (see Table 5.2.7.1.) agreed surprisingly well with the data reported by McClure (72), the nonlinearity of the decay from supposedly pure organic compounds was singularly distressing.

That the nonlinearity of the decay curves is due to instrumentation is ruled out by the quite linear phosphorescence decay of diacetyl (a result which is in agreement with the work presented by Bäckström (74). In order to determine whether the nonlinearity was due to concentration effects, measurements were made of the phosphorescence decay of freshly vacuum distilled acetophenone dissolved in EMPA glasses at 77°K. Sample concentrations ranged from 5×10^{-3} to 10^{-4} molar. The decay curves of these solutions were all alike and identical with the nonlinear curve shown in Fig. 5.4.3.

A possible explanation for the nonlinearity of the decay

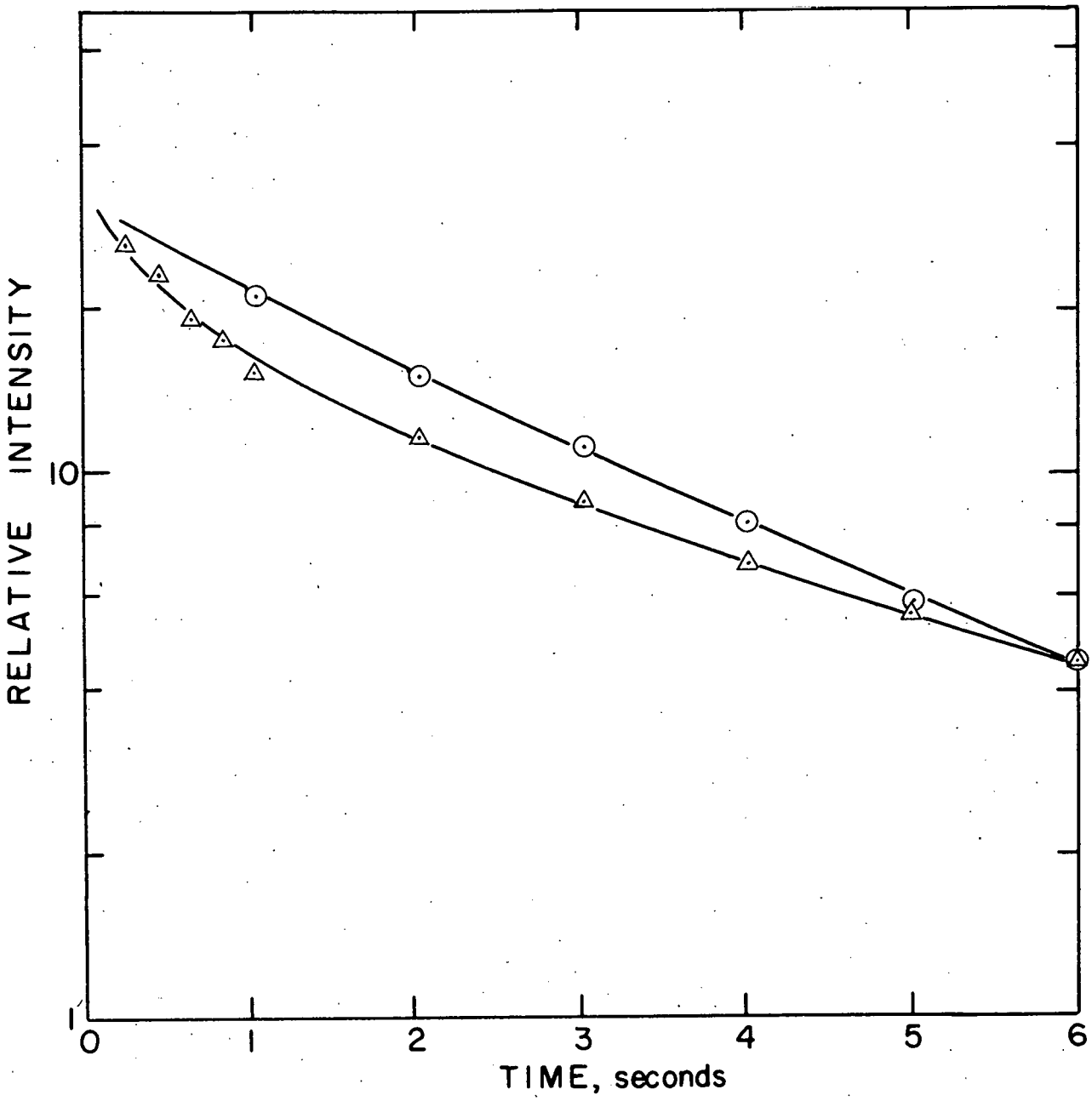

Fig. 5.4.1.--Phosphorescence decays of naphthalene and phenanthrene in EMPA glasses at 77°K.

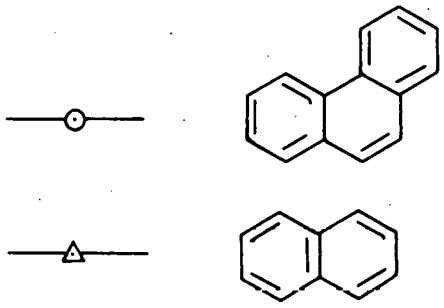

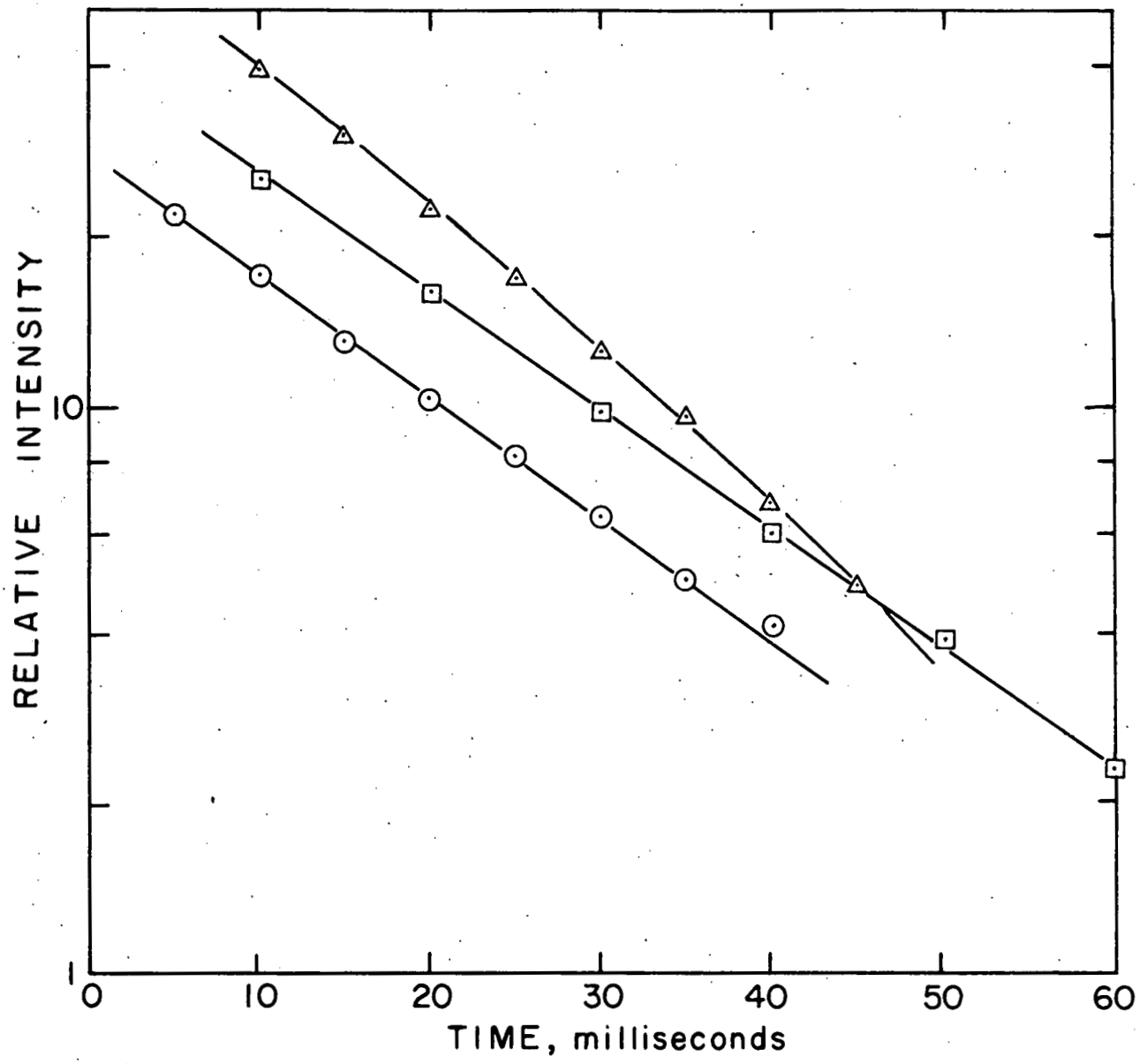

Fig. 5.4.2.--Phosphorescence decays of α-chloronaphthalene, α-bromonaphthalene, and β-bromonaphthalene in EMPA glasses at 77°K.

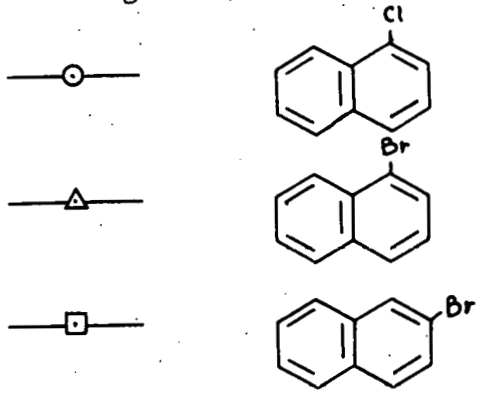

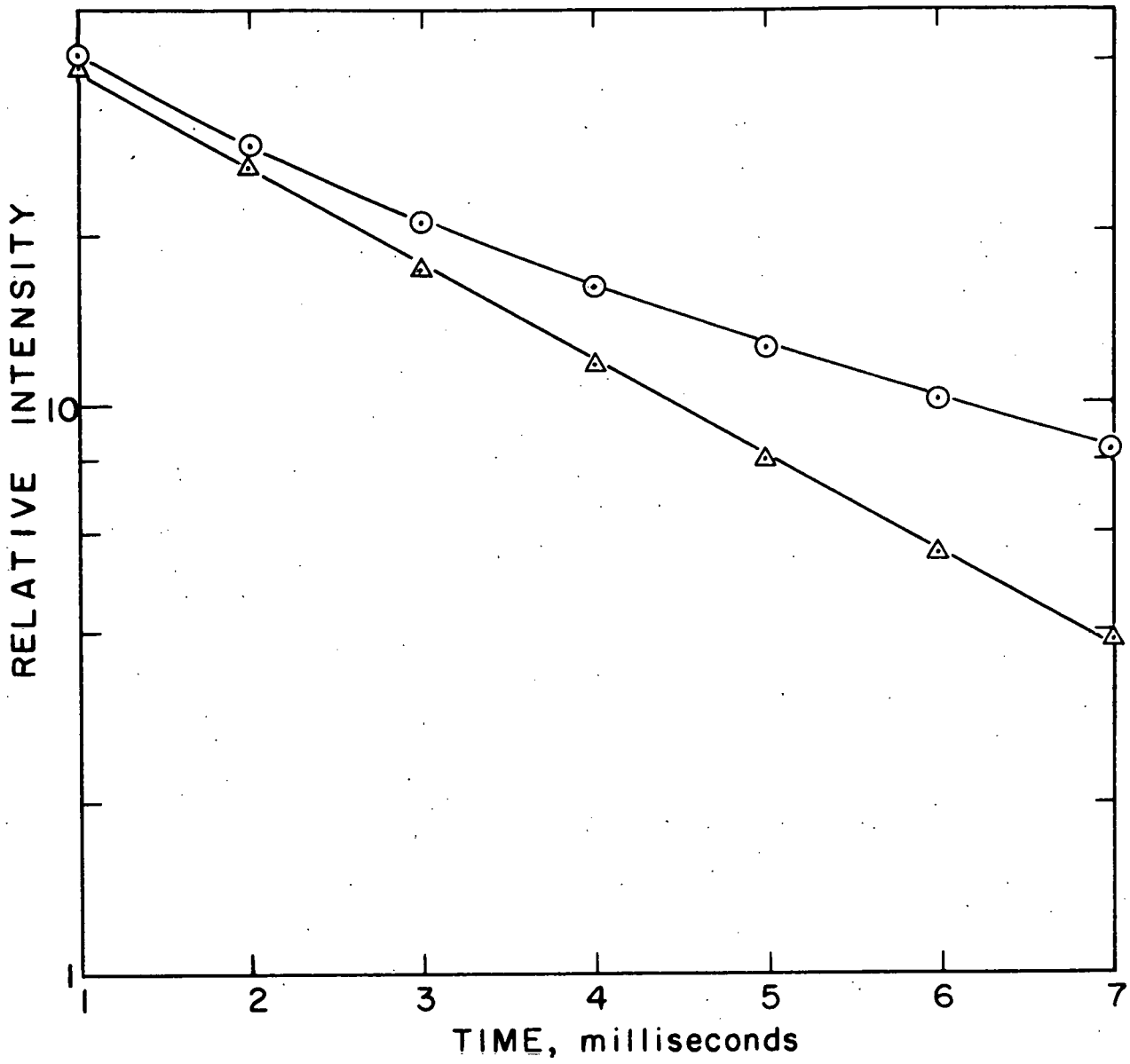

Fig. 5.4.3.--Phosphorescence decays of acetophenone and diacetyl in EMPA glasses at 77°K.

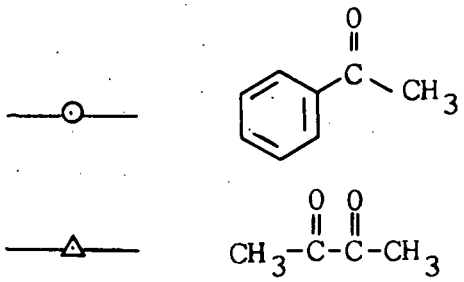

curves could be the formation of different organic species through association with trace contaminants--each specie possessing a slightly different decay time. The concentration of the contaminants need not be very high since the concentrations of the organic compounds used in these studies were between 10^{-5} to 10^{-3} molar. One such contaminant which could very well be causing the trouble is dissolved oxygen gas. Oxygen gas dissolved in solutions of organic compounds has been shown to increase the absorption strengths of the singlet-triplet band (75). An increased singlet-triplet absorption coefficient would imply that those compounds associated with oxygen gas have shorter phosphorescence decay times. No further work was done with the organic compounds.

Chelates of trivalent lanthanum, gadolinium, and lutetium derived from benzoylacetone were selected for the phosphorescence decay studies. Light filter combinations used to filter the exciting light from the flash lamp were the same as those listed in Table 2.4.4.1. The sample emission was filtered through two Corning #3385 cut-off filters. Only the green phosphorescence emission of the chelate reached the photomultiplier tube. The luminescence decay curves obtained from these chelates are presented in Figs. 5.4.4. and 5.4.5. (The phosphorescence decay times calculated from these curves are summarized in Table 3.2.2.1.)

The nonlinearity of the semilogarithmic plots of the luminescence decays was, as in the case of the organic compounds, an unsuspected result. No mention of this phenomenon

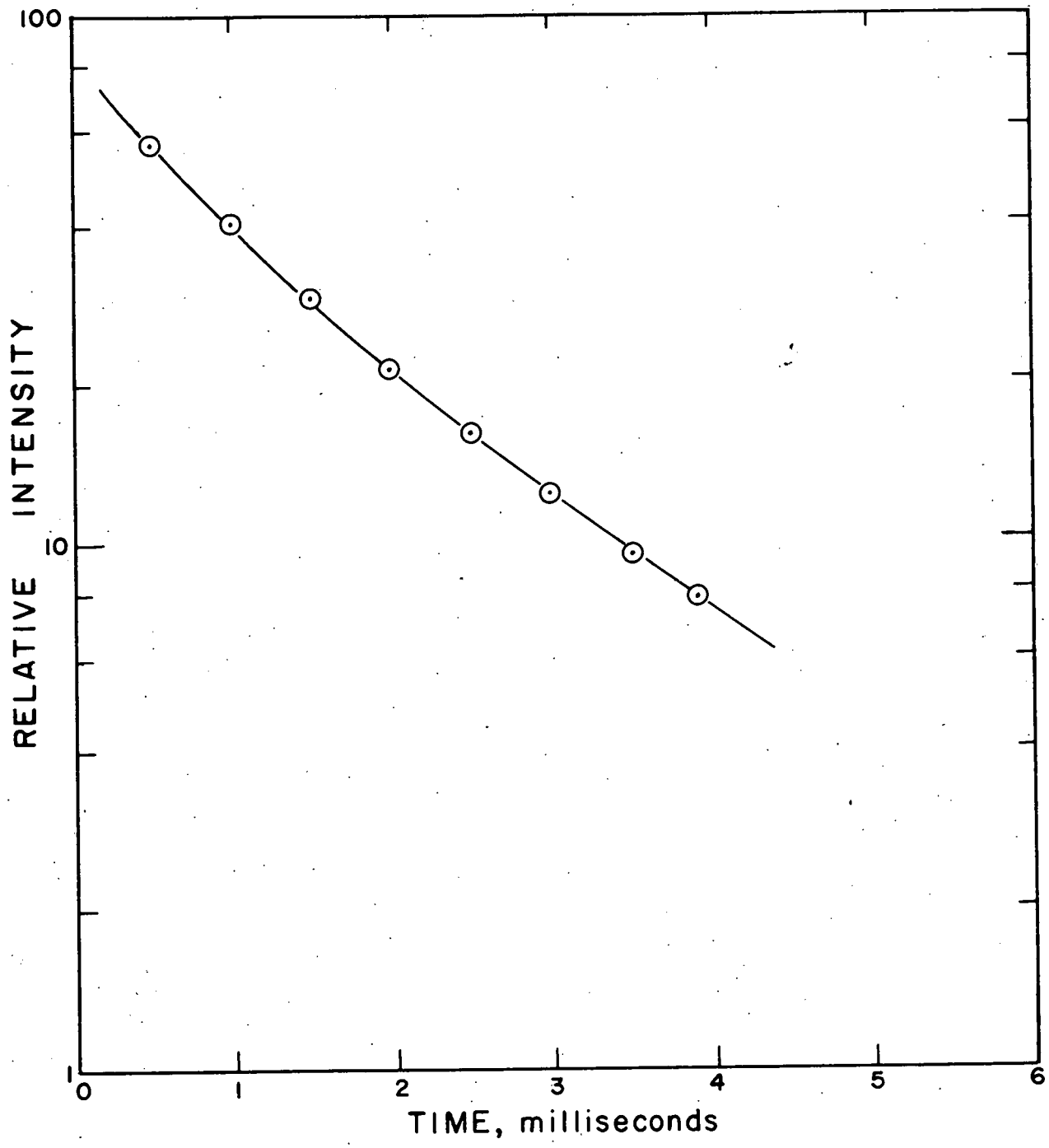

Fig. 5.4.4.--Phosphorescence decay of gadolinium trisbenzoylacetonate dihydrate in an EMPA glass at 77°K.

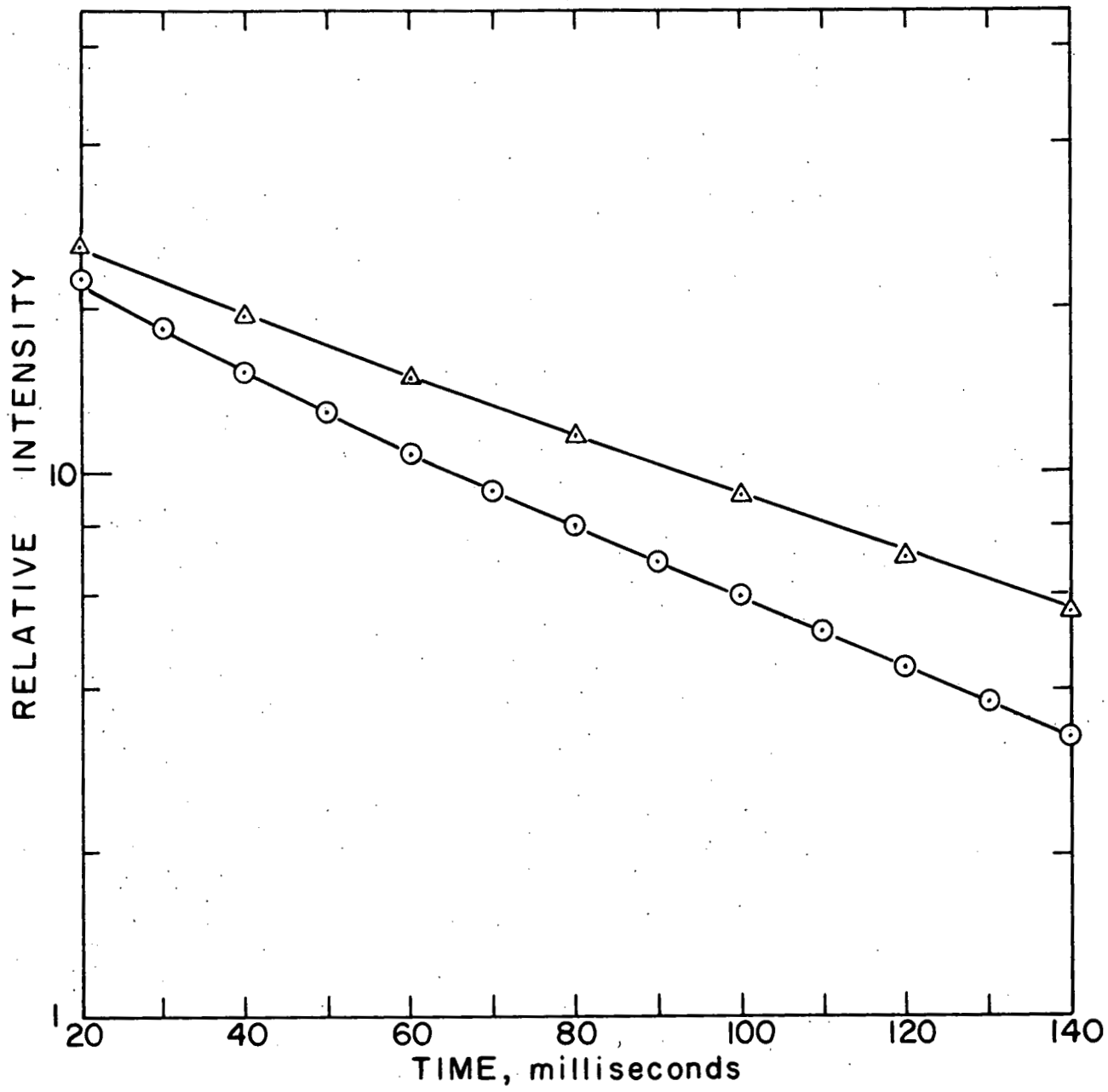

Fig. 5.4.5.--Phosphorescence decays of lanthanum and lutetium trisbenzoylacetonate dihydrates in EMPA glasses at 77°K.

—⊙— $LaB_3 \cdot 2H_2O$

—△— $LuB_3 \cdot 2H_2O$

was made by previous researchers (33,72). The existence of two or more emitting species of rare earth chelates in EMPA glasses is not too surprising in view of the dissociation of the chelates found to occur in these systems. As discussed in Section 3.3.2.6., the formation of clear EMPA glasses of rare earth chelates is accompanied by the formation of charged chelate species. Each of these species could very well have significantly different phosphorescence decay times.

Attempts to measure the phosphorescence decay times of benzoylacetonate chelates of other rare earth ions were unsuccessful because the phosphorescence emissions from the complexes were much too weak to be recorded by the apparatus. Due to the complexity of the phosphorescence decay curves and the low intensity of the phosphorescences emitted by the majority of the chelates, this phase of the investigation was discontinued.

5.5. Semilogarithmic Plots of Rare Earth Ion Luminescence Decays

5.5.1. Sodium Metaphosphate Glasses

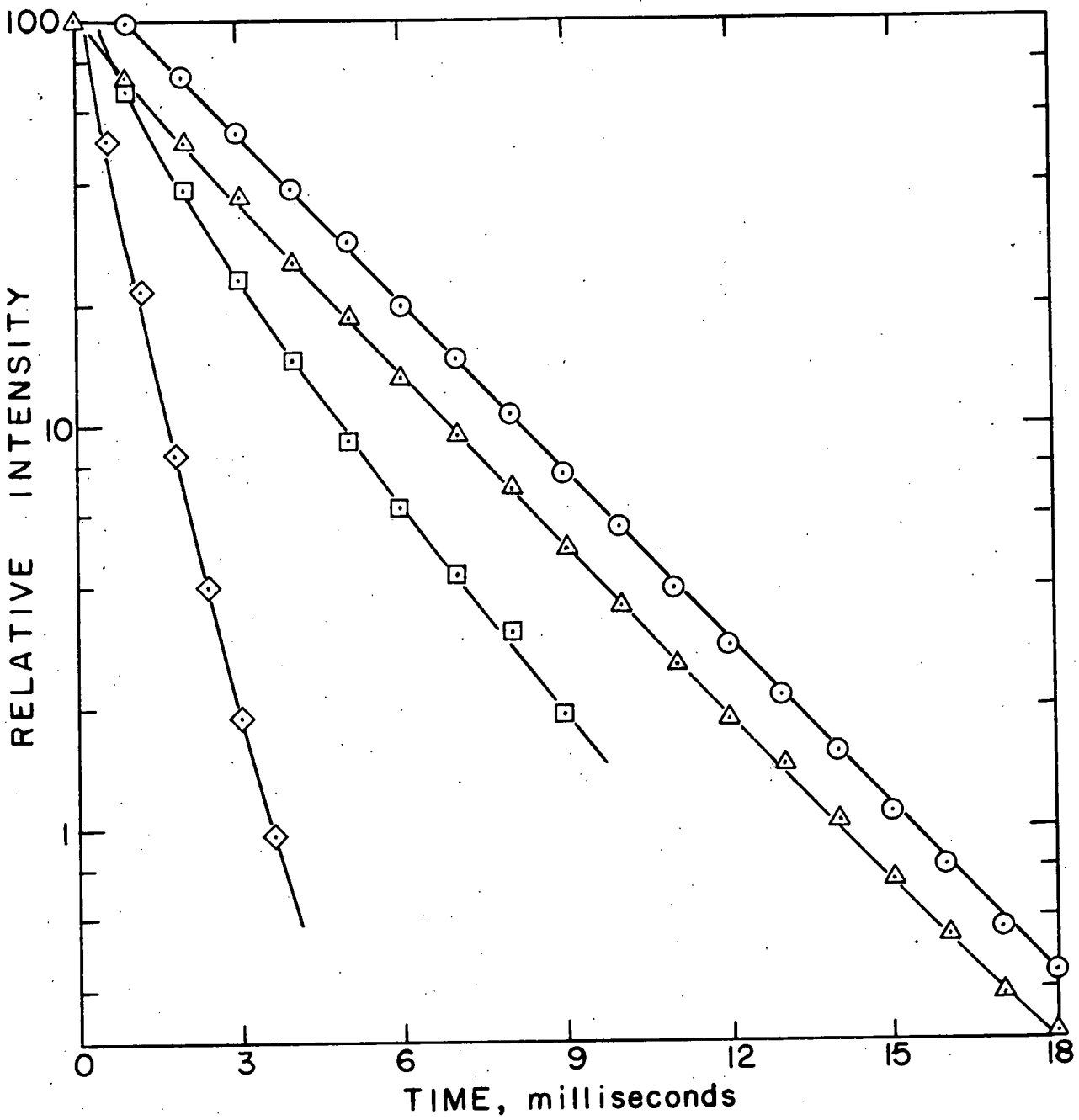

Fig. 5.5.1.1.--Luminescence decays of sodium metaphosphate glasses at 77°K containing 2 % by weight rare earth oxides.

—⊙— Terbium oxide

—△— Europium oxide

—□— Samarium oxide

—◇— Dysprosium oxide

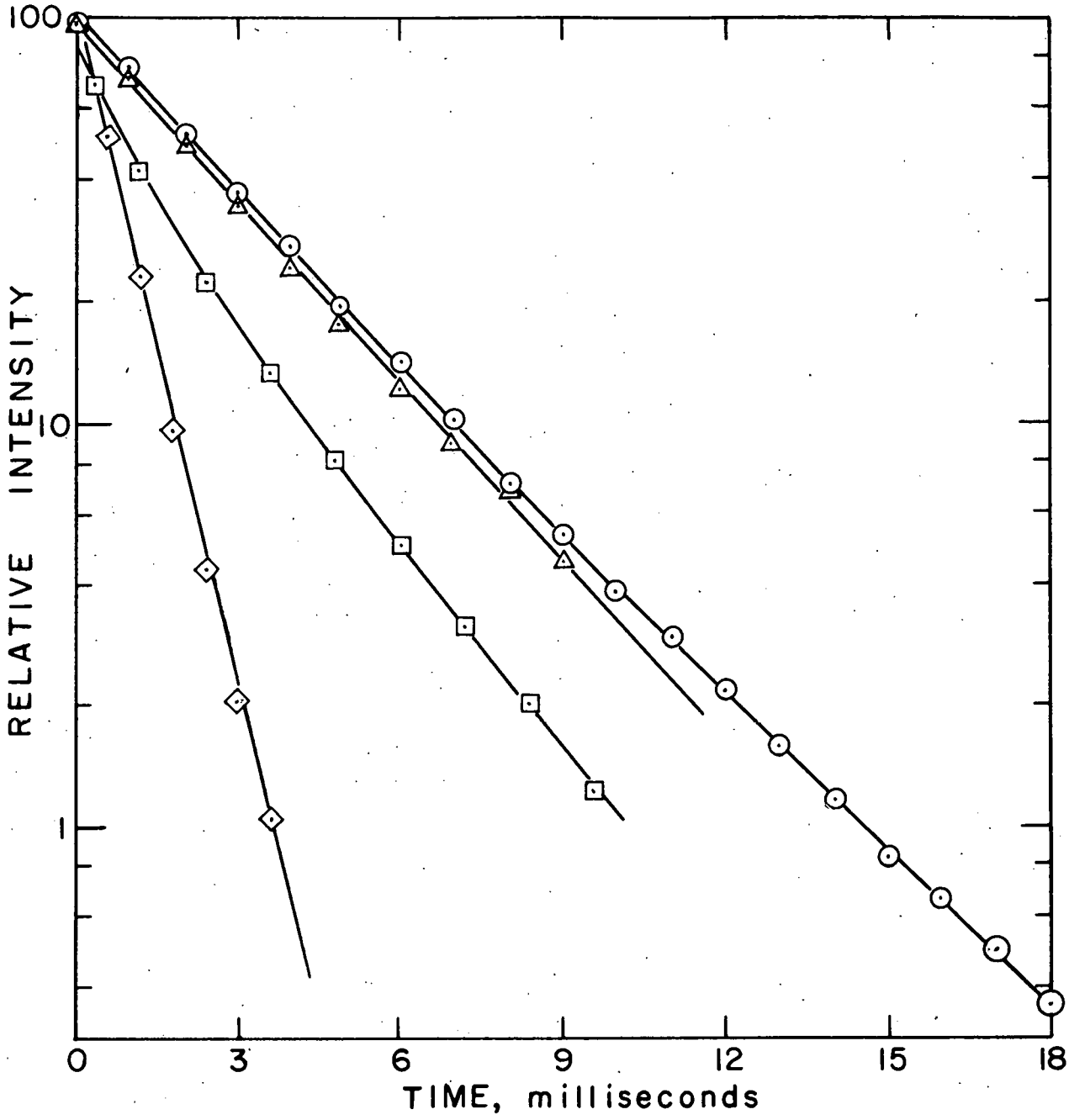

Fig. 5.5.1.2.--Luminescence decays of sodium metaphosphate glasses at 298°K containing 2 % by weight rare earth oxides.

—⊙— Terbium oxide

—△— Europium oxide

—□— Samarium oxide

—◇— Dysprosium oxide

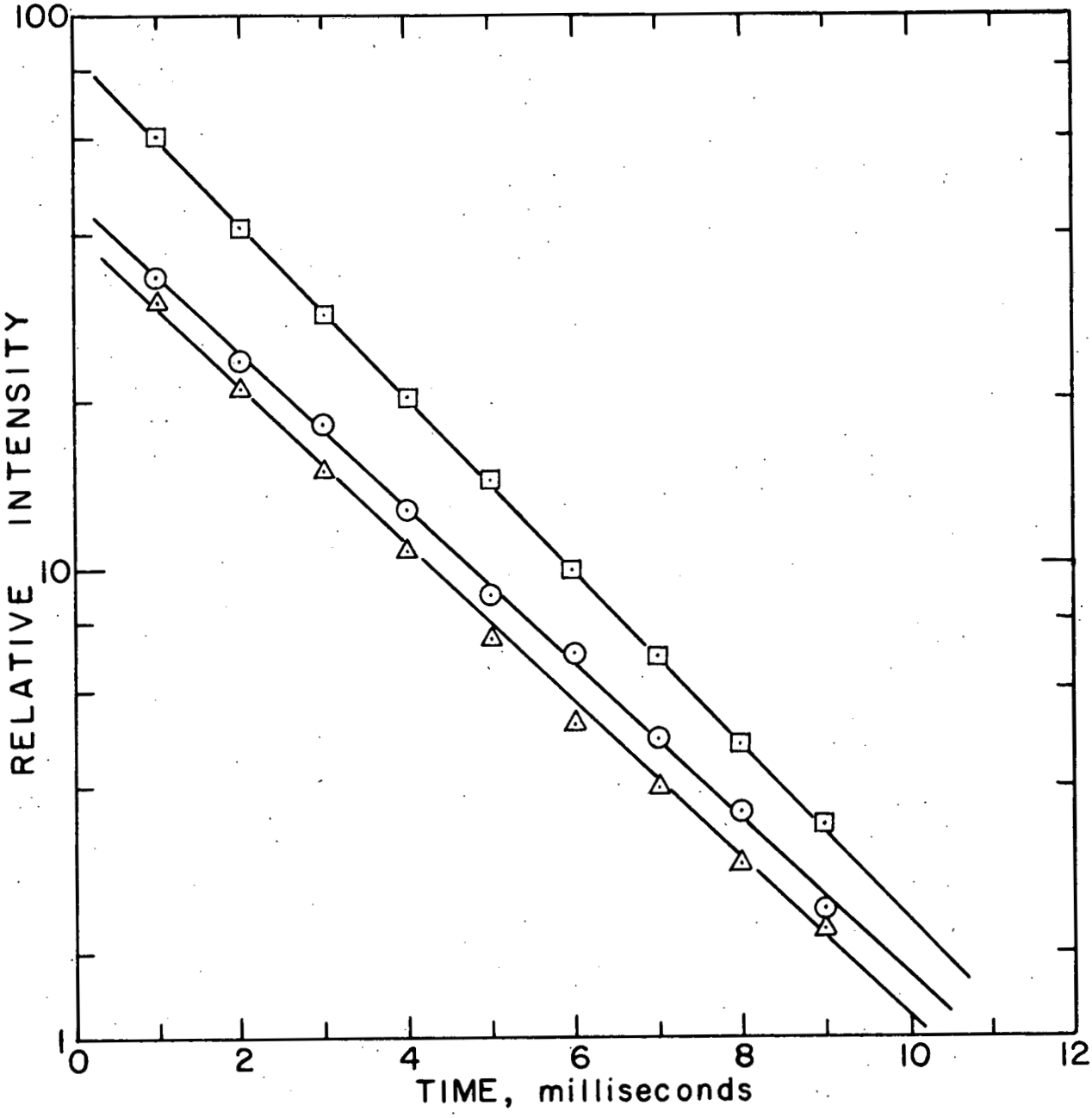

Fig. 5.5.1.3.--Luminescence decays of sodium metaphosphate glasses at 298°K containing 0.1, 1.0, and 10 % by weight europium oxide.

—⊙— 0.1 % europium oxide

—△— 1.0 % europium oxide

—⊡— 10 % europium oxide

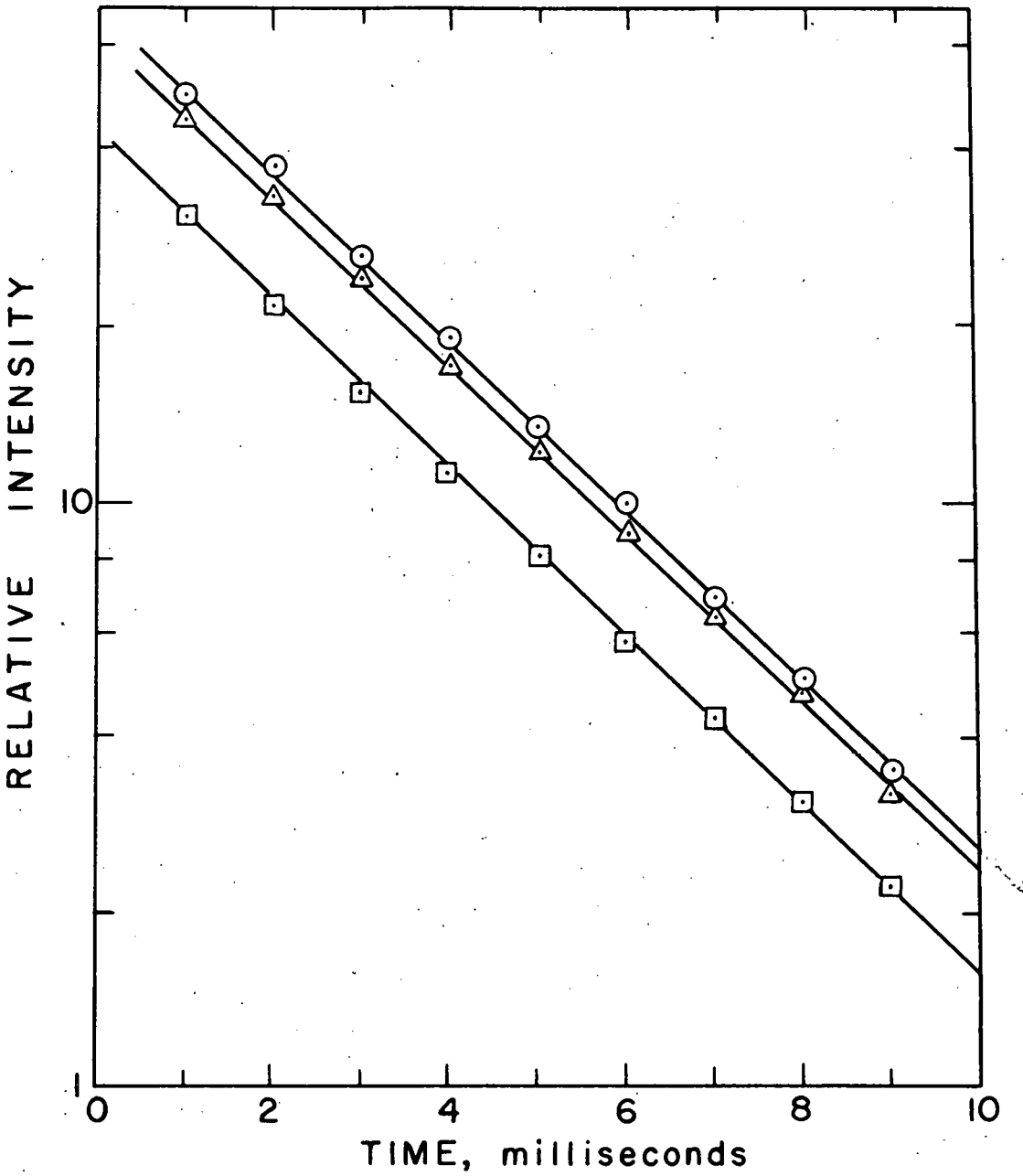

Fig. 5.5.1.4.--Luminescence decays of sodium metaphosphate glasses at 298°K containing 0.1, 1.0, and 10 % by weight terbium oxide.

—⊙— 0.1 % terbium oxide

—△— 1.0 % terbium oxide

—⊡— 10 % terbium oxide

5.5.2. Betadiketone Chelates

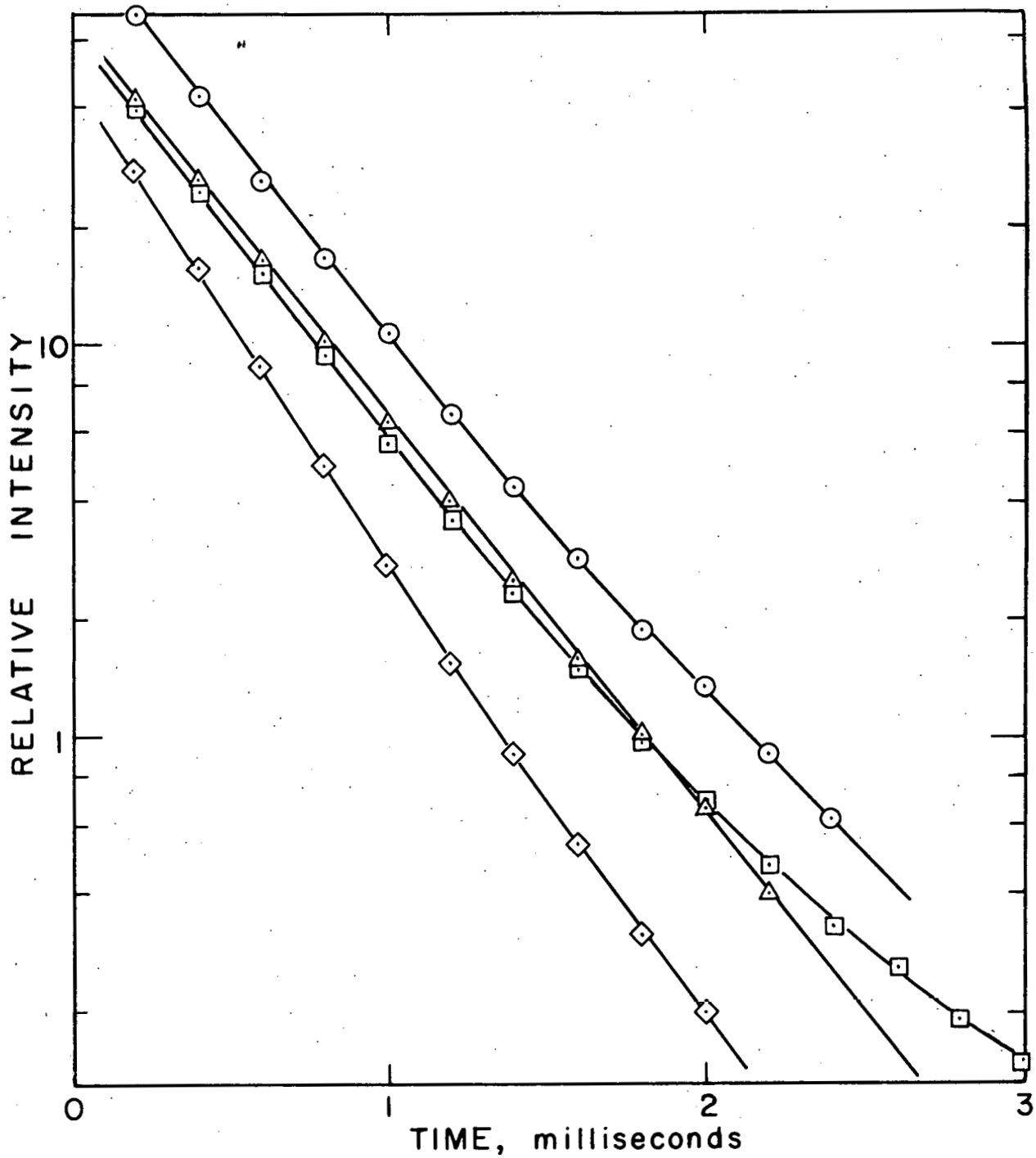

Fig. 5.5.2.1.--Luminescence decay of europium trisbenzoylacetonate dihydrate at 77°K.

—⊙— Microcrystalline solid

—△— EMPA glass

—□— EMP glass

—◇— MP glass

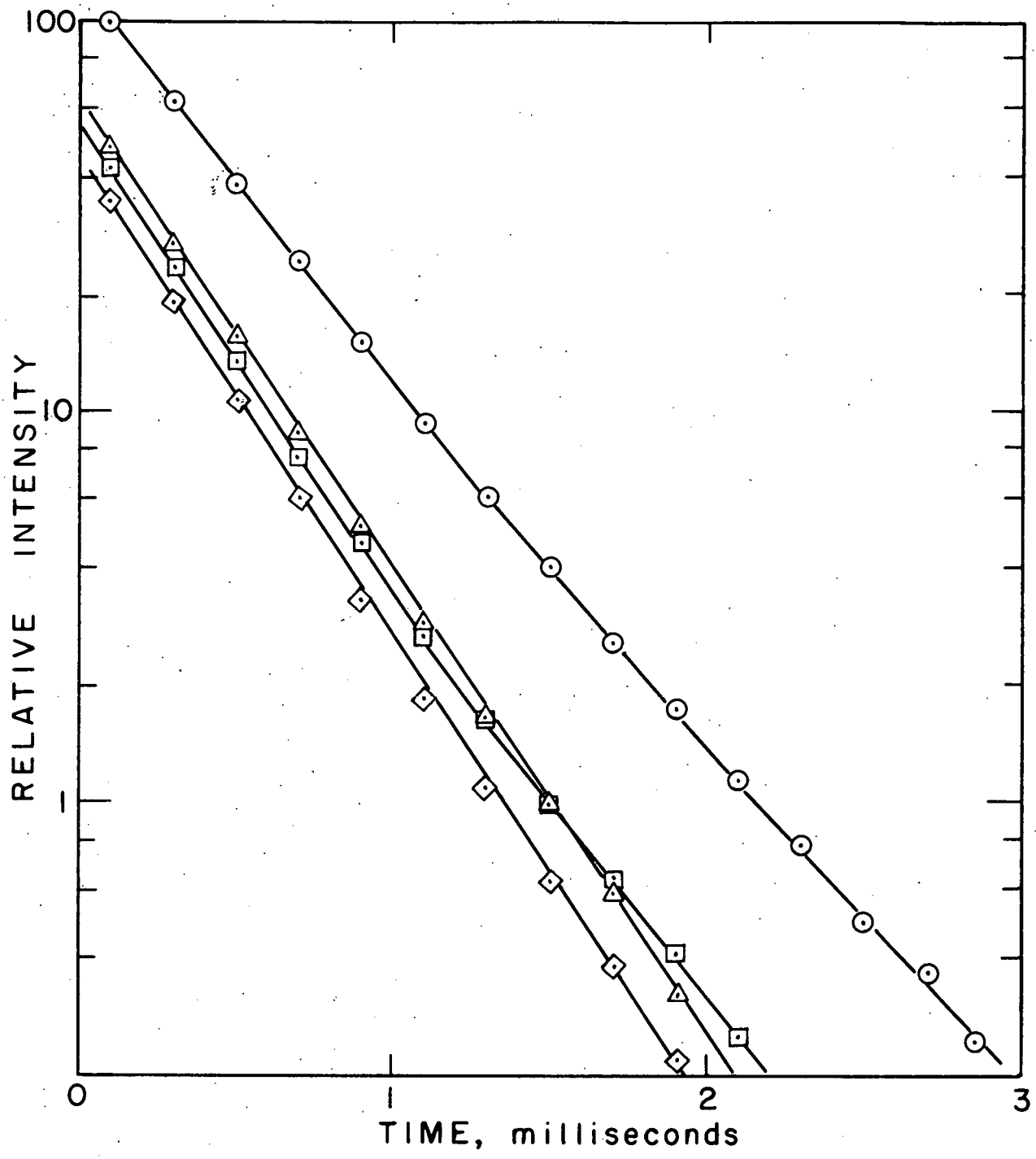

Fig. 5.5.2.2.--Luminescence decay of europium tris-dibenzoylmethide at 77°K.

—⊙— Microcrystalline solid

—△— EMPA glass

—□— EMP glass

—◇— MP glass

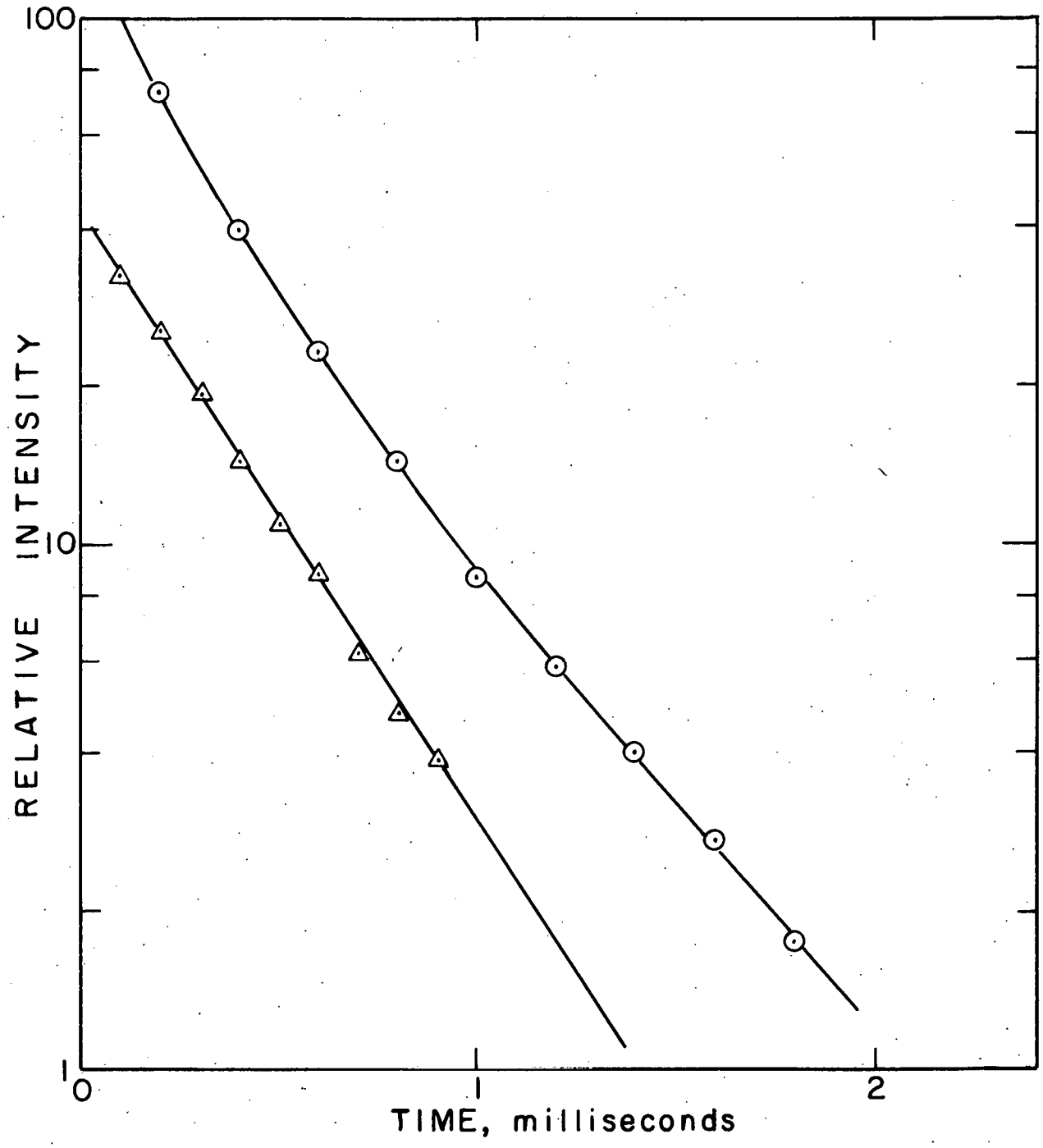

Fig. 5.5.2.3.--Luminescence decay of europium tris-dibenzoylmethide solvated with one mole of dibenzoylmethane at 77°K.

—⊙— Microcrystalline solid

—△— EMPA glass

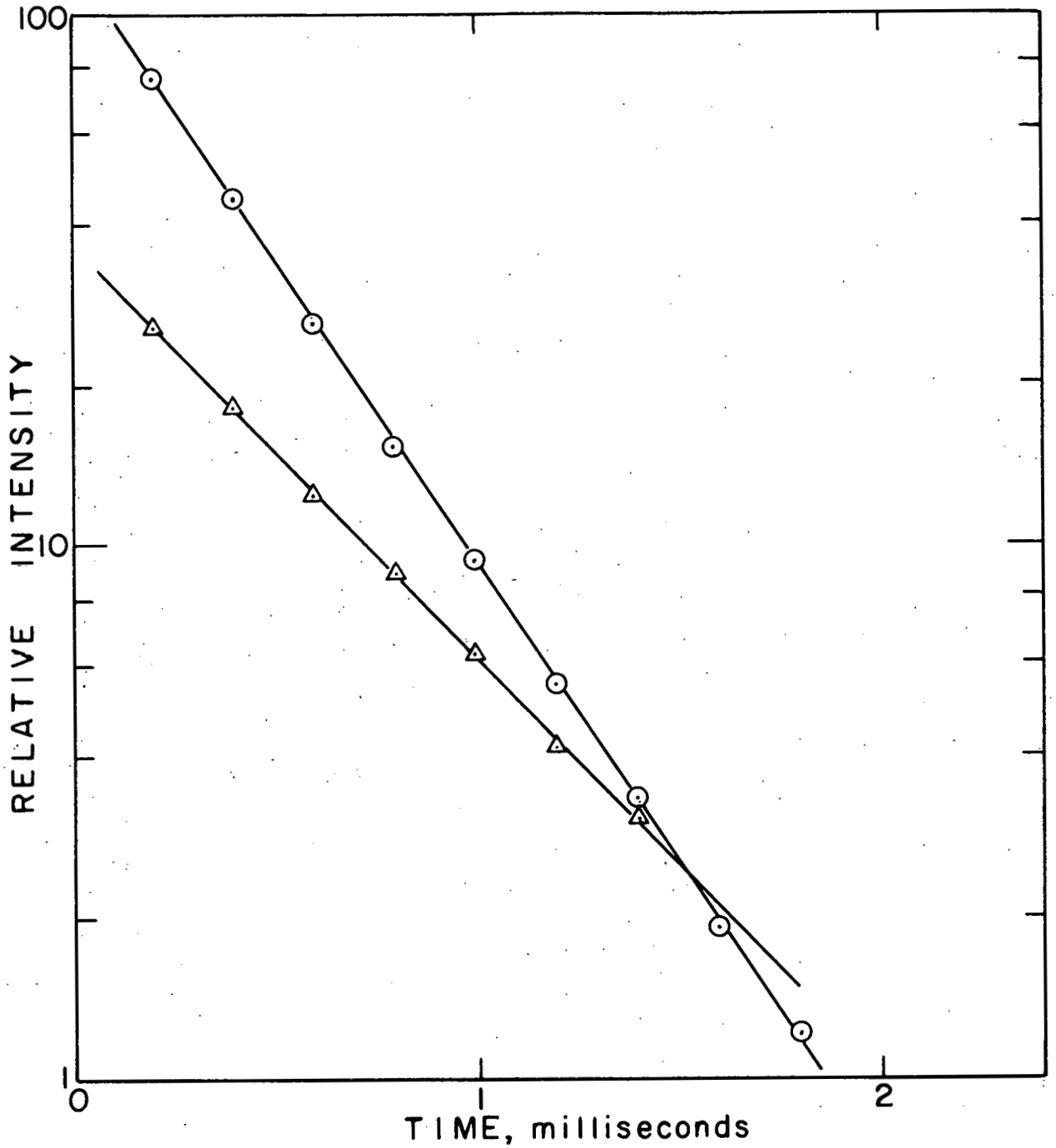

Fig. 5.5.2.4.--Luminescence decay of europium tris-acetylacetonate monohydrate at 77°K.

—⊙— Microcrystalline solid

—△— EMPA glass

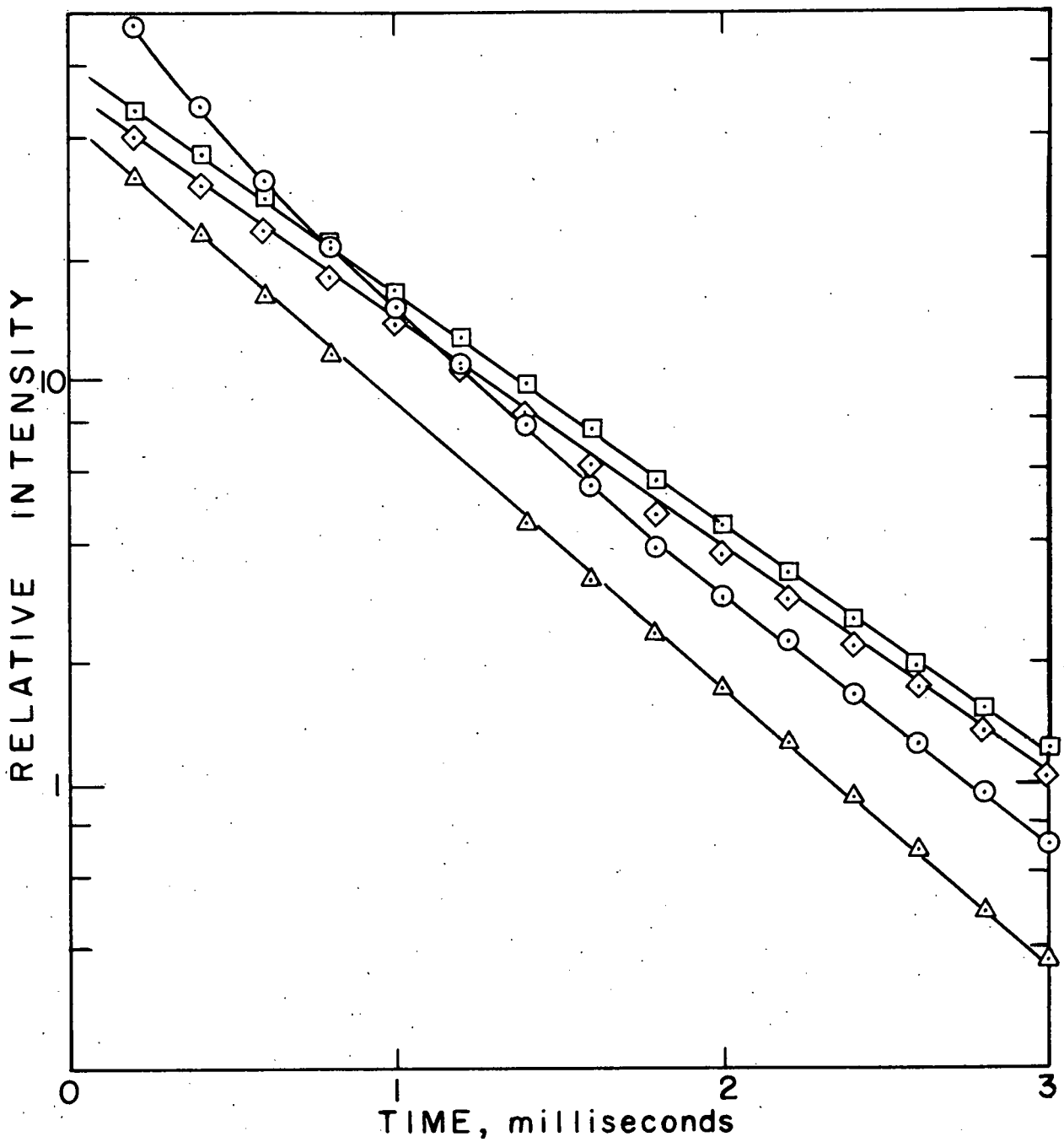

Fig. 5.5.2.5.--Luminescence decay of terbium tris-benzoylacetonate dihydrate at 77°K.

Microcrystalline solid

EMPA glass

EMP glass

MP glass

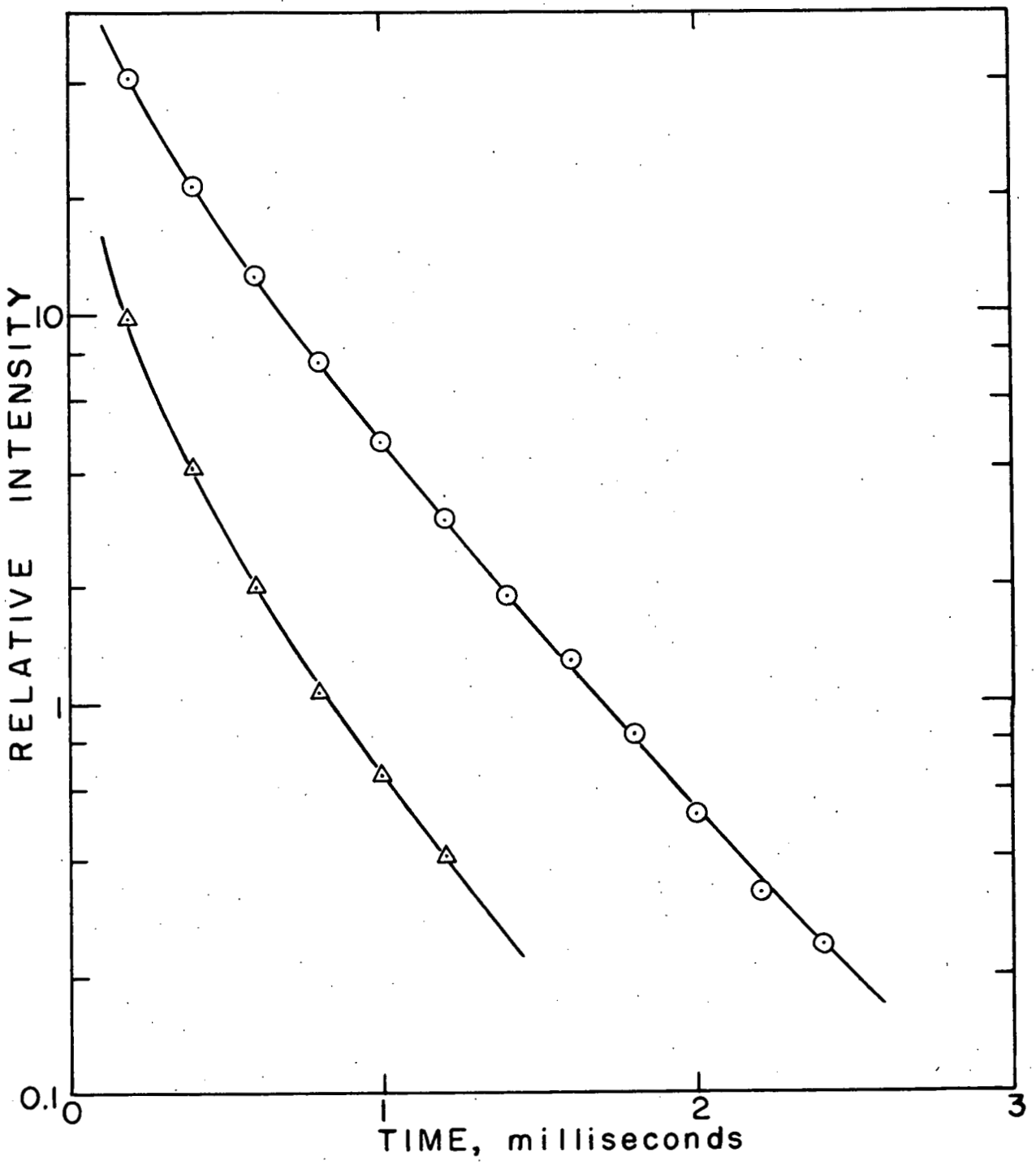

Fig. 5.5.2.6.--Luminescence decay of terbium trisdibenzoylmethide at 77°K.

—⊙— EMPA glass

—△— EMP glass

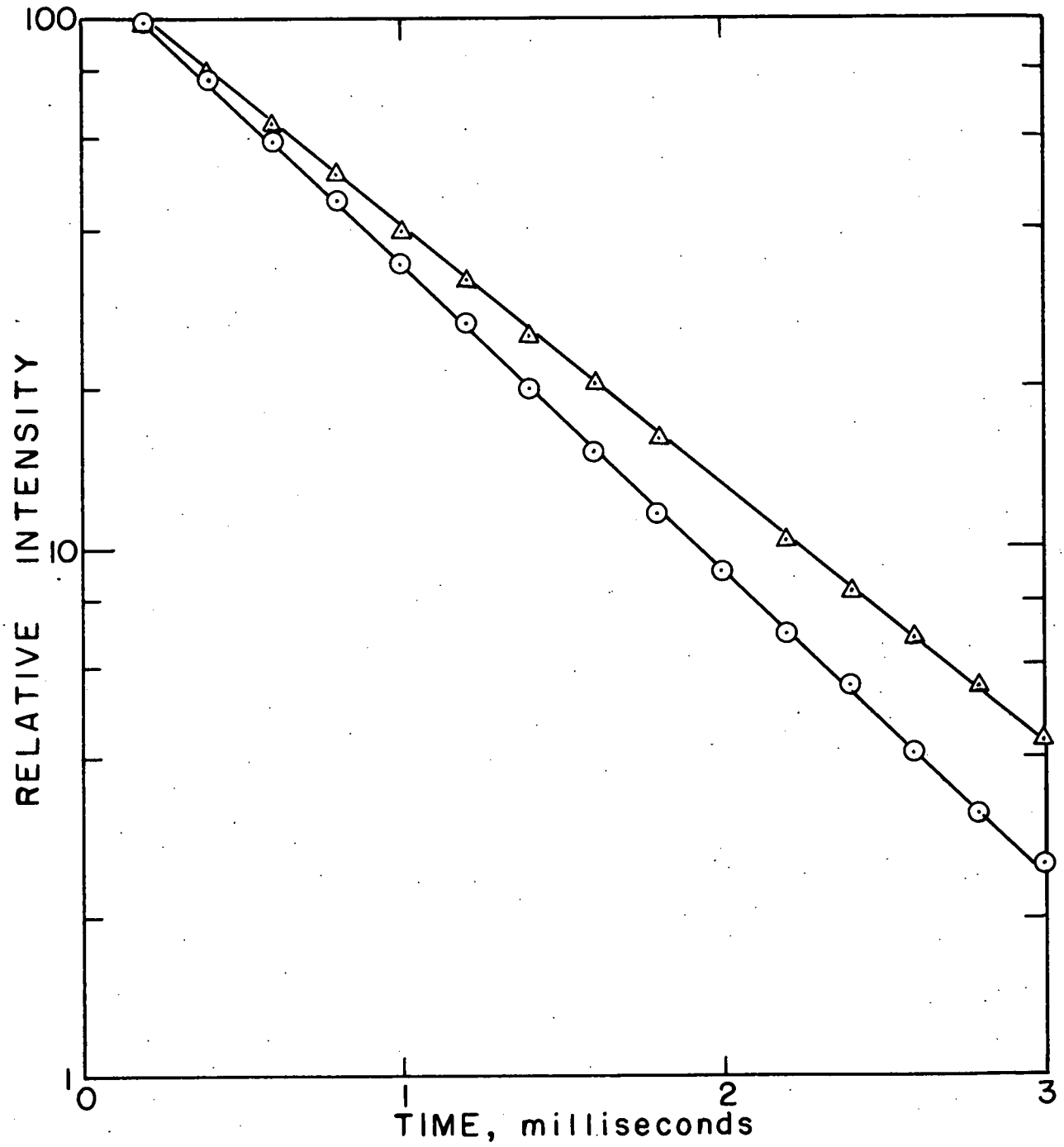

Fig. 5.5.2.7.--Luminescence decay of terbium tris-acetylacetonate monohydrate at 77°K.

—⊙— Microcrystalline solid

—△— EMPA glass

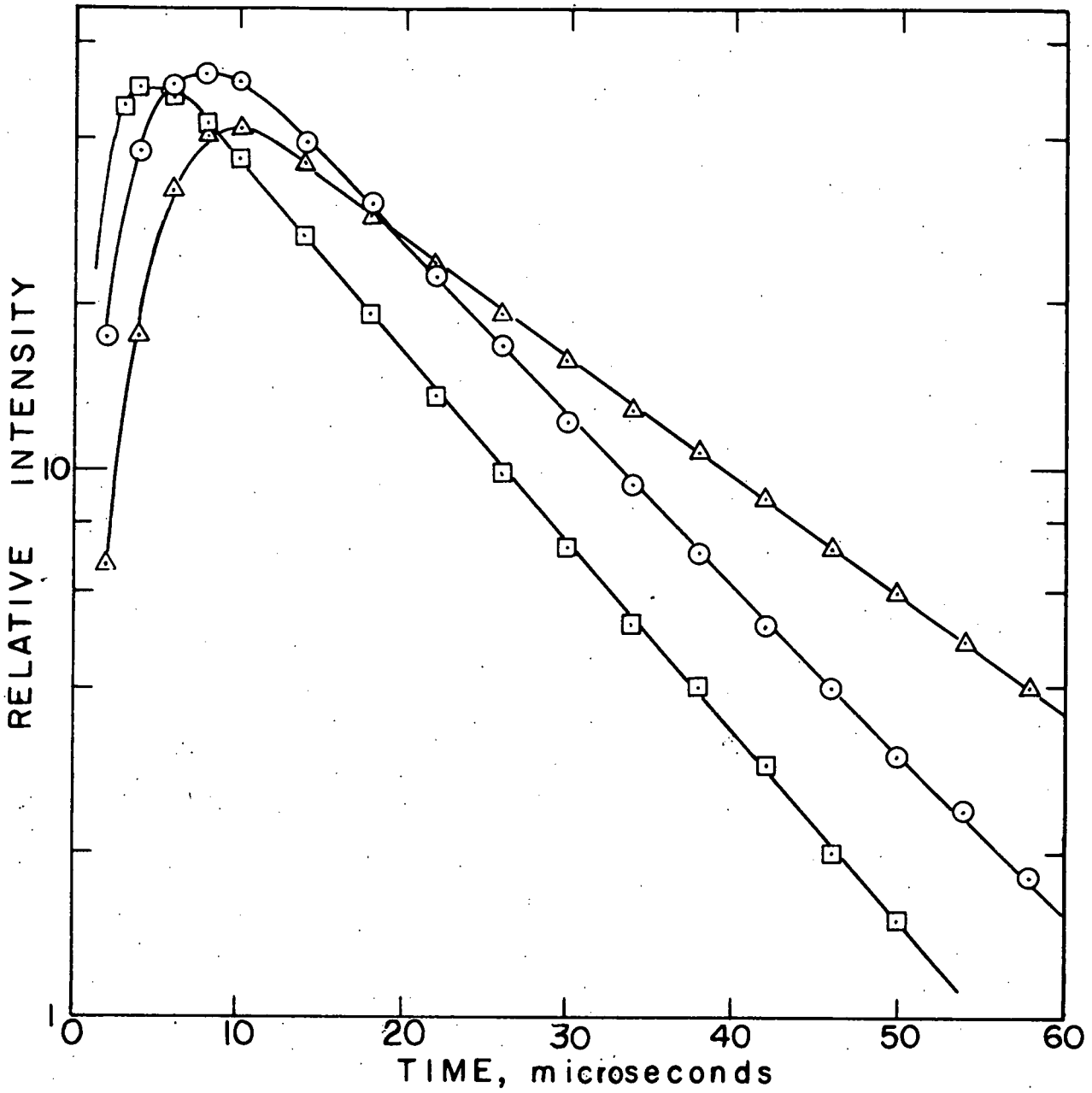

Fig. 5.5.2.8.--Luminescence decays of trivalent samarium and dysprosium chelates in EMPA glasses at 77°K.

—⊙— $SmB_3 \cdot 2H_2O$

—△— SmD_3

—⊡— $DyB_3 \cdot 2H_2O$

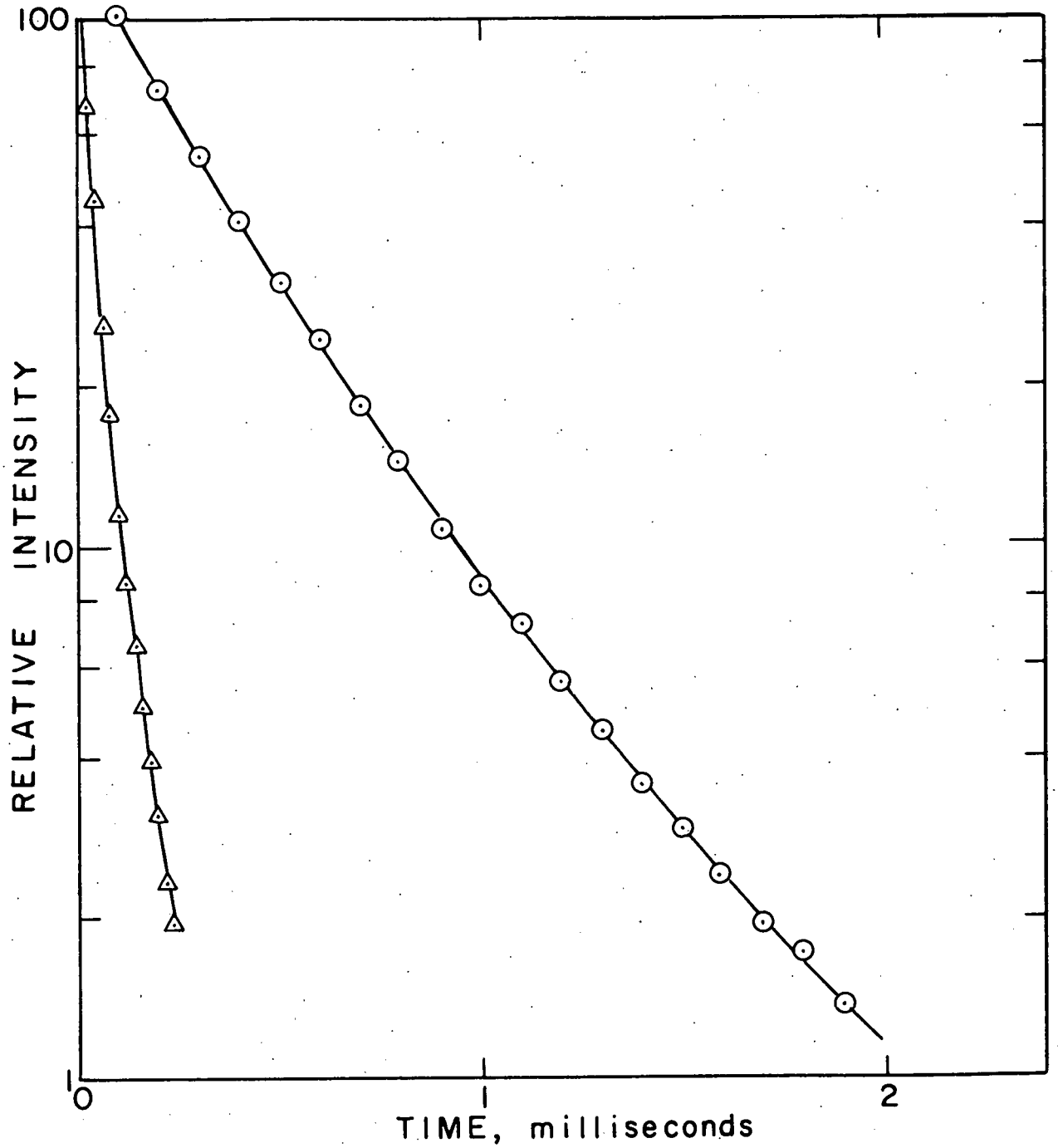

Fig. 5.5.2.9.--Luminescence decays of microcrystalline europium trisdibenzoylmethide and europium trisdibenzoylmethide solvated with dibenzoylmethane at 298°K.

—⊙— $EuD_3 \cdot DH$

—△— EuD_3

5.5.3. Solvated Inorganic Chlorides

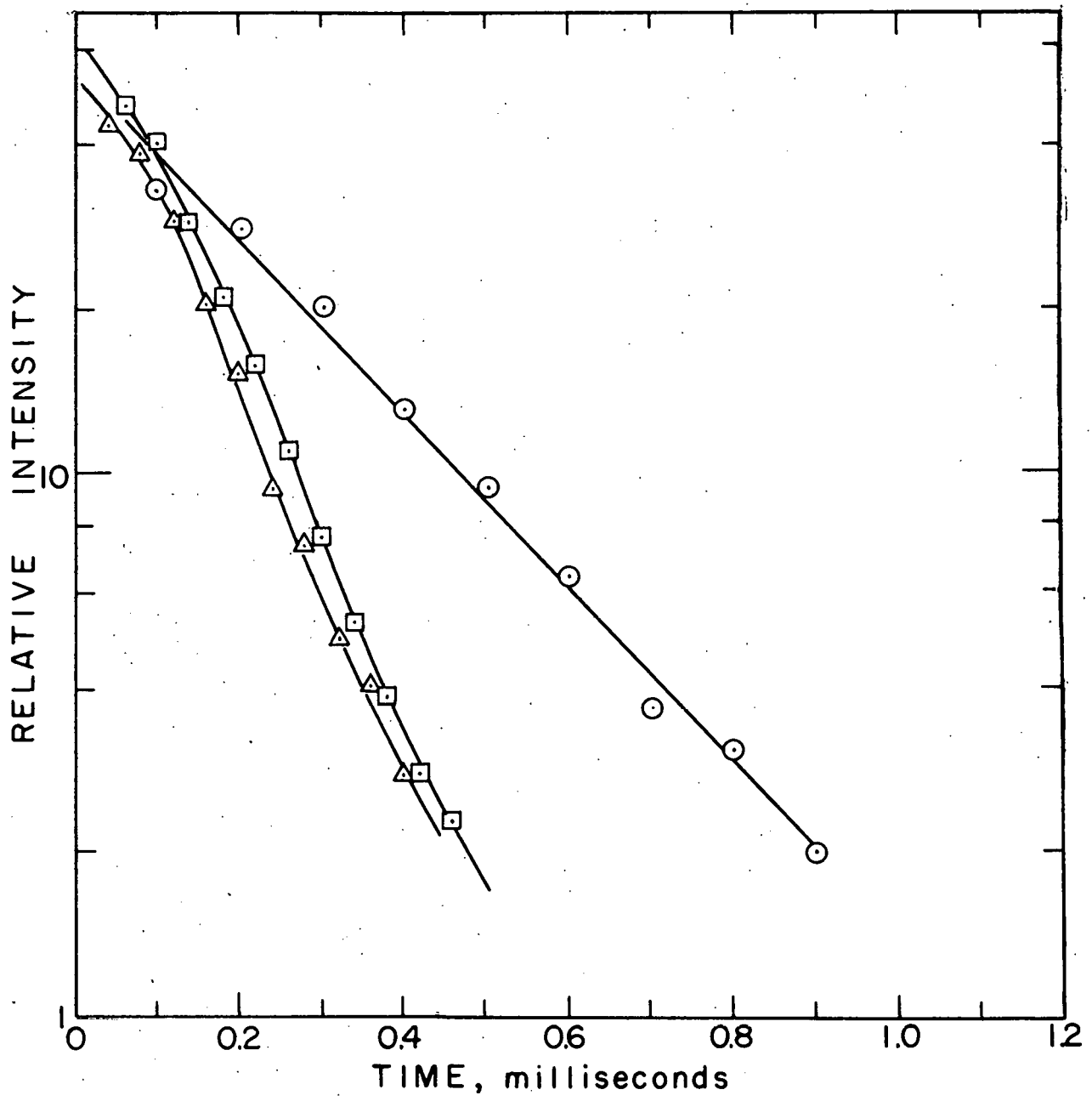

Fig. 5.5.3.1.--Luminescence decays of microcrystalline solvated europium chlorides.

—⊙— $EuCl_3 \cdot 6D_2O$ at 77°K

—△— $EuCl_3 \cdot 6H_2O$ at 77°K

—⊡— $EuCl_3 \cdot 6H_2O$ at 298°K

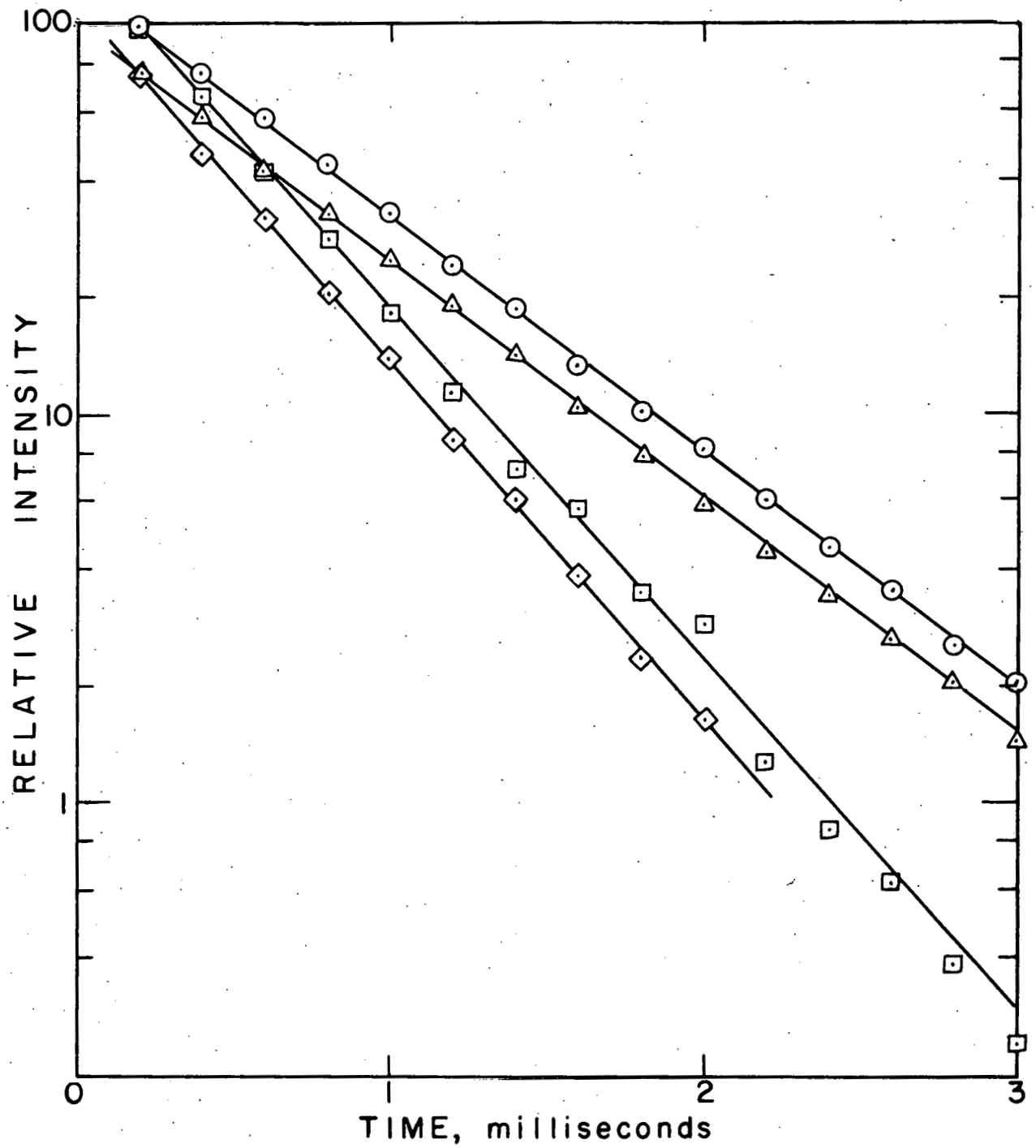

Fig. 5.5.3.2.--Luminescence decays of microcrystalline solvated terbium chlorides.

—⊙— $TbCl_3 \cdot 6D_2O$ at 77°K

—△— $TbCl_3 \cdot 6D_2O$ at 298°K

—□— $TbCl_3 \cdot 6H_2O$ at 77°K

—◇— $TbCl_3 \cdot 6H_2O$ at 298°K

6. Literature Cited

(1) R. C. Vickery, Analytical Chemistry of the Rare Earths (Pergamon Press, New York, 1961).

(2) L. J. F. Broer, C. J. Gorter, and J. Hoogschagen, Physica 11, 231 (1945).

(3) Donald S. McClure, "Electronic Spectra of Molecules and Ions in Crystals," Solid State Physics, eds. Frederik Seitz and David Turnbull (Academic Press, New York, 1959), Vol. 9, p. 399.

(4) G. H. Dieke, "Spectroscopic Observations on Maser Materials," Advances in Quantum Electronics, ed. J. R. Singer (Columbia University Press, New York, 1961), p. 164.

(5) G. H. Dieke and R. Sarup, J. Chem. Phys. 36, 371 (1962).

(6) F. Varsanyi and G. H. Dieke, J. Chem. Phys. 36, 835 (1962).

(7) M. S. Magno and G. H. Dieke, J. Chem. Phys. 37, 2354 (1962).

(8) L. G. DeShazer and G. H. Dieke, J. Chem Phys, 38, 2190 (1963).

(9) K. S. Thomas, S. Singh, and G. H. Dieke, J. Chem. Phys. 38, 2180 (1963).

(10) Bettina Rinck, Z. Naturforsch. 3a, 406 (1948).

(11) H. F. Geisler and K. H. Hellwege, Z. Physik 136, 293 (1953).

(12) S. I. Weissman, J. Chem. Phys. 10, 214 (1942).

(13) A. N. Sevchenko and A. G. Morachevskii, Izvest. Akad. Nauk S. S. S. R., Ser. Fiz. 15, 628 (1951).

(14) A. N. Sevchenko and A. K. Trofimov, Zhur. Eksp. i Teort. Fiz. 21, 220 (1951).

(15) G. A. Crosby and M. Kasha, Spectrochim. Acta 10, 377 (1958).

(16) G. A. Crosby and R. E. Whan, Naturwissenschaften 47, 276 (1960).

(17) G. A. Crosby and R. E. Whan, J. Chem. Phys. 32, 614 (1960).

(18) G. A. Crosby, R. E. Whan, and R. M. Alire, J. Chem. Phys. 34, 743 (1961).

(19) G. A. Crosby and R. E. Whan, J. Chem. Phys. 36, 863 (1962).

(20) R. E. Whan and G. A. Crosby, J. Mol. Spectroscopy 8, 315 (1962).

(21) G. A. Crosby, R. E. Whan, and J. J. Freeman, J. Phys. Chem. 66, 2493 (1962).

(22) Ruth Elaine Whan, Doctoral Dissertation (University of New Mexico, Albuquerque, New Mexico, 1962).

(23) T. D. O'Brien, "Scandium, Yttrium, and the Lanthanides," Comprehensive Inorganic Chemistry, ed. M. C. Sneed and R. C. Brasted (D. Van Nostrand Co., Inc., New York, 1955), Vol. 14.

(24) Albert F. Cotton and G. Wilkinson, Advanced Inorganic Chemistry (Interscience Publishers, New York, 1962).

(25) L. Halleck and L. Hartinger, Angew. Chem. 67, 648 (1955).

(26) Louis F. Fieser, Experiments in Organic Chemistry (D. C. Heath and Co., New York, 1941), p. 359.

(27) Glass Color Filters (Corning Glass Works, Corning, N. Y., 1948).

(28) M. Kasha, J. Opt. Soc. Amer. 38, 929 (1948).

(29) Gerhardt Friedlander and Joseph W. Kennedy, Nuclear and Radiochemistry (John Wiley & Sons, Inc., New York, 1960).

(30) G. H. Dieke and L. A. Hall, J. Chem. Phys. 27, 465 (1957).

(31) M. Kasha, Discussions Faraday Soc. 9, 14 (1950).

(32) G. H. Dieke and S. Singh, J. Opt. Soc. Amer. 46, 495 (1956).

(33) Phillip Yuster and S. I. Weissman, J. Chem. Phys. 17, 1182 (1949).

(34) G. H. Dieke and L. Leopold, J. Opt. Soc. Amer. 47, 944 (1957).

(35) Gerhard Herzberg, Atomic Structure and Atomic Spectra (Dover Publications, New York, 1944).

(36) Gordon M. Barrow, Molecular Spectroscopy (McGraw-Hill Book Company, Inc., New York, 1962), p. 310.

(37) Donald G. Miller, Edward V. Sayre, and Simon Freed, J. Chem. Phys. 29, 454 (1958).

(38) John L. Prather, Atomic Energy Levels in Crystals (National Bureau of Standards Monograph 19, Washington, D. C. 1961), p. 38.

(39) G. Joos and K. H. Hellwege, Ann. Physik 39, 128 (1941).

(40) L. G. Van Uitert, J. Electrochem. Soc. 110, 1 (1963).

(41) L. G. Van Uitert, J. Chem. Phys. 37, 981 (1962).

(42) L. G. Van Uitert and S. Iida, J. Chem. Phys. 37, 986 (1962).

(43) L. G. Van Uitert, J. Electrochem. Soc. 107, 803 (1960).

(44) Martin Gouterman, J. Chem. Phys. 36, 2846 (1962).

(45) Robert A. Satten, J. Chem. Phys. 27, 286 (1957).

(46) Simon Freed, Rev. Mod. Phys. 14, 105 (1942).

(47) Edward V. Sayre and Simon Freed, J. Chem. Phys. 24, 1213 (1956).

(48) G. W. Robinson and R. P. Frosch, J. Chem. Phys. 37, 1962 (1962).

(49) G. W. Robinson and R. P. Frosch, J. Chem. Phys. 38, 1187 (1963).

(50) R. Orbach, Proc. Roy. Soc. (London) A 264, 458 (1961).

(51) R. Orbach, Proc. Roy. Soc. (London) A 264, 485 (1961).

(52) R. D. Mattuck and M. W. P. Strandberg, Phys. Rev. 119, 1204 (1960).

(53) John C. Slater, Quantum Theory of Atomic Structure, Vol. 1 (McGraw-Hill Book Co. Inc., New York, 1960).

(54) Eran Nardi and Shaul Yatsiv, J. Chem. Phys. 37, 2333 (1962).

(55) Foster F. Rieke and Rinda Alison, J. Chem. Phys. 37, 3011 (1962).

(56) M. L. Bhaumik, H. Lyons, and P. C. Fletcher, J. Chem. Phys. 38, 568 (1963).

(57) A. Lempicki and H. Samelson, Physics Letters 4, 133 (1963).

(58) L. F. Johnson and K. Nassau, Proc. IRE 49, 1704 (1961).

(59) L. F. Johnson and R. R. Soder, J. Appl. Phys. 33, 757 (1962).

(60) L. F. Johnson, J. Appl. Phys. 33, 757 (1962).

(61) L. F. Johnson, Abstract No. 108, p. 260 Electrochem. Soc. Meeting (1962).

(62) E. Snitzer, Phys. Rev. Letter 7, 444 (1961).

(63) L. F. Johnson, G. D. Boyd, and K. Nassau, Proc. IRE 50, 86 (1962).

(64) Z. J. Kiss and R. C. Duncan, Jr., Proc. IRE 50, 1532 (1962).

(65) L. F. Johnson, G. D. Boyd, and K. Nassau, Proc. IRE 50, 87 (1962).

(66) Z. J. Kiss and R. C. Duncan, Jr., Proc. IRE 50, 1531 (1962).

(67) Z. J. Kiss and R. C. Duncan, Jr., Proc. IRE 50, 1531 (1962).

(68) A. Yariv, S. P. S. Porto, and K. Nassau, J. Appl. Phys. 33, 2519 (1962).

(69) H. W. Etzel, et. al., Applied Optics 1, 534 (1962).

(70) L. F. Johnson, G. D. Boyd, and K. Nassau, R. R. Soder, Phys. Rev. 126, 14 (1962).

(71) Handbook of Chemistry and Physics (39th ed., Chemical Rubber Publishing Co., Cleveland, 1957), p. 2550.

(72) Donald S. McClure, J. Chem. Phys. 17, 905 (1949).

(73) George W. Snedecor, Statistical Methods (5th ed., The Iowa State College Press, Ames, Iowa, 1956), p. 122.

(74) J. L. J. Bäckström and K. Sandros, Acta Chem. Scand. 12, 823 (1950).

(75) D. F. Evans, J. Chem. Soc. (London), 345 (1963).